2018-08-29

Investigation of LIN-28 Function in Somatic Gonadal Development and Fertility, and Characterization of the LIN-28 Isoforms in C. elegans Hermaphrodites

Sungwook Choi
University of Massachusetts Medical School

INVESTIGATION OF LIN-28 FUNCTION IN SOMATIC GONADAL DEVELOPMENT AND FERTILITY, AND CHARACTERIZATION OF THE LIN-28 ISOFORMS IN *C. elegans* HERMAPHRODITES

A Dissertation Presented
By
Sungwook Choi

Submitted to the Faculty of the
University of Massachusetts Graduate School of Biomedical Sciences, Worcester
In partial fulfilment of the requirements for the degree of
DOCTOR OF PHILOSOPHY
August, 2018
Program in Molecular Medicine

ACKNOWLEDGEMENTS

I want to express my sincere gratitude to my thesis advisor, Dr.Victor Ambros. He is an inspiring scientist. I learned a tremendous amount of knowledge and the attitude about science from his passion and his way of thinking. At the same time, he is a very supportive mentor. Whenever I have issues regarding my project, he offered advices and waited for me to pursue the project and also gave me a chance to solve them independently.

I thank all of my scientific committee members, Dr. Marian Walhout, Dr. Sean Ryder, Dr. William Theurkauf, Dr. Oliver Rando, Dr. Amy Walker, and Dr. Alexandra Byrne. Their critical questions have guided me to think in different ways and to refine my project. I also thank my outside committee member Dr. Erin Cram. She gave me the insightful comments about my thesis with her immense knowledge about *C. elegans* somatic gonads.

The past and current members of the Ambros Lab greatly contribute to my research. Rosalind Lee had created great lab environment for research. Dr. Anna Zinovyeva was my mentor when I first joined the laboratory and taught me how to perform various kinds of *C. elegans* experiments. Other lab members - Dr. Katherine McJunkin, Dr. Charles Nelson, Dr. Alrejandro Vasquez-Rifo, Dr.Hirosha Geekiyanage, Orkan Ilbay, Ye Duan, Mizra Zeynap, Reyyan Bulut – provided significant comments about my research at every step and also help to develop my presentation skills. Discussions with each lab member have made me a better scientist.

My classmates and Korean community in U Mass Medical School gave me emotional supports during my graduate study. Finally, I thank my mother, father and brother in Korea who always pray for my wellness and happiness.

ABSTRACT

lin-28 was first characterized as a developmental timing regulator in *Caenorhabditis elegans*. Loss of *lin-28* function (*lin-28(lf)*) mutants skip the hypodermal cell fates specific to the 2nd larval stage. Here, we studied two aspects of *lin-28* which had not yet been investigated.

First, we show that *lin-28(lf)* mutants exhibit reduced fertility associated with abnormal somatic gonadal morphology. In particular, the abnormal spermatheca-uterine valve morphology of *lin-28(lf)* hermaphrodites traps embryos in the spermatheca, which disrupts ovulation and causes embryonic lethality. The same genes downstream of *lin-28* in the regulation of hypodermal developmental timing also act downstream of *lin-28* in somatic gonadal morphogenesis and fertility. Importantly, we find that hypodermal expression, but not somatic gonadal expression, of *lin-28* is sufficient for restoring normal somatic gonadal morphology in *lin-28(lf)* mutants. We propose that the abnormal somatic gonadal morphogenesis of *lin-28(lf)* hermaphrodites results from temporal discoordination between the accelerated hypodermal development and normally timed somatic gonadal development. Thus, our findings exemplify how a cell-intrinsic developmental timing program can also control proper development of other interacting tissues, cell non-autonomously.

We also investigated the expression patterns and functions of two *lin-28* isoforms in *C. elegans*. Our analysis of spatial expression patterns suggests that *lin-28a* and *lin-28b* are co-expressed in diverse tissues. Consistently, neither of

isoform specific knock-out mutant, *lin-28a(lf)* or *lin-28b(lf),* exhibits defects in hypodermal development, somatic gonad, or fertility, indicating functional redundancy of two isoforms. Our study will contribute to further investigation of *lin-28* isoforms by providing the mutants of each isoform as well as the primary analysis of their phenotypes.

TABLE OF CONTENTS

LIST OF FIGURES

LIST OF TABLES

LIST OF ABBREVIATIONS

WT: wild type

L1: the 1st larval stage

L2: the 2nd larval stage

L3: the 3rd larval stage

L4: the 4th larval stage

TRIM-NHL family : Tripartite motif NCL-1/HT2A/LIN-41 protein family

CSD: cold shock domain

ZFD: zinc finger domain

CCHC zinc-knuckle : CysCysHisCys zinc-knuckle

pre-let-7: let-7 precursor

pri-let-7: primary *let-7* microRNA

CLIP-seq: Crosslinking immunoprecipitation -sequencing

eIF3β :eukaryotic initiation factor 3 beta

ER: endoplasmic reticulum

DTC: distal tip cell

Sp-Ut valve: spermathecal-uterine valve

sujn: spermathecal-uterine valve toroidal syncytium

sujc: spermathecal-uterine valve core cell syncytium

utse: uterine seam cells

EGF :epidermal growth factor

IP-3: inositol trisphosphate

MAPK: mitogen-activated protein kinase

Emo: Endomitotically replicating DNA

DAPI: 4′,6-diamidino-2-phenylindole

FM 4-64: *N*-(3-Triethylammoniumpropyl)-4-(6-(4-(Diethylamino) Phenyl) Hexatrienyl) Pyridinium Dibromide

GFP: Green fluorescent protein

KCl : Potassium Chloride

RNAi : RNA interference

mTOR: mammalian target of rapamycin

DIC microscopy: Differential interference contrast microscopy

NGM: nematode growth media

SL1 sequence: spliced leader 1 sequence

RT-PCR :reverse transcription polymerase chain reaction

EMS: ethyl methanesulfonate

ENU: N-ethyl-N-nitrosourea

VD neurons: GABAergic ventral D type neurons

DD neurons: GABAergic dorsal D type neurons

CRISPR-cas9: Clustered Regularly Interspaced Short Palindromic Repeats-Cas9 protein

PREFACE

The work presented in Chapter II is based on the manuscript "The *C. elegans* heterochronic gene *lin-28* coordinates the timing of hypodermal and somatic gonadal programs for hermaphrodite reproductive system morphogenesis" written by me and Dr. Victor Ambros, uploaded in bioRxiv server (https://www.biorxiv.org) as a preprint version. The manuscript is submitted as a research article to the journal of *Development* and is under review. Dr. Ambros and I designed the experiment and I performed all the experiments. Dr. Ambros and I wrote and reviewed the manuscripts. All the strain in this study were from Ambros Lab or the *Caenorhabditis* Genetics Center, except UN810 (donated by Dr. Erin Cram (Northeastern University)) and AG212 (donated by Dr.Anna Allen (Howard University)).

The work presented in Chapter III is unpublished. Dr. Ambros and I designed the experiment and I performed all the experiments. I wrote Chapter III which was reviewed by Dr. Ambros. The plasmid pWASR1 was donated by Dr. John Calarco (University of Toronto).

The preliminary data presented in Chapter IV was generated by me. I used a strain containing Punc-47::mCherry (donated by Dr. Alexandra Byrne (U Mass Medical School)) and a strain where GFP reporter is tagged at the 3' end coding sequence of the endogenous *lin-28* (generated by Orkan Ilbay, a PhD student in Ambros Lab)

Chapter I. Introduction

I-A. Heterochronic Genes as Developmental Timing Regulators during *C. elegans* Larval Stages

I-B. Functions of *lin-28* Homologs in Other Organisms

I-C. Molecular and Cellular Characteristics of LIN-28

I-D. Gonad Structure and Reproductive Process of *C. elegans* Hermaphrodites

I-E. Scope of This Thesis

I-A. Heterochronic Genes as Developmental Timing Regulators during *C. elegans* Larval Stages

In the context of evolution, the term “heterochrony” refers to modes of developmental alteration of an organism in which genetic changes lead to either accelerated or delayed development of certain body parts relative to others (Keyte and Smith, 2011; Klingenberg, 1998). Genetic mutations causing heterochrony in the nematode *Caenorhabditis elegans* revealed a gene regulatory network, the ‘heterochronic pathway’, that governs the relative timing of developmental events during the four larval stages (L1-L4), particularly in the hypodermis (Ambros and Horvitz, 1984a; Ambros and Horvitz, 1987) (Fig 1.1).

Mutation of each heterochronic gene can cause either precocious or retarded development. For example, loss-of-function (lf) mutations of *lin-14* or *lin-28* result in precocious development via the skipping of hypodermal cell fates specific to one or more larval stages. In contrast, *lin-4(lf)* and *let-7(lf)* mutations prevent the normal progression of certain stage-specific cell fates, leading to abnormal repetition of larval stages (Ambros, 2011; Ambros and Horvitz, 1984b)

lin-14 encodes a nuclear protein that specifies L1 hypodermal cell fates. Many *lin-14(lf)* alleles induce precocious hypodermal development, wherein L1-specific cell fates are skipped (Ambros and Horvitz, 1987). LIN-14 protein expression is highest in the L1 stage and decreased from the L2 stage onward (Ruvkun and Giusto, 1989). This downregulation requires the 3' untranslated region (UTR) of *lin-14* mRNA, which contains a complementary sequence to *lin-4*

microRNA (Arasu et al., 1991; Lee et al., 1993; Wightman et al., 1991). Therefore, *lin-4* microRNA is an essential component for progression from L1 to L2, and *lin-4(lf)* mutants reiterate L1-specific larval stages (Chalfie et al., 1981).

The transition from the L2 to L3 stage is regulated by multiple genes. Developmental down regulation of a transcription factor HBL-1, the homolog of *Drosophila* hunchback, is required for the transition (Abbott et al., 2005; Fay et al., 1999; Vadla et al., 2012). *let-7* family microRNAs (*mir-48*, *mir-241*, and *mir-84*) inhibit HBL-1 expression after the L2 stage. Thus, loss of these *let-7* family microRNAs results in repetition of L2-specific cell fates (Abbott et al., 2005). In contrast, LIN-28 is an upstream factor required for maintaining the HBL-1 level during the L2 stage (Moss et al., 1997; Vadla et al., 2012). Thus, *lin-28(lf)* mutants skip the L2-specific cell division patterns, causing precocious development of later cell fates. The precocious developmental features of *lin-28(lf)* mutants are restored to those of wild-type by loss of *lin-46* function (Pepper et al., 2004). *lin-46* acts downstream of *lin-28* and upstream of *hbl-1* in parallel with *let-7* family microRNAs. Both negative and positive regulation of *hbl-1* depends on the 3' UTR of its mRNA, which contains multiple *let-7* complementary sites (Abrahante et al., 2003; Lin et al., 2002; Vadla et al., 2012)

lin-29 is the most downstream of the heterochronic genes determining the transition timing from the 4th larval stage to the adult stage of *C. elegans* (Ambros, 1989; Rougvie and Ambros, 1995). As a zinc finger transcription factor, LIN-29 regulates many transcripts including *col-7* and *col-19*, which encode adult-specific

collagens (Abete-Luzi and Eisenmann, 2018; Liu et al., 1995). *lin-29(lf)* mutants undergo an additional larval stage after the L4, rather than differentiating into adults. Similarly, loss of *let-7* microRNA function causes retarded development, including a supernumerary larval stage after the 4th larval stage. *let-7* downregulates LIN-41 via *let-7* complementary sequences in the *lin-41* 3' UTR. LIN-41 is a member of the TRIM-NHL family protein, and LIN-41 negatively regulates *lin-29* expression (Slack et al., 2000). HBL-1 is another target of *let-7* microRNA. Loss of *hbl-1* function partially suppresses the retarded phenotype of *let-7(lf)* upstream of *lin-29* (Lin et al., 2002). Therefore, *let-7* microRNA functions to regulate the transition from L4 to adult via downregulation of LIN-41 and HBL-1. This reduction in the levels of LIN-41 and HBL-1 release their inhibition of *lin-29*, the downstream effector of the larval to adult switch (Figure 1.1).

In summary, protein coding genes, such as *lin-14*, *hbl-1*, and *lin-29*, control the transitions downstream of other heterochronic genes. Another important class of heterochronic genes are microRNAs, including *lin-4*, *let-7,* and the *let-7*-family microRNAs, *mir-48*, *mir-84*, and *mir-241*. MicroRNAs post-transcriptionally control the level of other heterochronic genes by targeting their mRNAs. Loss of one or more microRNA functions causes retarded larval development due to the failure of prompt downregulation of the corresponding target genes.

LIN-28 is a central regulator of the heterochronic pathway. *lin-28* functions to specify the proper timing of L2-to-L3 cell fate transitions by promoting the expression of HBL-1, as mentioned above. In addition, LIN-28 also prevents

premature expression of mature *let-7* microRNA and thus guards against precocious transition from L4 to adult (Abbott et al., 2005; Vadla et al., 2012; Van Wynsberghe et al., 2011). The expression of LIN-28 protein is highest in the late embryo and L1 stages and decreases from the L2 stage onward, mediated *by lin-4* microRNA. The 3' UTR of *lin-28* mRNA contains not only a *lin-4* binding site but also a *let-7*-family *s*eed complementar*y* binding site, and mutation of either site induces an increased level of *lin-28*, suggesting that *lin-4*, in combination with *let-7-family* microRNAs, function to suppress LIN-28 (Morita and Han, 2006).

Figure 1.1

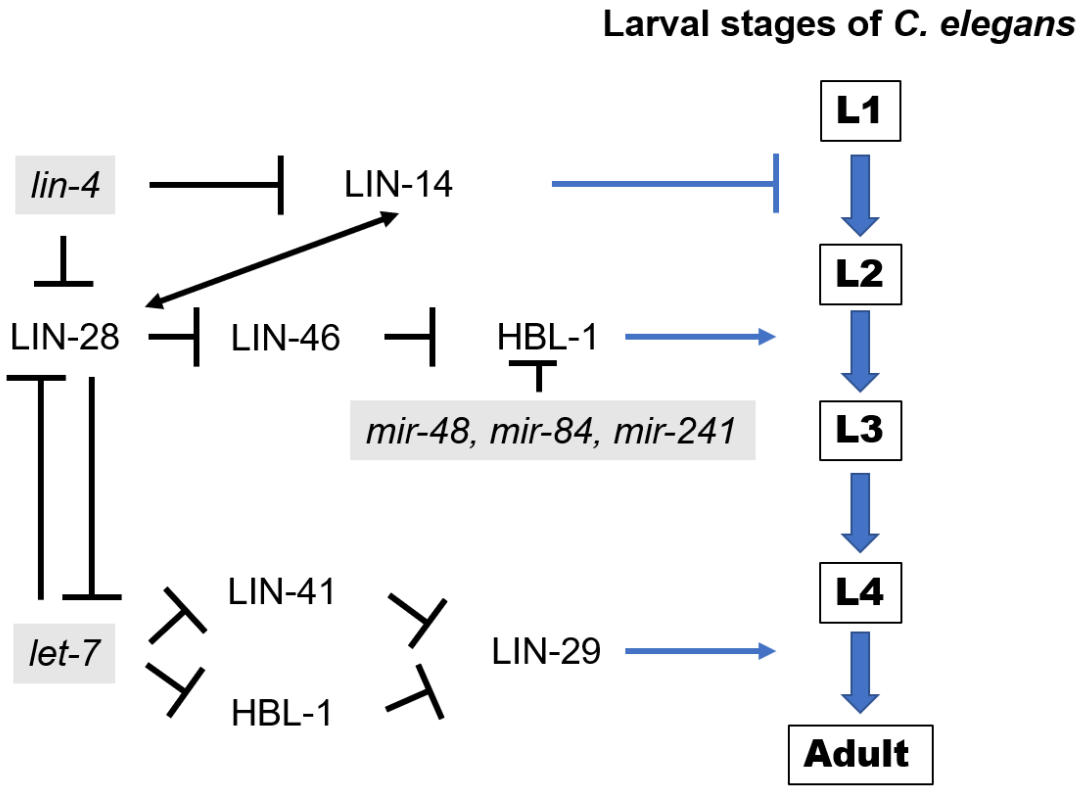
Larval stages of C. elegans
L1
L2
L3
L4
Adult
lin-4
LIN-14
LIN-28
LIN-46
HBL-1
mir-48, mir-84, mir-241
let-7
LIN-41
HBL-1
LIN-29

Figure 1.1. Heterochronic pathway in *C. elegans* larval development.

Schematic representation of heterochronic pathway genes that govern developmental timing of the *C. elegans* hypodermis. *lin-4*, *let-7, mir-48,mir-84,* and *mir-241* are microRNAs that negatively regulate other proteins.

I-B. Functions of *lin-28* Homologs in Other Organisms

Homologs of *lin-28* are found in many organisms, including flies, zebrafish, mice, and humans (Moss and Tang, 2003). Moreover, the reciprocal negative regulation between *let-7* and *lin-28*(See Fig 1.1), is also conserved in many organisms (Roush and Slack, 2008).

In *C. elegans*, larval hypodermal seam cell lineages exhibit a series of asymmetric divisions at each larval stage, with a distinctive symmetric division specifically in the L2 (Fig 1.2). These division patterns are exemplary of the self-renewing and proliferative behaviors typical of stem cells. At the end of the L4 stage, seam cells exit the cell cycle and differentiate, producing the adult-specific cuticular alae. In the absence of *lin-28*, the L2-specific proliferative division is omitted, and differentiation occurs precociously by one or two larval stages. (Ambros and Horvitz, 1984b; Reinhart et al., 2000; Vadla et al., 2012).

Consistent with the function of *C. elegans lin-28* in specifying early larval symmetric stem cell divisions, and opposing differentiation, mammalian embryonic stem cells express high levels of Lin28 (Moss and Tang, 2003). The pluripotency activity of mammalian Lin28 was demonstrated by the reprogramming of human fibroblasts into induced pluripotent stem cells (iPSCs) using Lin28, along with Oct4, Sox2, and Nanog (Yu et al., 2007). Many studies have shown that mammalian Lin28, directly or indirectly, interacts with other pluripotency factors such as Oct4 or Sox2 (Cox et al., 2010; Jin et al., 2011; Marson et al., 2008; Qiu et al., 2010). One mechanism by which mammalian Lin28 contributes to pluripotency is by

inhibiting biogenesis of mature *let-7*, because genes important for maintaining stemness, such as Hgma2 and c-Myc, are targets of *let-7* microRNA (Kim et al., 2009; Lee and Dutta, 2007). Furthermore, additional studies suggest that Lin28 regulates embryonic stem cell metabolism by binding to mitochondrial enzyme-encoding mRNAs (Peng et al., 2011). Theses enzymes are involved in the synthesis of essential cellular metabolites for self-renewal of embryonic stem cells (Alexander et al., 2011; Wang et al., 2009). Overexpression of *let-7* microRNA reduces the abundance of these metabolites, indicating that Lin28–mediated suppression of *let-7* maturation is necessary to maintain their levels (Shyh-Chang et al., 2013).

In humans, Lin28 is also implicated in tumorigenesis in various cancer types, including breast cancer, lung cancer, and hepatocellular carcinoma (Carmel-Gross et al., 2016; Jiang and Baltimore, 2016). High levels of Lin28 expression are detected in both patient samples and cancer cell lines. Lin28 regulates tumorigenesis by inhibiting biogenesis of mature *let-7*, which suppresses many oncogenes, including K-Ras, c-Myc, and other cyclins (Dong et al., 2010; Kim et al., 2009; Oh et al., 2010). Recent studies showed that mammalian Lin28 functions in the metastasis of colon cancer and breast cancer (Chen et al., 2015a; King et al., 2011; Liu et al., 2013).

Finally, findings suggest that mammalian Lin28 is involved in the development of immune cells. Ectopic expression of mammalian Lin28 can reprogram (via repression of *let-7*) adult bone marrow cells into hematopoietic

stem cells, enabling the production of various immune cells including B cells, gamma/delta T cells, and natural killer cells (Lee et al., 2013; Yuan et al., 2012; Zhou et al., 2015)(Lee et al., 2013; Yuan et al., 2012; Zhou et al., 2015) Furthermore, Lin-28 overexpression leads to peripheral T-cell lymphoma in mouse thymus (Beachy et al., 2012).

In *Drosophila melanogaster, lin-28* loss-of-function mutations cause precocious fusion of the egg chamber in the early oogenesis of female files, resulting in reduced fertility. Ectopic expression of *let-7* induces the same defects, implying that *let-7* is involved in this process (Stratoulias et al., 2014). In addition, *Drosophila lin-28* functions to maintain adult intestinal stem cell populations by binding directly to mRNAs of insulin receptors and promoting their expression independent of *let-7* regulation (Chen et al., 2015b). *fmr1,* a *Drosophila* homolog of human fragile X mental retardation protein (FMRP), opposes the *lin-28* functions of regulating insulin receptors and the expansion of adult intestinal progenitor cells, to control the population of intestinal stem cells depending on nutrient availability (Luhur et al., 2017).

In zebrafish, heterochronic genes, including *lin-28*, *let-7*, *lin-4*, and *lin-41,* share a similar expression pattern with their homologs in *C. elegans* (Ouchi et al., 2014). Zebrafish embryos express high levels of *lin-28,* and knockdown of *lin-28* in zebrafish causes embryonic defects in gastrulation and neural expansion (Ouchi et al., 2014). Zebrafish *lin-28* induces proliferation of Muller glial cells, the source of retina stem cells. This proliferation is crucial for retina regeneration upon injury,

and wnt signaling activates *lin-28* expression to abrogate *let-7* function (Kaur et al., 2018; Yao et al., 2016).

In *Xenopus*, *lin-28* similarly affects embryonic development. *lin-28* knockdown embryos fail to form proper mesoderm independently of *let-7* microRNA (Faas et al., 2013). Interestingly, *lin-28* promotes expression of *Xenopus* mir-17~92. (Warrander et al., 2015). Mammalian mir-17~92 is implicated in diverse types of cancers, cardiovascular disease and neurodegenerative diseases.(Mogilyansky and Rigoutsos, 2013)

Figure 1.2.

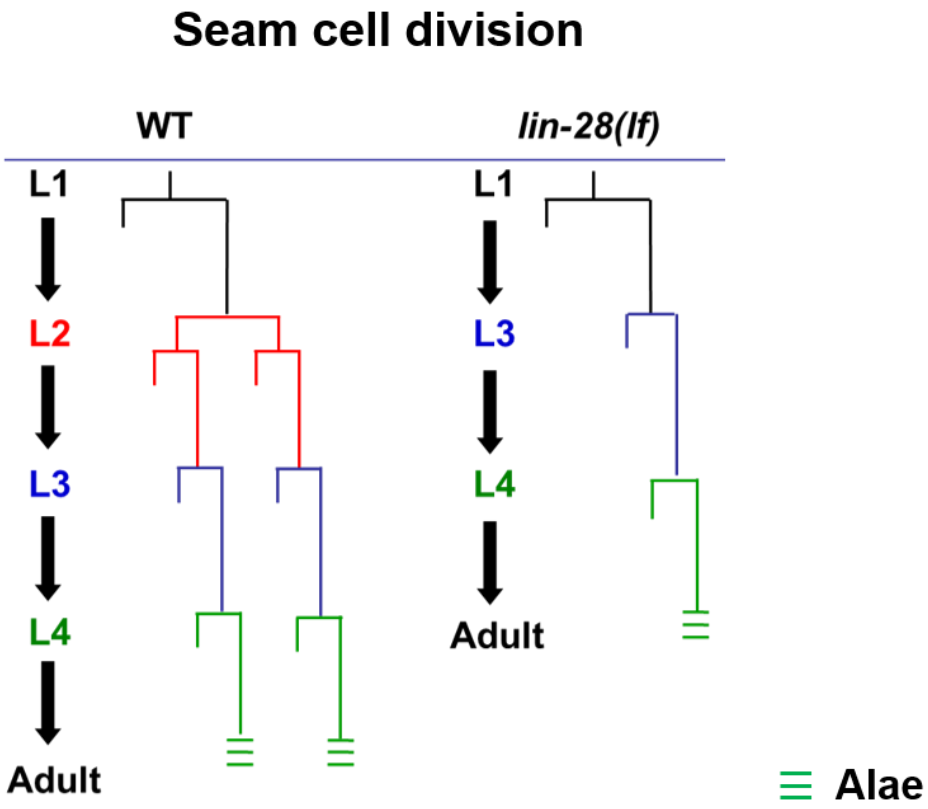
Seam cell division
WT
lin-28(lf)
L1
L2
L3
L4
Adult
L1
L3
L4
Adult
Alae

Figure 1.2. Seam cell division pattern of wild type and *lin-28(lf)* mutants during *C. elegans* larval developments

Division patterns of seam cell (V1-V4, V6), *C. elegans* hypodermal stem cell, of wild type (WT) or *lin-28(lf)* mutants are depicted. L2 specific proliferative cell division is skipped in *lin-28(lf)* mutants. Seam cells are finally differentiated into adult specific alae.

I-C. Molecular and Cellular Characteristics of LIN-28

The LIN-28 protein contains two types of RNA-binding domains: one cold shock domain (CSD) in the amino terminal portion of the protein, and two C-terminal zinc finger domains (ZFDs) (Moss et al., 1997). The CSD contain RNP1 and RNP2 motifs, which are also present in bacterial cold shock proteins and the family of eukaryotic Y-Box proteins (Graumann and Marahiel, 1996; Landsman, 1992). The two LIN-28 ZFDs contains CCHC (CysCysHisCys) zinc-knuckle type motifs initially identified in retroviruses (Gorelick et al., 1988; Pappalardo et al., 1997). These two types of domains are highly conserved across diverse species (Moss and Tang, 2003), and their roles in LIN-28 function have been investigated extensively (Mayr et al., 2011; Nam et al., 2011; Triboulet et al., 2015; Wang et al., 2017c).

Mammalian Lin28 can inhibit maturation of *let-7* by binding directly to the loop region of the *let-7* precursor (*pre-let-7*) (Heo et al., 2008; Newman et al., 2008; Viswanathan et al., 2008). The conserved GGAG sequence in the *pre-let-7* terminal loop is required for recognition by LIN-28 (Heo et al., 2009). LIN-28 is reported to recruit TUTase4 to promote uridylation at the 3' terminus of *pre-let-7*, causing degradation of pre-let-7 (Heo et al., 2008; Heo et al., 2009).

Structural analysis using crystallography revealed that both the CSD and ZFD of Lin28 interact with the loop region of *pre-let-7* (Nam et al., 2011). Two CCHC motifs in the ZFD recognize GGAG sequences, and the CSD prefers to bind GNGAY sequences in the loop. Later, it was reported that binding of the CSD with

pre-let-7 causes a conformational change in the *pre-let-7* structure, exposing the GAGG sequence (Mayr et al., 2011). Therefore, the CSD is essential for the change in *pre-let-7* structure needed for the ZFD to recognize GGAG and trigger subsequent uridylation. Consistent with this finding, *let-7a-3*, a human *let-7* family member, bypasses Lin28 regulation, because it does not bind the LIN-28 CSD domain. Switching the pre-loop region of *let-7a-3* with that of other *let-7* family members restores its interaction with Lin28 (Triboulet et al., 2015). Another study suggested that the ZFD is crucial for stabilizing the binding of Lin28 with *pre-let-7*. The dissociation rate was increased by either mutating the ZFD domain of Lin28 or the GGAG sequence motif of *pre-let-7* (Wang et al., 2017c).

The mammalian genome encodes two paralogs of Lin28: Lin28A and Lin28B. Both proteins are involved in a variety of cancers in a *let-7*–dependent manner (Viswanathan et al., 2009). Depending on cancer subtype, either Lin28A or Lin28B may be found to be overexpressed (Piskounova et al., 2011).

Lin28A and Lin28B show ~70% homology with each other and contain both a CSD and ZFDs. Nonetheless, Lin28B inhibits *let-7* biogenesis via a different mechanism than Lin28A (Piskounova et al., 2011). Lin28B localizes in the nucleus due to its functional nuclear localization signal. Thus, Lin28B does not recruit Terminal Uridylyl Transferase (TUTase) or uridylate *pre-let-7* in the cytoplasm as does Lin28A. Instead, Lin28B directly binds to primary *let-7* microRNA (*pri-let-7*) in the nucleus. Lin28B localizes to the nucleoli, where microRNA processors such as DGCR8 and Drosha are absent, implying that Lin28B sequesters *pri-let-7* from

microprocessing.

Unlike in mammals, *C. elegans* contains one genomic location where LIN-28 is encoded, although this genomic locus can encode two isoforms of LIN-28. The two isoforms differ only in the first exon, whereas they share the second and third exons, which include the CSD and ZFD coding sequences. Differences in their expression and function have not yet been investigated.

Interestingly, recent studies have indicated that *C. elegans* LIN-28 regulates pri-*let-7* in the nucleus, as in the case of mammalian Lin28B. *C. elegans* LIN-28 binds directly to *pri-let-7* and inhibits microprocessing. Therefore, although *pri-let-7* is expressed from the L1 stage onward, neither *pre-let-7* nor mature *let-7* are detected until the L3 stage, when LIN-28 is depleted (Van Wynsberghe et al., 2011). Furthermore, Crosslinking immunoprecipitation (CLIP)-sequencing (seq) data showed that the GGAG motif bound by LIN-28 is located in the *C. elegans pri-let-7* outside of its terminal loop region (Stefani et al., 2015). However, another study suggested that LIN-28 can bind to *pre-let-7* and the poly(U) polymerase (PUP)-2 uridylates *pre-let-7*, similar to mammalian Lin-28A and TUT4 (Lehrbach et al., 2009).

Although the role of LIN-28 in regulating *let-7* microRNA is essential in various biological contexts, much evidence indicates that Lin28 also directly binds to and regulates mRNAs, such as those of insulin-like growth factor 2 (IGF2), OCT4, and bone morphogenetic protein 4 (BMP4) (Ma et al., 2013; Polesskaya et al., 2007; Qiu et al., 2010). Lin28A is localized in the processing body where mRNA

and microRNA are processed, or to stress granules where some non-translating mRNAs are temporarily stored (Balzer and Moss, 2007). During myoblast differentiation, Lin28 promotes translation of IGF2 independently of *let-7*. Biochemical analysis revealed that Lin28 binds to the translation initiation factor eukaryotic initiation factor 3 beta (eIF3β) and elongation factors (EFs) such as EF1-α and EF1-α2 in skeletal muscles (Polesskaya et al., 2007). It has been also suggested that Lin28 also recruits RNA helicase to target mRNA and enhance translation (Jin et al., 2011). Crosslinking immunoprecipitation (CLIP)-sequencing (seq) and photoactivatable ribonucleoside-enhanced (PAR)-CLIP data revealed that Lin28 binds to the mRNA that encodes itself, cell cycle regulators, and splicing factors, increasing their expression levels (Hafner et al., 2013; Wilbert et al., 2012). Thus, ectopic expression of Lin28 induces a wide range of alternative splicing events (Wilbert et al., 2012). In contrast, another study showed that LIN-28 localizes in the periendoplasmic reticulum (ER) area and inhibits the expression of ER-associated mRNAs, which encode transmembrane proteins, ER and Golgi proteins, and secretory proteins (Cho et al., 2012). In *C. elegans*, CLIP-seq data suggest that LIN-28 can bind to mRNAs of proteins in the heterochronic pathway, such as LIN-46, LIN-14, and DIN-1 (Stefani et al., 2015).

In summary, *lin-28* has a wide range of functions in both vertebrates and invertebrates, although generally, these functions fit a theme wherein *lin-28* functions early in development to inhibit *let-7*-associated differentiation, and thereby promote proliferation and pluripotency. While the *lin-28/let-7* axis is

important in many contexts, there is evidence that *lin-28* can also directly bind to and regulate mRNA independently of *let-7*. The mechanisms by which LIN-28 regulates mRNA expression require further investigation. For example, further research is needed to understand how Lin28 functions as a translational activator (Polesskaya et al., 2007; Wilbert et al., 2012) or suppressor (Cho et al., 2012) depending on context. In addition, the functions of the CSD and ZFD in regulating mRNA expression are of particular interest.

I-D Gonad Structure and Reproductive Processes in *C. elegans* Hermaphrodites

The hermaphrodite gonad consists of germ cells, which originate from proliferation of two germline precursor cells (Z2 and Z3), and somatic gonadal tissues, which are derived from two somatic precursor cells (Z1 and Z4); Z1, Z2, Z3, and Z4 comprise within the gonadal primordium of L1 larvae (Kimble and Hirsh, 1979).

Germline precursors Z2 and Z3 originate from P4 cells in the embryo, which are characterized by the presence of P-granules and the expression of *pie-1*. Germline proliferation occurs from mid L1 to L3. From the L3 stage, mitotic division is restricted to the distal germline, and proximal germline nuclei (organized around the periphery of a tubular syncytium) begin to enter meiosis. Spermatogenesis occurs during L4 in hermaphrodites, and many genes have been identified that are required to produce mobile and fertile sperm (Chatterjee et al., 2005; Kroft et al.,

2005; Nishimura and L'Hernault, 2008; Singson et al., 1998). Oogenesis occurs during young adulthood, characterized by an increase in volume of the oocyte cytosol. A subset of germline nuclei undergo apoptosis and are engulfed by surrounding gonad sheath cells (Gartner et al., 2008).

Somatic gonadal development occurs during the L1–L4 larval stages and is characterized by stage-specific patterns of cell division, morphogenesis, and differentiation into tissues with specific functions, including distal tip cells (DTCs), gonadal sheath cells, spermatheca, the spermathecal-uterine valve (Sp-Ut valve), uterus, and uterine seam cell (utse) syncytium (Kimble and Hirsh, 1979; Newman and Sternberg, 1996).

DTCs are single, large somatic cells located in the most distal region of each gonad arm (Kimble and White, 1981). Directed migration of the two DTCs leads to elongation of the gonad arms during the larval stages in the anterior and posterior directions, respectively. Also, signals from DTCs regulate cell division, cell cycle, and entry into meiosis of the distal germline. Gonadal sheath cells enclose each gonad arm, covering the germline cells and syncytium, and form connections between germline and other somatic tissues. Yolk proteins are produced in the intestine and delivered to the oocytes through the gonadal sheath cell pores (Grant and Hirsh, 1999; Hall et al., 1999).

The spermatheca is a sac structure where sperm cells are stored and fertilization occurs (Gissendanner et al., 2008; Kimble and Hirsh, 1979). The spermatheca first forms two narrow rows of 12 cells next to proximal oocytes

during the young adult stage. Spermathecal actomyosin network changes dynamically during stretching and contraction in the process of ovulation (Wirshing and Cram, 2017).

The Sp-Ut valve connects the spermatheca to the uterus in hermaphrodites. The Sp-Ut valve comprises two syncytia. The toroidal syncytium (sujn) results from the fusion of four cells and provides the pathway for fertilized embryos to the uterus. The core cell syncytium (sujc), which contains two nuclei, resides inside of the toroidal syncytium (Kimble and Hirsh, 1979). The core cell syncytium forms a dumbbell-like structure in wild-type young adult stages, with one arm in the spermathecal side and the other arm in the uterus (Palmer et al., 2002).

Fertilized embryos are held in the uterus before they are laid outside of animals. The adult hermaphrodite uterus is composed of eight syncytia, which each contain four or six nuclei. Uterine cells fuse after multiple rounds of division during the mid-L4 stage. As a result, the uterine lumen forms and extends during the mid-L4 stage in wild-type hermaphrodites (Newman et al., 1996). The uterus is structurally connected to the lateral seam cells, and this connection is mediated by the uterine seam (utse). Utse is formed by fusion of 8 cells of uterine lineage and the anchor cell by the mid-L4 stage (Newman et al., 1996). The eight cells are daughter cells of ventral uterine precursors, which require notch signals from the anchor cell. After forming the utse syncytium, the nuclei spread laterally during the L4 stage (Newman et al., 1995; Newman et al., 2000).

Oocyte meiotic maturation occurs before ovulation and fertilization in young adult hermaphrodites. Oocyte maturation requires major sperm protein (MSP) from sperm to antagonize VAB-1 receptor and CEH-18 transcription factor, which inhibit the maturation process via a MAPK-dependent pathway (Miller et al., 2001; Miller et al., 2003). In addition, the female germline expresses OMA-1 and OMA-2 proteins, which redundantly regulate completion of oocyte maturation. Breakdown of the nuclear envelope and a cortical rearrangement are characteristics of oocyte maturation (Detwiler et al., 2001).

Ovulation is the process wherein the mature oocytes one-by-one enter the spermatheca where hermaphrodite sperm reside. Contraction of gonadal sheath cells and dilation of the distal spermatheca region occur during ovulation and are modulated by the epidermal growth factor (EGF) signaling pathway including *lin-3* and *let-23* as well as inositol trisphosphate (IP-3)–mediated calcium signaling (Clandinin et al., 1998; Kariya et al., 2004; Yin et al., 2003).

Ovulated oocytes are fertilized in the spermatheca. Many mutations have identified in spermathecal genes that are required for successful fertilization via the recognition of or fusion with the oocyte (Nishimura and L'Hernault, 2008). Right after fertilization, embryos rapidly establish an egg shell in the spermatheca. The egg shell consists of multiple layers, including the outermost vitelline membrane and chitin membrane, that form a protective barrier for the embryo (Johnston and Dennis, 2011). Many egg shell-defective mutants show multiple sperm cells in their fertilized embryo, indicating that the egg shell functions as a polyspermy barrier

(Johnston et al., 2010; Parry et al., 2009). Furthermore, some egg shell mutants fail to exhibit extrusion of the second polar body from the embryos, suggesting the abnormal cytokinesis (Johnston et al., 2006) .

The fertilized embryo exits from the spermatheca to the uterus via the contraction of spermathecal muscle. This process also requires induction of calcium signaling by a Phospholipase C (PLC-1), a cytoskeletal proteins such as structural filamin (FLN-1), and a gap junction subunit (INX-12) are involved in the release, oscillation, and propagation of calcium signaling (Kovacevic and Cram, 2010; Kovacevic et al., 2013). Embryos are temporally stored in the uterus until they are expelled through the vulva into the outside world.

Figure 1.3.

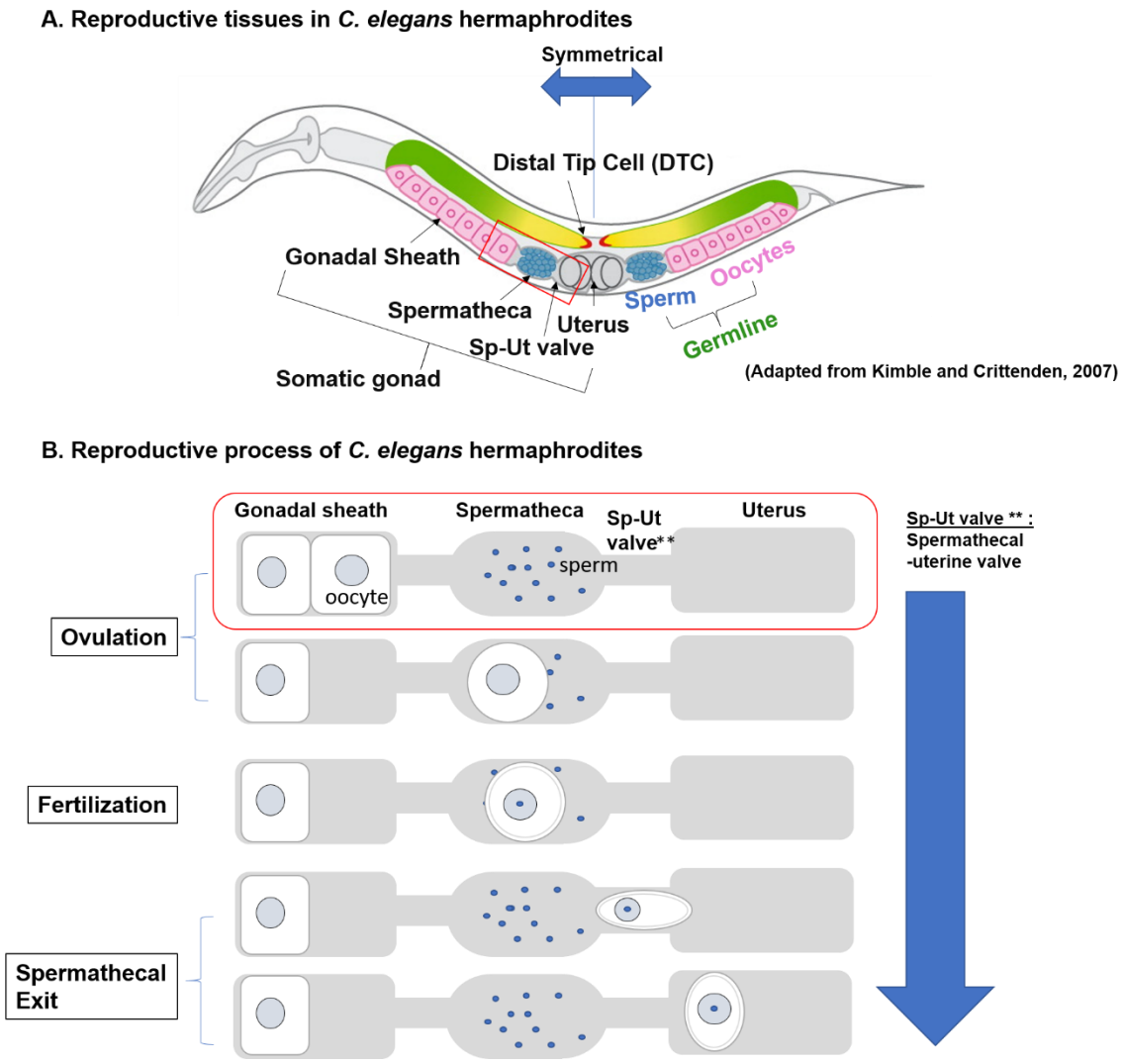
A. Reproductive tissues in *C. elegans* hermaphrodites
Symmetrical
Distal Tip Cell (DTC)
Gonadal Sheath
Spermatheca
Uterus
Sp-Ut valve
Somatic gonad
Sperm
Oocytes
Germline
(Adapted from Kimble and Crittenden, 2007)
B. Reproductive process of *C. elegans* hermaphrodites
Gonadal sheath
Spermatheca
Sp-Ut valve**
Uterus
oocyte
sperm
Sp-Ut valve ** :
Spermathecal
-uterine valve
Ovulation
Fertilization
Spermathecal Exit

Figure 1.3. Reproductive system in *C. elegans* hermaphrodites

(A) *C. elegans* hermaphrodites contains both sperm and oocytes. Other than germ cells, somatic gonadal tissues including distal tip cells (DTCs), gonad sheath cells, spermatheca, spermathecal-uterine valve, and uterus are also crucial for reproductive process in hermaphrodites (Picture adapted from Kimble and Crittenden 2007).

(B) Schematic representation of reproductive process in *C. elegans* hermaphrodites. The most proximal oocyte in gonadal sheath ovulates into spermatheca wherein oocytes is fertilized with sperm. Fertilized embryos exit to uterus via Sp-Ut valve, and they are held in the uterus until they are laid outside of the animal.

I-E Scope of This Thesis

The research presented in this thesis covers two separate topics, but all are related to investigating the functions of *C. elegans lin-28*.

In Chapter II, I present our findings regarding the roles of *lin-28* in somatic gonadal development and how *lin-28* affects the fertility of *C. elegans* hermaphrodites. This project began with the discovery that *C. elegans lin-28(lf)* mutants exhibit fertility defects. We asked why the mutants have fertility defects and how the defects are related to developmental timing regulation. To answer these questions, we investigated: 1) the physiological cause of the mutants' fertility defects, 2) the correlation between fertility defects and developmental timing defects in *lin-28(lf)* mutants, and 3) the tissue-specific requirement of *lin-28* for fertility. Our aim was to identify fertility problems that are specifically induced by developmental timing defects.

In the research presented in Chapter III, we examined the roles of each *lin-28* isoform in *C. elegans* mutants. 1) We first investigated the expression pattern of each isoform by differential fluorescent reporters. 2) Next, to determine the function of each isoform, we generated two individual knock-out mutants (*lin-28a(lf)* and *lin-28b(lf)*) using CRISPR-Cas9 technology. We determined whether each mutant exhibits the defects shown in *lin-28(lf)* mutants.

In Chapter IV, I summarize the presented findings and also discuss remaining questions and future directions regarding this research.

Chapter II. *lin-28* Coordinates the Timing of Hypodermal and Somatic Gonadal Programs for Hermaphrodite Reproductive System morphogenesis

- **Abstract**
- **Background and Significance**
- **Results**
- **Discussion**
- **Material and Methods**

Abstract

C. elegans heterochronic genes determine the timing of expression of specific cell fates in particular stages of developing larva. However, their broader roles in coordinating developmental events across diverse tissues have been less well investigated. Here, we show that loss of *lin-28*, a central heterochronic regulator of hypodermal development, causes reduced fertility associated with abnormal somatic gonadal morphology. In particular, the abnormal spermatheca-uterine valve morphology of *lin-28(lf)* hermaphrodites traps embryos in the spermatheca, which disrupts ovulation and causes embryonic lethality. The same genes that act downstream of *lin-28* in the regulation of hypodermal developmental timing also act downstream of *lin-28* in somatic gonadal morphogenesis and fertility. Importantly, we find that hypodermal expression, but not somatic gonadal expression, of *lin-28* is sufficient for restoring normal somatic gonadal morphology in *lin-28(lf)* mutants. We propose that the abnormal somatic gonadal morphogenesis of *lin-28(lf)* hermaphrodites results from temporal discoordination between the accelerated hypodermal development and normally timed somatic gonadal development. Thus, our findings exemplify how a cell-intrinsic developmental timing program can also control proper development of other interacting tissues, presumably by cell non-autonomous signal(s).

Background and Significance

Animal development is an intricate process which requires spatial and temporal regulation of diverse cell types. Spatial regulation such as that of the Hox gene family has been the subject of intense research (Mallo et al., 2010). Temporal control of cell-fate decision is another crucial feature for time appropriate developmental events such as organ morphogenesis and sexual maturation. Moreover, orchestrating developmental timing of complex tissues and constructing timely connections between them are essential to achieve normal development for the organism as a whole (Rougvie, 2001).

Previous studies in *C. elegans* identified a gene regulatory network of "heterochronic genes" that govern hypodermal developmental timing (Ambros, 2011). LIN-28 is one of the central heterochromatic gene which determines the L2 hypodermal fates of the animals. Their roles in developmental timing and genetic relationship with other heterochronic genes have been the main focus of previous study (Ambros and Horvitz, 1984b; Moss et al., 1997; Pepper et al., 2004; Seggerson et al., 2002).

Here, we investigated the role of *lin-28* in maintaining fertility of *C. elegans* hermaphrodites. Our results show that certain aspects of somatic gonadal development are abnormal in *lin-28(lf)* hermaphrodites, reflected by abnormal morphology of the uterus, uterine seam, and Sp-Ut valve. These morphological defects, particularly the abnormal Sp-Ut, dramatically limit *lin-28(lf)* fertility. Our

results further indicate that the normal development of the somatic gonad relies on temporal coordination of hypodermal developmental events with somatic gonadal events, and that *lin-28* acts in the hypodermis to specify a schedule of hypodermal events that is properly coordinated with a corresponding schedule of somatic gonadal developmental events. We demonstrate that the hypodermal function of *lin-28* is sufficient to regulate somatic gonadal development non-autonomously, consistent with a role for *lin-28*, and downstream heterochronic genes, in controlling the hypodermal components of critical developmental signaling between the gonad and hypodermis. This study shows one example of physiological defects which stem from the failure to control developmental timing of different tissues

Results

lin-28(lf) mutants exhibit defects in embryo production and embryo viability

lin-28(n719) hermaphrodites produced dramatically fewer larval progeny than wild-type hermaphrodites (Fig 2.1A). *lin-28(n719)* mutants are unable to lay eggs, due to precocious vulva development, which results in abnormal vulva morphogenesis (Euling and Ambros, 1996). Like other egg-laying defective mutants, *lin-28(lf)* hermaphrodites contain their entire brood of embryos trapped inside the limited space of the somatic gonad. To test whether the reduced number of progeny of *lin-28(lf)* hermaphrodites could be simply the result of their egg-laying defects, we compared the number of progeny of *lin-28(n719)* hermaphrodites with that of *lin-2(e1309). lin-2(e1309*) mutants exhibit defective egg-laying due to their vulvaless phenotype, which results from cell lineage defects not related to developmental timing (Hoskins et al., 1996). *lin-28(n719)* mutants produce substantially fewer progeny than *lin-2(e1309)* (Fig 2.1A), suggesting the reduced brood number of *lin-28(n719)* animals is not merely the result of an egg-laying defect. To test for reduced embryo production in *lin-28(n719)* hermaphrodites, we dissected mature, gravid hermaphrodites to count the embryos retained inside. *lin-28(n719)* gravid adults contained fewer embryos than *lin-2(e1039)* animals (Fig 2.1C and 2.1D), indicating that *lin-28(n719)* mutants are defective in embryo production. To test embryonic viability, we harvested embryos from dissected gravid adults and counted the number that hatched and developed into larva. Approximately 70% of *lin-28(n719)* embryos failed to develop, whereas essentially

all of the *lin-2(e1309)* embryos were viable (Fig 2.1B). These results suggest that reduced embryo production and embryonic lethality contribute to the reduced progeny number of *lin-28(n719)* mutants. *lin-28(n719)* mutants also displayed these same defects at 20°C, although at a somewhat reduced penetrance compared to 25°C (Fig 2.1). We conducted all our subsequent experiments at 25°C, where those defects are most prominent.

Figure 2.1.

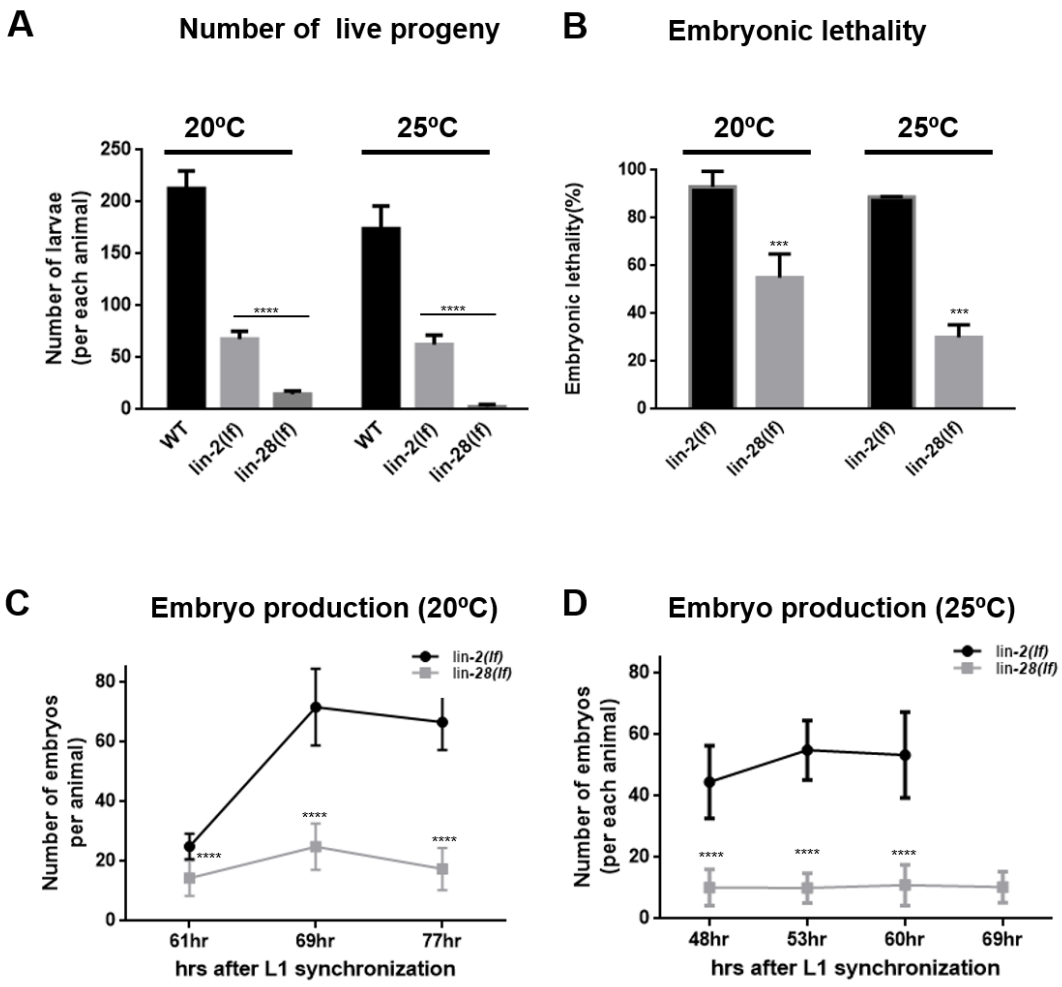
A
Number of live progeny
20ºC
25ºC
Number of larvae (per each animal)
250
200
150
100
50
0
****
****
WT
lin-2(lf)
lin-28(lf)
WT
lin-2(lf)
lin-28(lf)
B
Embryonic lethality
20ºC
25ºC
Embryonic lethality(%)
100
80
60
40
20
0
***
***
lin-2(lf)
lin-28(lf)
lin-2(lf)
lin-28(lf)
C
Embryo production (20ºC)
lin-2(lf)
lin-28(lf)
Number of embryos per animal)
80
60
40
20
0
****
****
****
61hr
69hr
77hr
hrs after L1 synchronization
D
Embryo production (25ºC)
lin-2(lf)
lin-28(lf)
Number of embryos (per each animal)
80
60
40
20
0
****
****
****
48hr
53hr
60hr
69hr
hrs after L1 synchronization

Figure 2.1. Fertility phenotypes of *lin-28(lf)* mutants at 20°C and 25°C.

(A)Total number of live larval progeny per animal for wild-type N2 animals(n=5), *lin-2(e1309)* mutants(n=17 for 25°C, n=16 for 20°C) and *lin-28(n719)* (n=19) mutants at 20°C and 25°C. (B) Embryonic lethality for *lin-2(e1309)* and *lin-28(n719)* mutants at 20°C and 25°C. (Number of animlals≥15 per each assay; number of independent replicate assays = 3) (C) The number of embryos produced at varying time points after feeding of synchronized L1 larvae, for *lin-2(e1309)* and *lin-28(n719)* mutants at 20°C and 25°C. (n= 10,8,8 (*lin-2(e1039*), 12,15,13 (*lin-28(n719)*) for 61hr, 69hr, and 77hr respectively at 20°C. n= 12,10,10, 0(*lin-2(e1039*), 15,13,12,3 (*lin-28(n719)*) for 48hr, 53hr, 60hr and 69hr respectively at 25°C.) (A-C: Data are shown as mean ± SD. Unpaired t-test compared to *lin-2(lf)*, ****p<0.0001)

Defects in ovulation and the spermathecal exit cause reduced embryo production in *lin-28(lf)* mutants

To investigate the cause of reduced embryo production in *lin-28(n719)* mutants, we checked whether ovulation and spermathecal exit proceed normally. We examined the spermatheca of *lin-28(n719)* mutants using the expression of a spermatheca reporter, *fkh-6::GFP* (Chang et al., 2004). Approximately 80% of *lin-28(n719)* mutants contained embryos in their spermathecae, whereas less than 10% of wild-type spermathecae contained embryos (Fig 2.2A,B). Unlike in the wild type, many embryos in *lin-28(n719)* hermaphrodites had undergone multiple rounds of cell division inside the spermathecae. This suggests that *lin-28(n719)* mutants have defects in the process of spermathecal exit. We used time-lapse video microscopy to monitor spermathecal exit. In wild type hermaphrodites, the process of ovulation, fertilization, and spermathecal exit of an individual embryo happens within less than 10 minutes (McCarter et al., 1999). In *lin-28(n719)* mutants however, an embryo was trapped in the spermatheca and unable to exit into the uterus at least for 40 minutes.

Next, we addressed whether the process of ovulation is also defective in *lin-28(n719)* mutants. Endomitotically replicating DNA (Emo) oocytes is a characteristic of many ovulation mutants (Iwasaki et al., 1996), where oocytes undergo several DNA replications without ovulation and fertilization. Gonadal DAPI staining revealed that some *lin-28(n719)* hermaphrodites contain endomitotic oocytes (Fig 2.2D) in the oviducts. We speculate that the defective ovulation in *lin-*

28(n719) mutants may result from impairment of the spermathecal exit process, wherein the presence of fertilized embryos trapped within the limited spermathecal space would prevent entry of mature oocytes. We conclude that the poor fertility of *lin-28(n719)* mutants is the consequence of embryos becoming trapped in the spermathecae, stalling subsequent ovulation.

Figure 2.2.

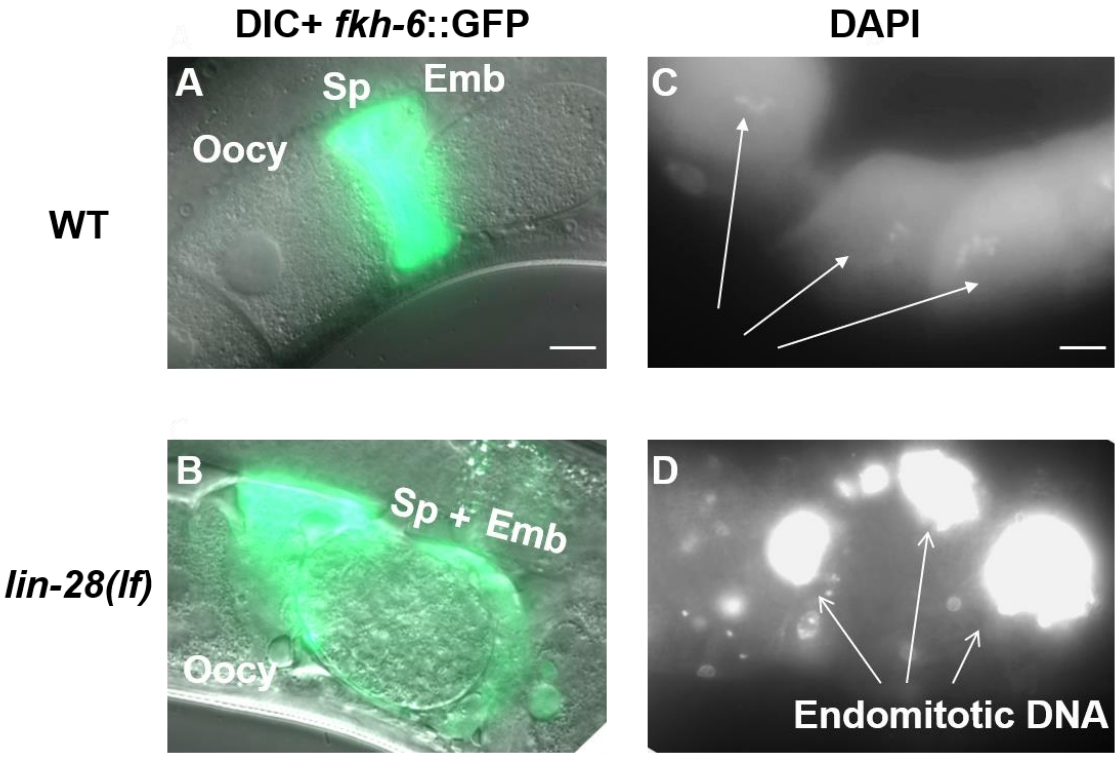
DIC+ fkh-6::GFP
DAPI
WT
lin-28(lf)
A
Sp
Emb
Oocy
C
B
Sp + Emb
Oocy
D
Endomitotic DNA

Figure 2.2. *lin-28(lf)* hermaphrodites have defects in exit of embryos from the spermatheca, and defects in ovulation.

(A, B) Spermatheca labeled by *fkh-6:GFP* of representative wild-type and *lin-28(n719)* adult hermaphrodites. (A) In the wild type, oocytes (Oocy) pass into the spermatheca (Sp), where they are fertilized, and rapidly exit as a one-cell embryo (Emb), and so most spermathecae are not observed to contain an embryo. (B) In a *lin-28(n719)* hermaphrodite, an embryo (around ~150 cells) was trapped in the spermatheca. (C, D) DAPI staining of oocytes in wild-type (C) and *lin-28(n719)* hermaphrodites. (C) In the wild type, individual oocytes (Oocy) contained a haploid complement of condensed chromosomes (arrows). (D) In the *lin-28(n719*) mutant, endomitotic DNA was evidenced by an excessively bright DAPI signal, a characteristic of ovulation defective mutants. (Scale bar = 10 μm in this paper, except where noted).

Sp-Ut valve core morphogenesis, uterine lumen formation, and utse migration are abnormal in *lin-28(lf)* mutants

Spermathecae in *C. elegans* hermaphrodites consist of two rows of 12 cells forming a long tube structure at the young adult stage (Gissendanner et al., 2008; Kimble and Hirsh, 1979). Long spermathecal tube structures, labeled by *fkh-6:GFP*, are also observed in the *lin-28(n719)* mutants at the 4th stage (Fig 2.3B), which corresponds to L4 and adult stage in wild type (Fig 2.6C). Wild-type spermathecae become constricted horizontally as somatic gonadal tissues continue morphogenesis before the first ovulation. *lin-28(n719)* spermathecae exhibited a similar constricted and extended morphology as in the wild type (Fig 2.3A,B). Overall, we did not detect appreciable differences in spermathecal morphology between wild-type animals and *lin-28(n719)* mutants.

The Sp-Ut valve connects the spermatheca to the uterus in wild type hermaphrodites, and serves as a portal through which fertilized embryos exit the spermatheca into the uterus (McCarter et al., 1999). The mature Sp-Ut valve consists of the toroidal syncytium and the core cell syncytium. We examined the structure of the Sp-Ut valve in *lin-28(n719)* mutants according to the expression of *cog-1:GFP*, which is expressed in the Sp-Ut valve core cell syncytium from the late L3 or early L4 stage (Palmer et al., 2002). In wild type animals, the core cell syncytium stretches during the L4 stage, and in young adults, the Sp-Ut valve core forms a dumbbell-like structure with one end in the spermatheca and the other end in the uterus (Fig 2.3C). Although we observed apparently normal expression of

cog-1:GFP in the Sp-Ut valve core cell region of *lin-28(n719)* mutants in late 3rd larval stage, the stretching of a core cell syncytium did not occur in the mutants and the Sp-Ut valve core cell remained as a single lobe structure in old 4th stage and later (Fig 2.3D).

Figure 2.3.

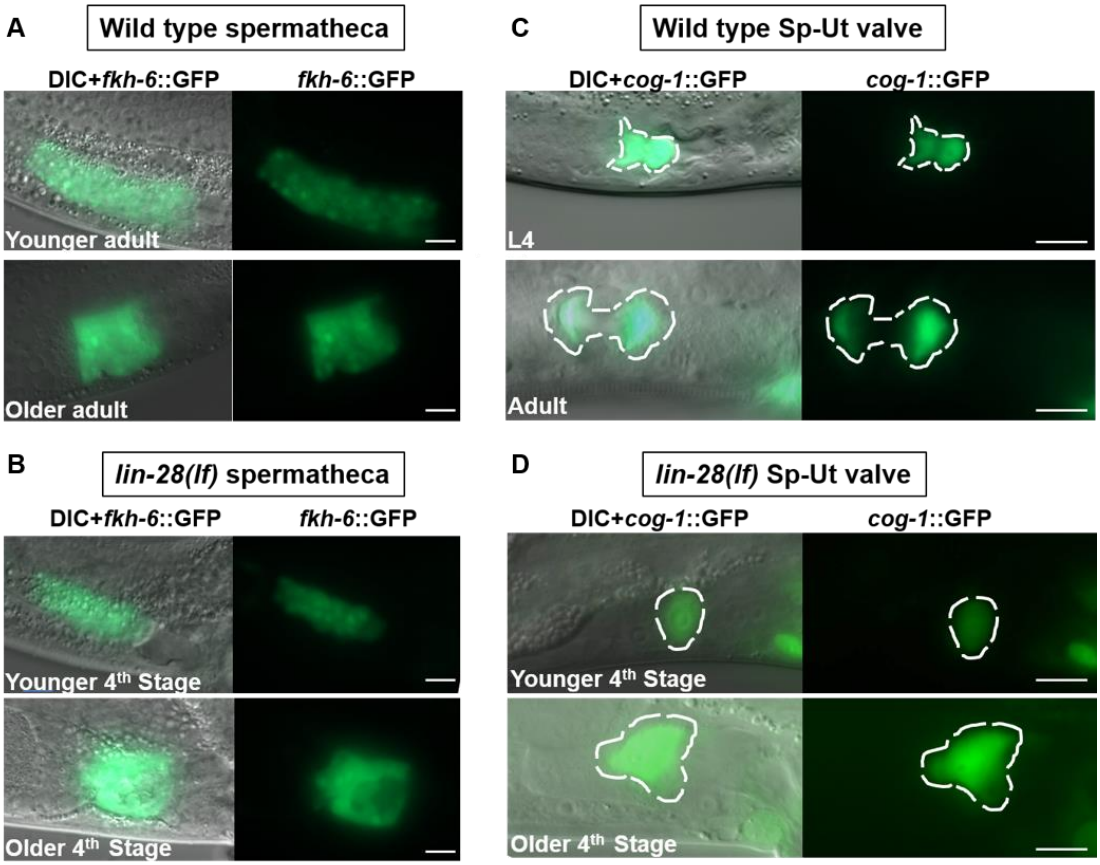
A
Wild type spermatheca
DIC+fkh-6::GFP
fkh-6::GFP
Younger adult
Older adult
C
Wild type Sp-Ut valve
DIC+cog-1::GFP
cog-1::GFP
L4
Adult
B
lin-28(lf) spermatheca
DIC+fkh-6::GFP
fkh-6::GFP
Younger 4th Stage
Older 4th Stage
D
lin-28(lf) Sp-Ut valve
DIC+cog-1::GFP
cog-1::GFP
Younger 4th Stage
Older 4th Stage

Figure 2.3. *lin-28(lf)* mutants show essentially normal spermathecal primordium structure, but display defects in spermathecal-uterine (Sp-Ut) valve core cell morphology.

Spermathecal primordium visualized by *fkh-6*:GFP expression (A, B) and Sp-Ut valve core cell structure visualized by *cog-1*:GFP expression (C, D) in wild-type and *lin-28(n719)* hermaphrodites at successive times in the advancement towards the first ovulation. In each panel, the upper images are of hermaphrodites at the L4 or early young adult stage, and the lower images are of hermaphrodites somewhat later in development, just before the time of first ovulation. (*lin-28(n719)* hermaphrodites skipped one larval stage; therefore, the “4th stage” corresponds to L4 and adult stage in wild-type [See Fig 2.6].) (A, B) In both wild type and *lin-28(n719)* mutants, similar tube-shaped spermathecal primordia were detected, which contracted horizontally to form similar sac-like structures in older adults (A, B lower panels). (C, D) Sp-Ut valve core cell structure (Sp-Ut, dashed oval) labeled by *cog-1*:GFP at successive stages in L4-adult developmental progression of a wild type and *lin-28(n719)* hermaphrodite. (C) In wild type, the Sp-Ut valve core stretches to form a fully developed “dumbbell” structure, with one side residing in the spermatheca and the other side in the uterus. The distance between each side shown here was ~10 μm. (D) In *lin-28(n719)* mutants, the Sp-Ut valve core does not stretch and remained as “single lobe” structure, indicating an abnormal connection between the spermatheca and uterus in the mutants

This observation indicates that the Sp-Ut valve morphology is abnormal in *lin-28(n719)* mutants, suggesting the connection between the spermatheca and the uterus is also disrupted in the mutants. We conclude that the aberrant connection between the uterus and the spermatheca induced by the atypical morphology of the Sp-Ut valve causes the spermathecal exit defect in *lin-28(lf)* mutants. To assess whether the abnormal Sp-Ut valve morphology of *lin-28(n719)* could reflect somatic gonadal cell lineage defects analogous to the precocious hypodermal cell lineages exhibited by *lin-28(n719)* (Ambros and Horvitz, 1984a), we investigated whether the Sp-Ut valve syncytium in the mutant contains a normal number of nuclei as in the wild-type. The Sp-Ut valve is derived from daughter cells of the dorsal uterus lineage, and the valve core syncytium is comprised of a fusion of two cells (Kimble and Hirsh, 1979). We used confocal microscopy to count the number of nuclei in the Sp-Ut valve core region based on labeling by *cog-1:GFP*. Two nuclei were present in Sp-Ut core cell of both wild-type and *lin-28(n719)* mutants, suggesting the morphological defect is not caused by abnormal cell division in the lineage generating the Sp-Ut valve core (Fig 2.4 A,B).

Figure 2.4.

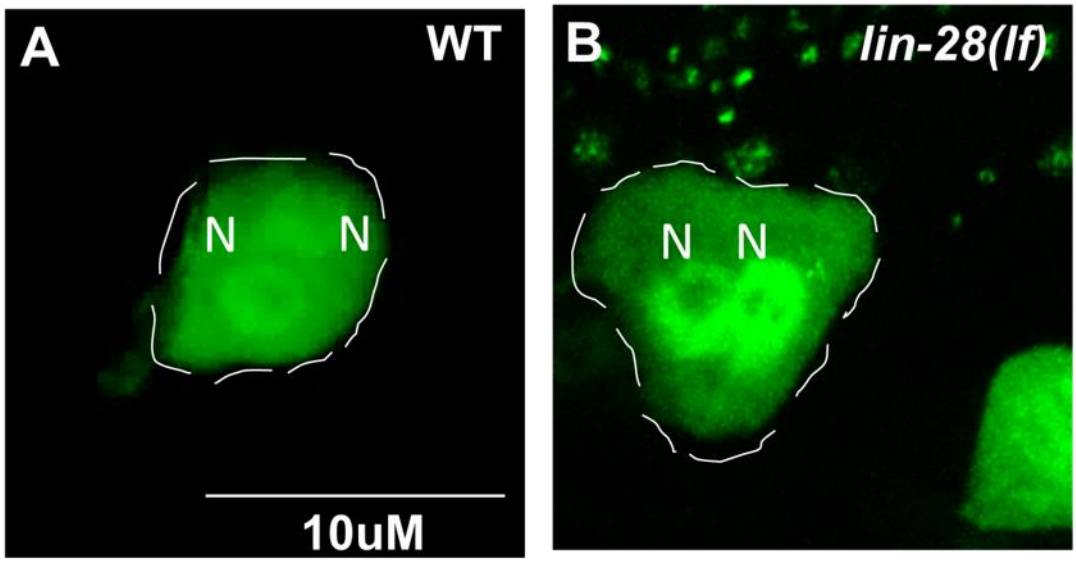

Figure 2.4. Both wild type and *lin-28(lf)* mutants have two nuclei that comprise Sp-Ut valve core syncytium.

Confocal microscopic images of Sp-Ut valve core syncytium labeled by *cog-1:GFP*. Both wild type animals (A) and *lin-28(lf)* mutants (B) exhibit two nuclei in their Sp-Ut valve core region (dashed oval), suggesting cell division in the Sp-Ut valve core occurs normally in *lin-28(lf)* mutants.

In addition to the abnormal Sp-Ut valve core morphology, other somatic gonadal defects were evident in *lin-28(n719)* mutants. In wild-type animals, the uteruine lumen forms between the dorsal and ventral uterus during the L4 stage when uterine toroidal cells fuse to generate a syncytium (Newman et al., 1996). In *lin-28(n719)* mutants at the 4th stage, we observed abnormally small, incompletely-connected, and/or less elongated uterine luminal structures, compared to the wild type (Fig 2.5B,C).

Figure 2.5.

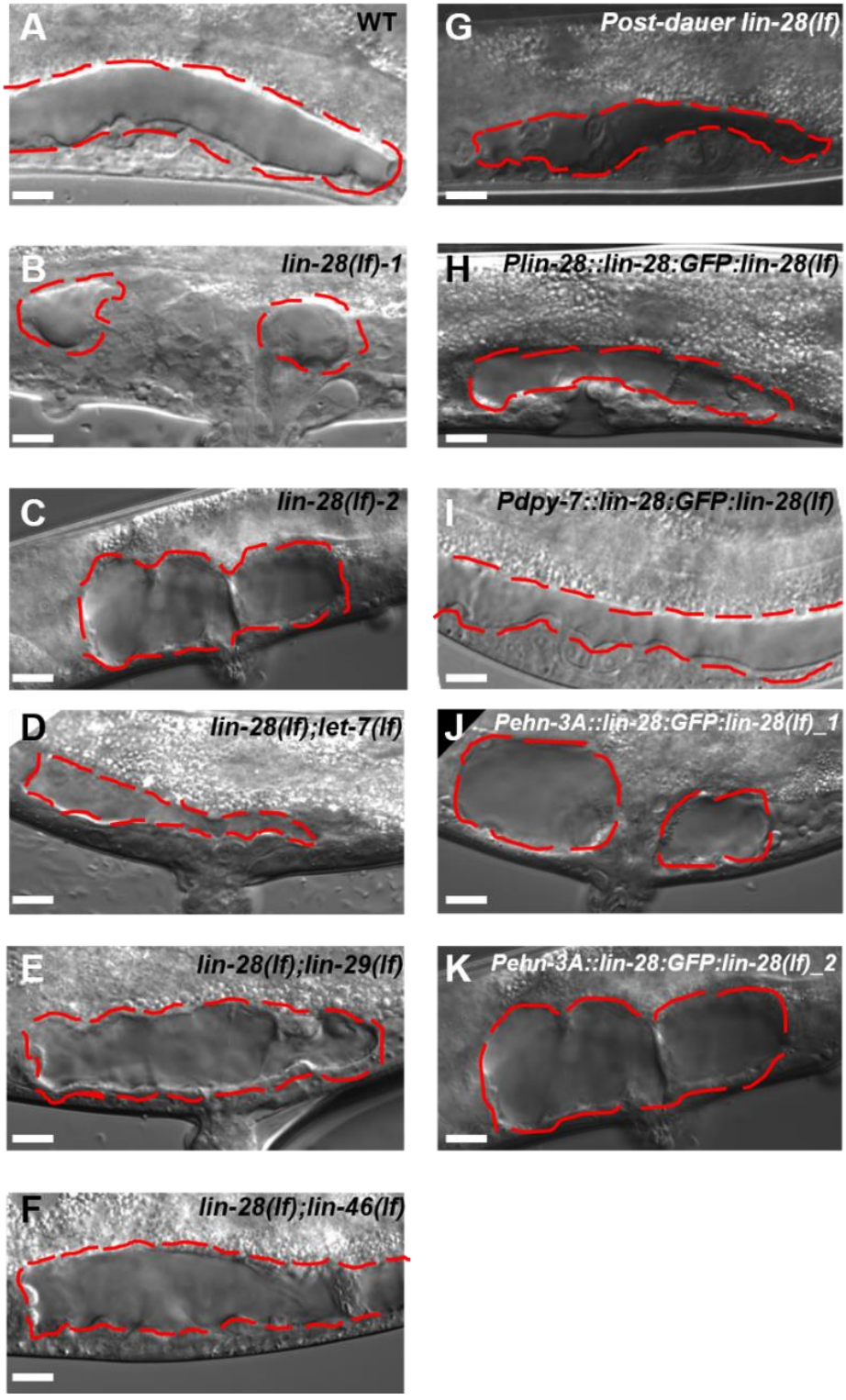
A
WT
G
Post-dauer lin-28(lf)
B
lin-28(lf)-1
H
Plin-28::lin-28:GFP:lin-28(lf)
C
lin-28(lf)-2
I
Pdpy-7::lin-28:GFP:lin-28(lf)
D
lin-28(lf);let-7(lf)
J
Pehn-3A::lin-28:GFP:lin-28(lf)_1
E
lin-28(lf);lin-29(lf)
K
Pehn-3A::lin-28:GFP:lin-28(lf)_2
F
lin-28(lf);lin-46(lf)

Figure 2.5 Defective formation of the uterine lumen in *lin-28(lf)* mutants is restored by the loss of function of *lin-28* downstream genes, or post-dauer development, or hypodermal *lin-28* expression.

(A-C) Uterine lumen formation in wild type and *lin-28(n719)* mutants. (A) Wild-type animals form a long uterine lumen between the dorsal uterus and ventral uterus in the mid L4 stage (red dashed oval), whereas, (B) the majority of *lin-28(n719)* mutants at an analogous point in 4th stage development exhibit an immature, partially-formed lumen. (C) Some 4th stage *lin-28(n719)* mutants show a connected lumen, which is shorter and rounder than that in wild-type animals. (D-F) Uterine lumen formation in *lin-28(n719);let-7(mn112), lin-28(n719);lin-29(n836)*,and *lin-28(n719);lin-46(ma164)* double mutants. (D) Lumen formation is restored in ~50% of *lin-28(n719);let-7(mn112)* mutants. (E) The majority of *lin-28(n719);lin-29(n836)* animals, and (F) the majority of *lin-28(n719);lin-46(ma164)* mutants show uterine lumen formation similar to the wild type. (G) *lin-28(n719)* mutants form an elongated uterine lumen similar to wild type after post-dauer development. (H-K) Rescue of *lin-28(lf)* uterine lumen phenotype by transgenes expressing LIN-28 driven by specific promotors. *Plin-28::lin-28:GFP;lin-28(n719)* (H) and *Pdpy-7::lin-28:GFP;lin-28(n719)* (I) show normal uterine lumen formation as wild-type animals. *Pehn-3A::lin-28:GFP;lin-28(n719)* show only partial uterine lumen (J) or shorter and rounder uterine lumen (K) similar to the defects exhibited by *lin-28(n719)* alone (B and C, respectively).

The uterine seam (utse) is a component of the hermaphrodite somatic gonad that mediates structural attachment between the hypodermis and uterine (Newman and Sternberg, 1996). The utse syncytium forms in the early L4 stage and extends laterally during progression to mid L4. The utse connects the uterus to the seam cells laterally and also to uv1 and the vulva. *egl-13:GFP* is expressed in the nuclei of π cell lineage, whose products includes the utse, from late L3 to L4 stages (Ghosh and Sternberg, 2014). Utse labeled by *egl-13:GFP* migrated laterally in wild-type hermaphrodites (Fig 2.6A,B). However, the utse nuclei did not migrate during the 4th stage in *lin-28(n719)* mutants, although *egl-13:GFP(+)* cells were detected in the utse region (Fig 2.6C,D).

Figure 2.6.

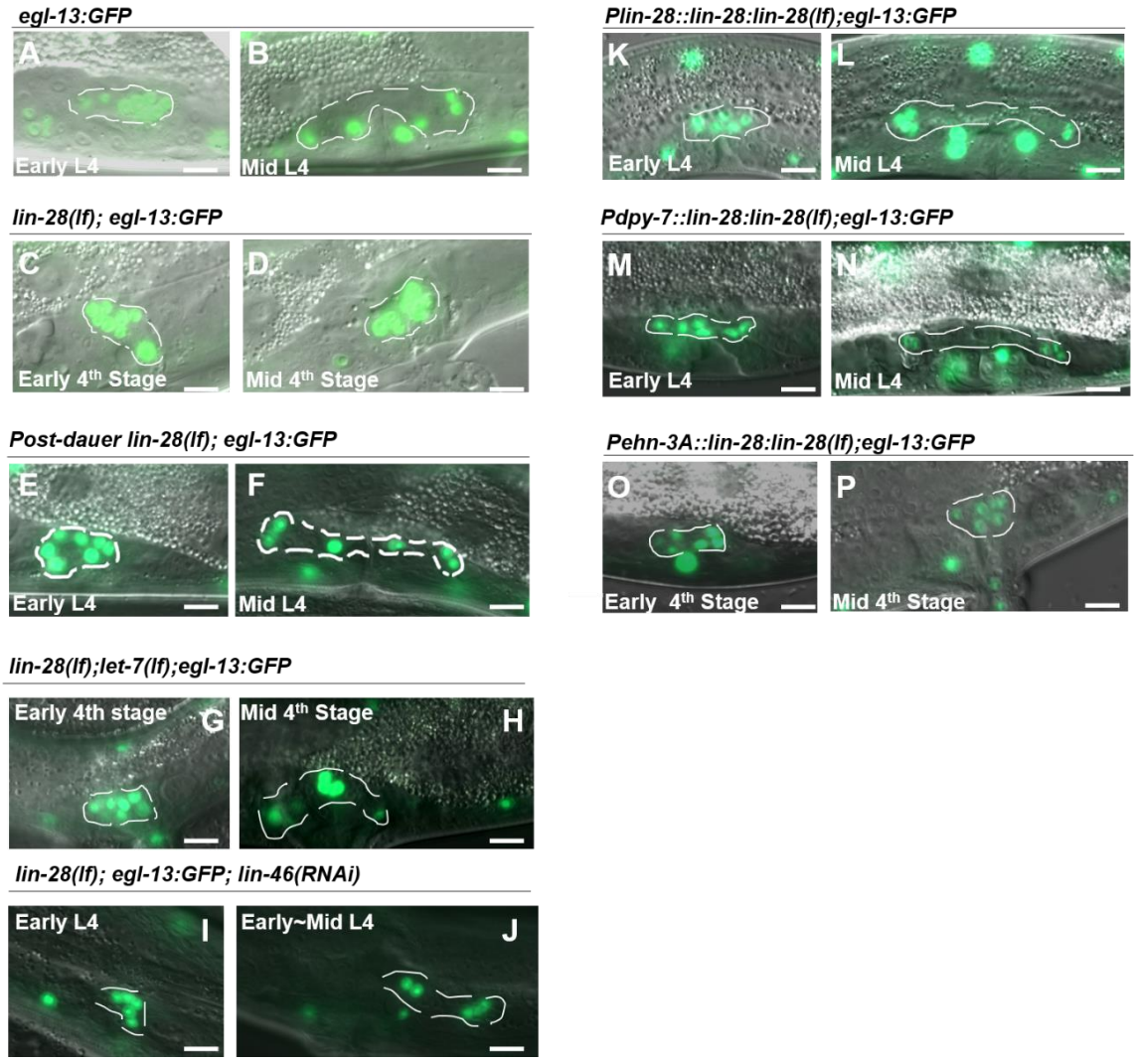
egl-13:GFP
A
Early L4
B
Mid L4
lin-28(lf); egl-13:GFP
C
Early 4th Stage
D
Mid 4th Stage
Post-dauer lin-28(lf); egl-13:GFP
E
Early L4
F
Mid L4
lin-28(lf);let-7(lf);egl-13:GFP
Early 4th stage
G
Mid 4th Stage
H
lin-28(lf); egl-13:GFP; lin-46(RNAi)
Early L4
I
Early~Mid L4
J
Plin-28::lin-28:lin-28(lf);egl-13:GFP
K
Early L4
L
Mid L4
Pdpy-7::lin-28:lin-28(lf);egl-13:GFP
M
Early L4
N
Mid L4
Pehn-3A::lin-28:lin-28(lf);egl-13:GFP
O
Early 4th Stage
P
Mid 4th Stage

Figure 2.6. Defective migration of uterine seam cell (utse) nuclei in *lin-28(lf)* mutants is rescued by loss of function of *lin-28* downstream genes, or by post-dauer development, or by hypodermal *lin-28* expression.

(A-D) utse nuclei, labeled by *egl-13:GFP*, in wild type and *lin-28(n719)* mutants. *egl-13:GFP* expression in the utse region (dashed oval) is shown in early L4 (A) and mid-L4 (B) of the wild-type, and at analogous steps (C, D) of 4th stage *lin-28(n719)* animals. utse nuclei expressing *egl-13:GFP* migrate laterally during the early to mid L4 stage in wild type (A, B), but no such migration occurs in *lin-28(n719)* mutants (C, D). (E,F) utse migration defects of *lin-28(n719)* mutants are suppressed when the mutants develop via post-dauer stages. (G-J) Loss of function of *let-7* or *lin-46* can partially suppress the utse migration defects in *lin-28(lf)* mutants. (G,H) *lin-28(n719);let-7(mn112)* mutants show a more normal migration of utse nuclei compared to *lin-28(n719)* mutants (C, D). (I,J) utse nuclei of *lin-28(n719)* mutants migrated laterally when *lin-46* function was knocked down by RNAi. (K-P) Rescue of *lin-28(lf)* utse migration phenotype by transgenes expressing LIN-28 driven by specific promotors. *lin-28* expression with *lin-28* endogenous promoter (*Plin-28::lin-28:GFP;lin-28(n719);egl-13:GFP*) restores utse migration as wild type (K, L). Hypodermal expression of *lin-28* (*Pdpy-7::lin-28:GFP;lin-28(n719);egl-13:GFP*) also rescues utse migration defects in *lin-28(n719)* mutants (M, N), whereas *lin-28* expression driven by early somatic gonadal promoter (*Pehn3-A::lin-28:GFP;lin-28(n719);egl-13:GFP*) does not rescue the phenotype (O, P). (Note: In these experiments (K-P), the promoter-

driven *lin-28* transgene is also tagged with GFP, but *lin-28:GFP* expression is not detectable at these stages, so all the GFP signal here corresponds to *egl-13:GFP.*)

lin-28(n719);lin-2(e1309) double mutants, which lack vulva formation, have the same somatic gonadal defects as *lin-28(n719)* mutants, indicating these defects are not indirect consequences of the abnormal vulva morphology in *lin-28(n719)* mutants (Fig 2.7).

Defects in uterine lumen formation and utse migration in *lin-28(n719)* mutants, together with Sp-Ut valve morphological defects, suggest that *lin-28* activity is required for multiple aspects of proper hermaphrodite somatic gonadal development.

Figure 2.7

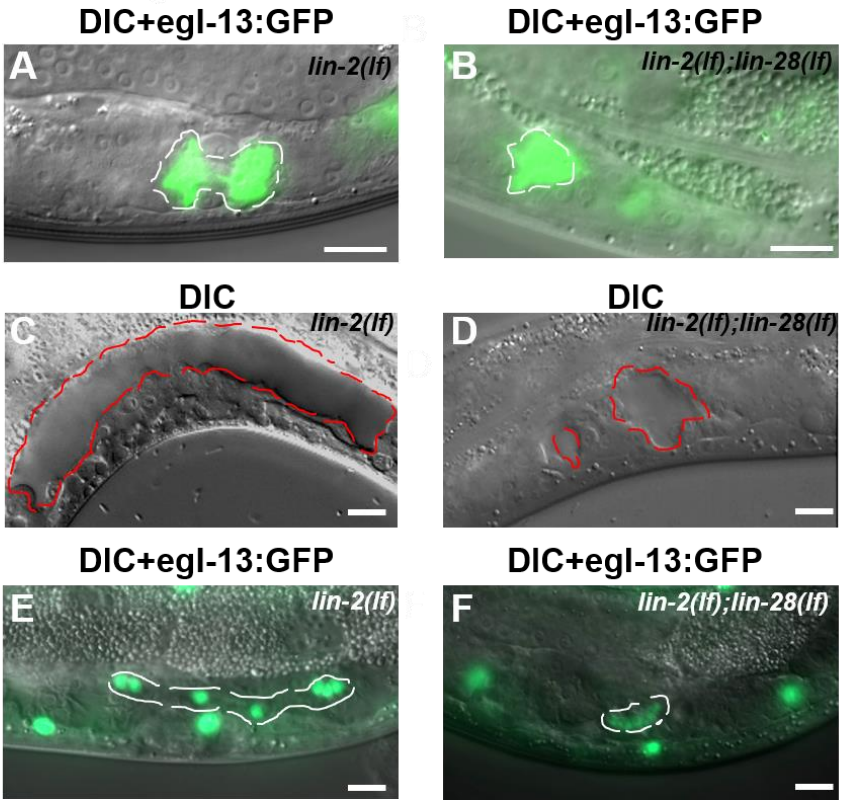
DIC+egl-13:GFP
A
lin-2(lf)
DIC+egl-13:GFP
B
lin-2(lf);lin-28(lf)
DIC
C
lin-2(lf)
DIC
D
lin-2(lf);lin-28(lf)
DIC+egl-13:GFP
E
lin-2(lf)
DIC+egl-13:GFP
F
lin-2(lf);lin-28(lf)

Figure 2.7. Defective Sp-Ut valve morphogenesis, uterine lumen formation, and utse migration are not results of the abnormal vulva morphogenesis of *lin-28(lf)* animals.

(A, B) Sp-Ut valve core structure (dashed oval) visualized by *cog-1:GFP* in *lin-2(e1309)* and *lin-2(e1309);lin-28(n719)* animals. (A) The "dumbbell" structure of Sp-Ut valve core cell is shown in *lin-2(e1309)* mutants like wild type animals (Fig 2.3C). (B) *lin-2(e1309); lin-28(n719)* mutants exhibit the "single-lobe" structure of Sp-Ut valve core, similar to *lin-28(n719)* mutants (Fig 2.3D). (C, D) Uterine lumen formation (dashed oval) visualized by DIC in *lin-2(e1309)* and *lin-2(e1309);lin-28(n719)* animals. (C) fully extended and connected uterine lumen (red-dashed oval) is formed in *lin-2(e1309)* mutants like wild type animals (Fig S3A). (D) By contrast, *lin-2(e1309);lin-28(n719)* mutants form only partial uterine lumen, similar to *lin-28(n719)* (Fig 2.5B). (E, F) utse nuclei (surrounded by a dashed line) are labeled by *egl-13:GFP* in *lin-2(e1309)* and *lin-2(e1309);lin-28(n719)* animals. (E) utse migration appears normal in *lin-2(e1309)* (Fig 2.6B), whereas (F) utse nuclei remain tightly clustered in *lin-2(e1309);lin-28(n719)* animals, similar to *lin-28(n719)* (Fig 2.6D).

Eggshell integrity is compromised in *lin-28(lf)* mutant embryos

To understand the cause of embryonic lethality in *lin-28(n719)* mutants, we first dissected and imaged the embryos produced by the mutants. The *lin-28(n719)* embryos displayed abnormal, irregular shapes (Fig 2.8A), reminiscent of the misshapen phenotypes exhibited egg-shell mutants (Johnston et al., 2006; Maruyama et al., 2007; Zhang et al., 2005). The *C. elegans* eggshell is formed rapidly after fertilization in the spermatheca and consists of chitin, lipid, and structural proteins, and functions as a protective barrier between the embryo and outside environment. Eggshell abnormalities often result in embryo lethality (Johnston et al., 2010).

Chitin-binding domain-protein 1 (CBD-1) is a component of the eggshell cortex, and CBD-1::mCherry expression marks the periphery of wild-type embryos. CBD-1::mCherry expression was evident surrounding embryos from *lin-28(n719)* hermaphrodites, indicating that an eggshell does form (Fig 2.8B). However, *lin-28(n719)* embryos were abnormally permeable to the lipophilic dye FM 4-64. The wild-type eggshell prevents FM 4-64 from infiltrating the embryo (Johnston et al., 2006). In our study, about 50% of *lin-28(n719)* embryos were permeable to FM4-64, while around 10% of *lin-2(e1309)* embryos were permeable (Fig 2.8C).

This finding indicates that eggshell integrity is compromised in embryos produced by *lin-28(n719)* mutants. In support of this conclusion, *lin-28(n719)* embryos exhibited osmotic stress sensitivity. Wild-type embryos maintained their

oval shape upon exposure to 0, 150, and 300 mM KCl, whereas *lin-28(n719)* embryos swelled upon treatment with 0 or 150 mM KCl (Fig 2.8D).

Interestingly, embryos of *fln-1(tm545)* mutants, which have defective spermathecal exit (Kovacevic and Cram, 2010), also exhibited permeability to FM4-64, suggesting an association of eggshell permeability with the spermathecal exit phenotype (Fig 2.8C). Delay in the spermathecal exit might decrease the physical integrity of eggshell in *lin-28(lf)* mutants (see Discussion).

In summary, *lin-28* is required for normal somatic gonadal development, including uterine lumen formation, utse morphogenesis, and proper Sp-Ut valve formation. The abnormal Sp-Ut valve structure in *lin-28(n719)* mutants causes defects in spermathecal exit and ovulation, resulting in reduced embryo production. In addition, the embryos stalled in the spermatheca seem to suffer eggshell damage, resulting in embryonic lethality (Fig 2.8E).

Figure 2.8

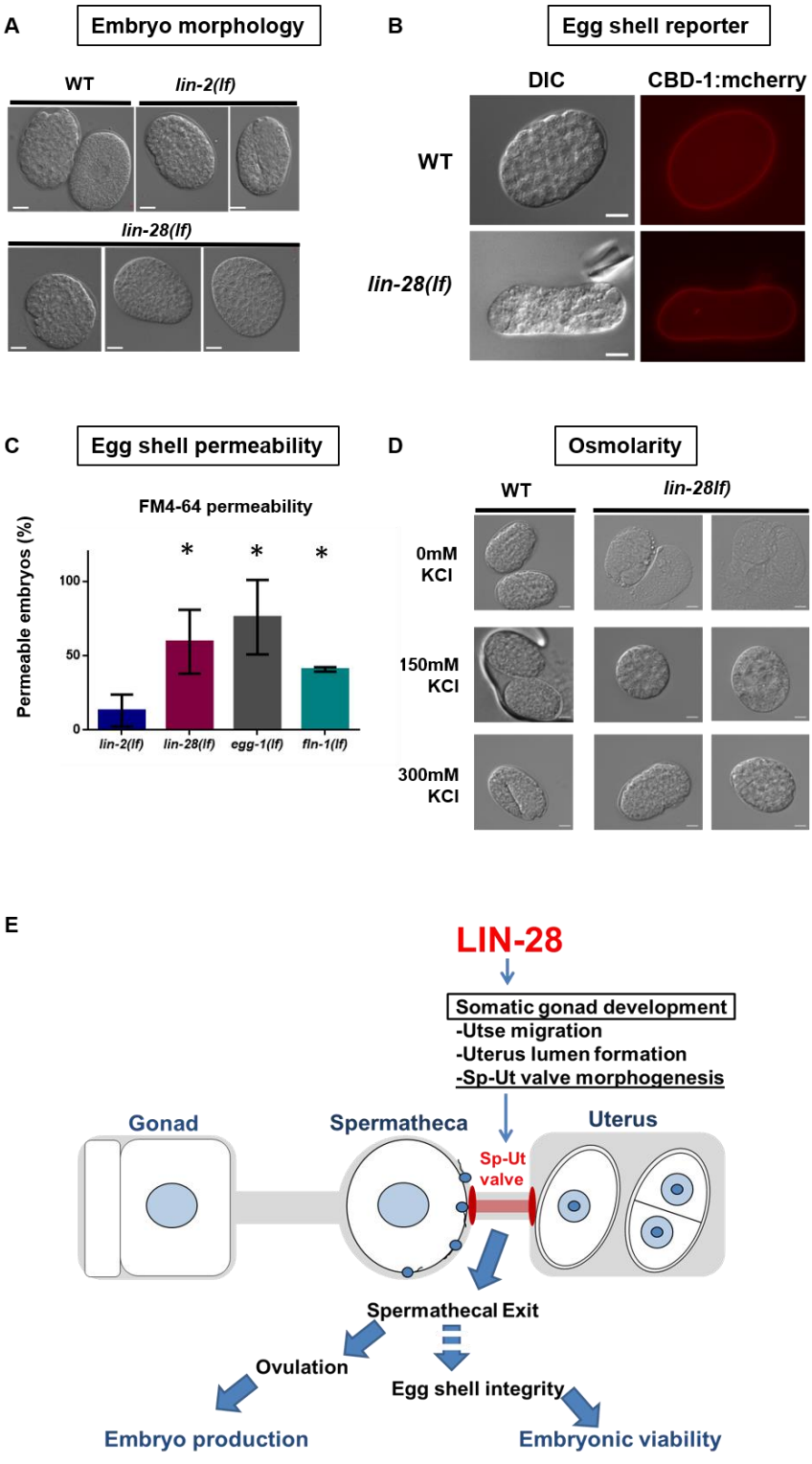
A
Embryo morphology
WT
lin-2(lf)
lin-28(lf)
B
Egg shell reporter
DIC
CBD-1:mcherry
WT
lin-28(lf)
C
Egg shell permeability
FM4-64 permeability
Permeable embryos (%)
100
50
0
*
*
*
lin-2(lf)
lin-28(lf)
egg-1(lf)
fln-1(lf)
D
Osmolarity
WT
lin-28lf)
0mM KCl
150mM KCl
300mM KCl
E
LIN-28
Somatic gonad development
-Utse migration
-Uterus lumen formation
-Sp-Ut valve morphogenesis
Gonad
Spermatheca
Uterus
Sp-Ut valve
Spermathecal Exit
Ovulation
Egg shell integrity
Embryo production
Embryonic viability

Figure 2.8. *lin-28(lf)* embryos are misshapen and are defective in egg shell integrity.

(A) DIC images of wild-type, *lin-2(e1309)* and *lin-28(n719)* embryos from dissected adult animals. Wild type and *lin-2(e1309)* mutants produce ovoid embryos, but *lin-28(n719)* embryos exhibit irregular shapes. (B) *cbd-1::mCherry* expression indicates that egg shells were present in *lin-28(n719)* embryos despite their misshapen morphology (lower panels). (C) Egg shell permeability of embryos produced by *lin-2(e1309)*, *lin-28(n719), egg-1(tm1071),* and *fln-1(tm545)* hermaphrodites. Egg shell mutant *egg-1(tm1071)* served as a control. Embryos from *lin-28(n719), fln-1(tm545)*, and *egg-1(tm1071)* were more permeable to the lipophilic dye FM 4-64 than *lin-2(e1309)* embryos. Like *lin-28(n719), fln-1(tm545)* hermaphrodites exhibit defects in spermathecal exit. Permeability was calculated as the percentage of permeable embryos/total embryos from dissected adult animals (Number of animlals≥15 per each assay; number of independent replicate assays = 3 for each strain, Data are shown as mean ± SD. unpaired t-test compared to *lin-2(e1309)*, *p<0.05). (D) Morphology of embryos under different osmotic conditions. *lin-28(n719)* embryos were more sensitive than wild type to low salt conditions, indicating a lack of protection from osmotic stress. (E) Model for physiological causes of fertility defects in *lin-28(lf)* mutants. *lin-28(lf)* animals have abnormal Sp-Ut valve structure, which leads to defects in spermathecal exit and ovulation, and hence a reduced embryo

production. In addition, retention of embryos in the spermatheca compromises egg shell integrity, which causes embryonic lethality.

Embryonic lethality of *lin-28(n719)* mutant is rescued by maternal expression of *lin-28*

We speculated that the lethality of embryos produced by *lin-28(n719)* hermaphrodites results from defects in maternal somatic gonadal morphology, rather than from an absence *lin-28* function in the embryos. If so, then maternal expression of *lin-28* should rescue the embryonic lethality of *lin-28(n719)* homozygous embryos. To test this, we crossed *lin-28(n719)* hermaphodites with wild-type males to obtain heterozygous mutants (*lin-28(n719)/+),* and then assessed the viability of *lin-28(n719)* homozygous self-progeny from these *lin-28(n719)/+* hermaphrodites. Viable *lin-28(n719)* homozygotes were identified by their characteristic egg-laying defective phenotype as adults. Amongst the self-progeny of heterozygous (*lin-28(n719)/+)* hermaphrodites, we observed a ratio of wild type progeny (+/+ or *lin-28(n719)/+*) to egg-laying defective progeny (*lin-28(n719)/lin-28(n719)*) of 2.89(±0.2):1 which is very close to the expected 3:1 ratio for complete maternal rescue of embryonic lethality (Table 2.1). This finding suggests that *lin-28(n719)* embryonic lethality reflects a requirement for *lin-28* activity in the mother to enable proper development of the somatic gonad, which is required for the production of viable embryos.

Table 2.1. Viability of embryos produced by *lin-28(n719)* heterozygous hermaphrodites

Maternal Genotype (P0)	Progeny Genotype (F1)	Maternal or Zygotic LIN-28 products	Egg laying phenotype (F1)	Zygotic effect		Maternal effect		Experimentally determind Ratio (egg laying vs egg laying defective)
				Expected Genotype ratio	Expected Phenotype ratio	Expected Genotype ratio	Expected Phenotype ratio	
$\frac{lin-28(+)}{lin-28(+)}$	$\frac{lin-28(+)}{lin-28(+)}$	m+/z+	Egg laying	1	10.3	1	3	2.89(±0.2)**
	$\frac{lin-28(+)}{lin-28(-)}$	m+/z+	Egg laying	2		2		
	$\frac{lin-28(-)}{lin-28(-)}$	m+/z-	Egg laying defective	0.29*	1	1	1	1

Genes downstream of *lin-28* in developmental timing regulation also function downstream of *lin-28* in somatic gonadal morphogenesis and fertility

Functional interactions of *lin-28* with other heterochronic genes for the control of *C. elegans* hypodermal cell lineage developmental timing have been described previously (Ambros, 2011; Resnick et al., 2010) (see Fig 2.9E). *lin-28* functions upstream of *lin-46* and *hbl-1* to control the timing of L2 to L3 fate transitions in hypodermal cell lineages, and *lin-28* also acts via a pathway consisting of *let-7*, *hbl-1*, *lin-41*, and *lin-29* to regulate the transition from L4 fates to adult fates in the hypodermis.

We conducted RNAi knockdown experiments to determine whether these same heterochronic genes that act downstream of *lin-28* for hypodermal cell fate timing are also involved in Sp-Ut valve morphogenesis downstream of *lin-28*. After treatment of *cog-1:GFP* hermaphrodites with *lin-28* RNAi, 95% of the animals showed an abnormal Sp-Ut valve core morphology similar to that in *lin-28(n719)* mutants. However, around 70% of *lin-28(RNAi)*-treated *let-7(mn112);cog-1:GFP* hermaphrodites showed a normal Sp-Ut valve core. Also, genetic absence of *lin-46* or *lin-29* abolished the Sp-Ut valve defects caused by *lin-28(RNAi)*. Thus, *lin-46(lf)*, *lin-29(lf)* or *let-7(lf)* can fully or partially rescue the Sp-Ut valve defects in *lin-28(RNAi)* animals (Fig 2.9A), supporting the idea that these heterochronic genes act downstream of *lin-28* for somatic gonadal development. *hbl-1*(RNAi) phenocopied the fertility phenotypes of *lin-28(n719)* mutants, including abnormal

Sp-Ut valve core morphology (Fig 2.10A,B). Loss of *lin-46* or *let-7* function rarely affected the Sp-Ut valve core morphological defect in *hbl-1*(RNAi) animals, indicating *hbl-1* is epistatic to these genes. Finally, approximately 70% of *lin-29(lf)*;*cog-1:GFP* animals showed the wild-type Sp-Ut valve core morphology when *hbl-1* function was compromised (Fig 2.9A).

Figure 2.9

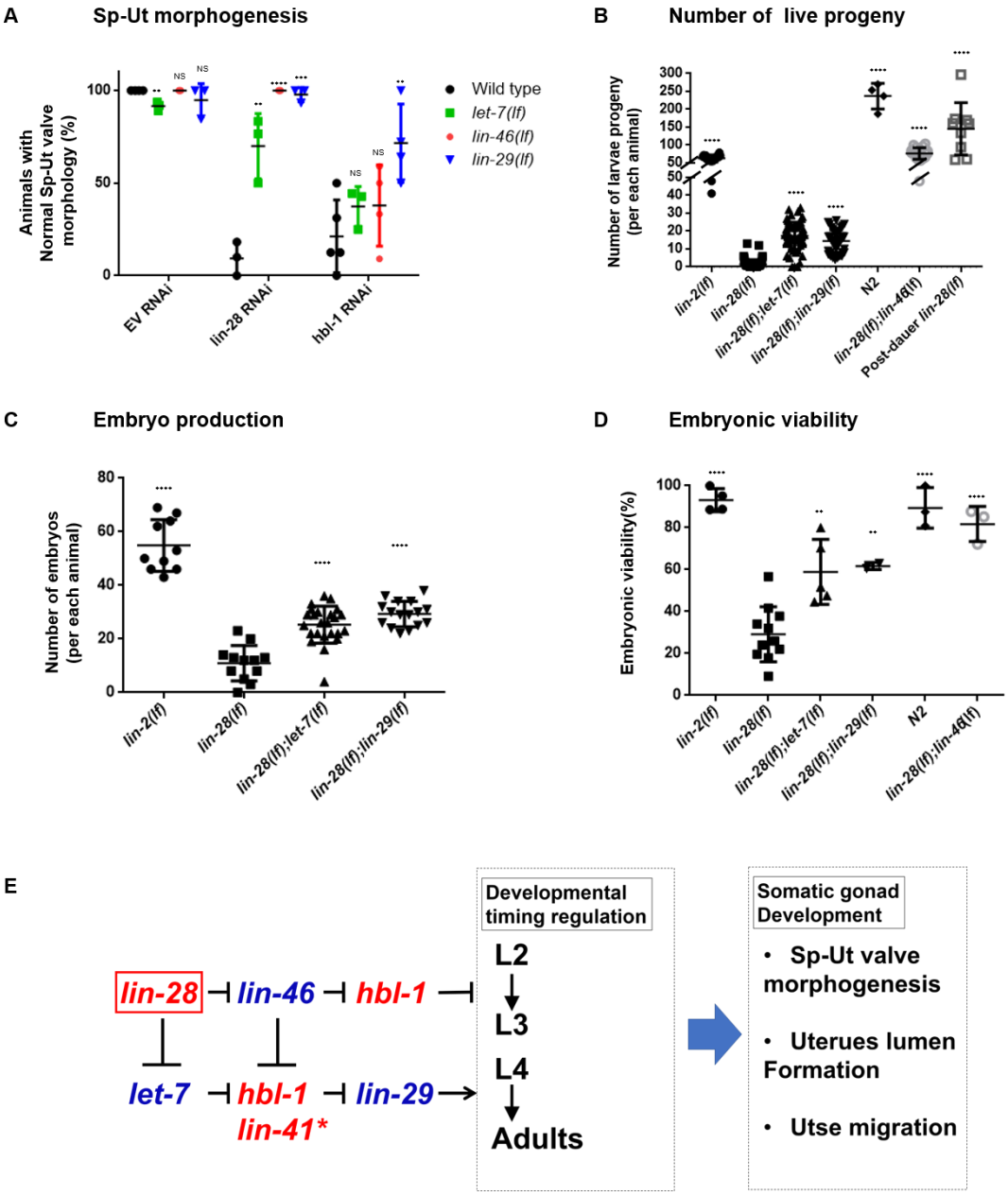
A
Sp-Ut morphogenesis
Animals with Normal Sp-Ut valve morphology (%)
Wild type
let-7(lf)
lin-46(lf)
lin-29(lf)
EV RNAi
lin-28 RNAi
hbl-1 RNAi
B
Number of live progeny
Number of larvae progeny (per each animal)
lin-2(lf)
lin-28(lf)
lin-28(lf);let-7(lf)
lin-28(lf);lin-29(lf)
N2
lin-28(lf);lin-46(lf)
Post-dauer lin-28(lf)
C
Embryo production
Number of embryos (per each animal)
lin-2(lf)
lin-28(lf)
lin-28(lf);let-7(lf)
lin-28(lf);lin-29(lf)
D
Embryonic viability
Embryonic viability(%)
lin-2(lf)
lin-28(lf)
lin-28(lf);let-7(lf)
lin-28(lf);lin-29(lf)
N2
lin-28(lf);lin-46(lf)
E
lin-28
lin-46
hbl-1
let-7
hbl-1
lin-29
lin-41*
Developmental timing regulation
L2
L3
L4
Adults
Somatic gonad Development
• Sp-Ut valve morphogenesis
• Uterues lumen Formation
• Utse migration

Figure 2.9. Genetic epistasis analysis of *lin-28* and other heterochronic genes for effects on Sp-Ut valve core morphogenesis and fertility.

(A) The percentage of animals with normal Sp-Ut valve core morphology, visualized by *cog-1*:GFP expression in wild type*, let-7(mn112), lin-46(ma164)* and *lin-29(n836)* mutants, treated with control RNAi (EV, empty vector strain L4440), *lin-28*(RNAi) or *hbl-1*(RNAi). Wild type*, lin-46(ma164)*, and *lin-29(n836)* mutants treated with L4440 empty vector RNAi rarely showed Sp-Ut valve defects. *let-7(mn112)* mutants with control RNAi showed less than 10% of Sp-Ut valve defects. *lin-28*(RNAi) treatment of wild type led to ~95% Sp-Ut valve defects, an effect that was partially or fully suppressed by *let-7(mn112), lin-46(ma164)* and *lin-29(n836). hbl-1*(RNAi) treatment of wild type also led to Sp-Ut valve defects that were rarely suppressed by *let-7(mn112)* and *lin-46(ma164)* and moderately suppressed (~70%) by *lin-29(n836)*. (Number of animlals ≥12 per each assay; number of independent replicate assays = 5 for WT with *hbl-1* RNAi, 4 for *lin-46(ma164)* or *lin-29(n836)* with *hbl-1* RNAi, 3 for all other assays, Data are shown as mean ± SD, unpaired t-test, p-values denoted as asterisks or "NS" were calculated by each mutant compared to wild type in each RNAi set. NS; not significant, **p<0.01,***p<0.001,****p<0.0001) (B-D) Fertility phenotypes of *lin-2(e1309), lin-28(n719), lin-28(n719);let-7(mn112), lin-28(n719);lin-29(n836)*, *lin-46(ma164);lin-28(n719)* mutants, post-dauer *lin-28(n719)*, and wild type. (B) Total number of viable larva progeny of *lin-2(e1309)* (n=16), *lin-28(n719)* (n=64)*, lin-28(n719);let-7(mn112)* (n=62)*, lin-28(n719);lin-29(n836)* (n=41), *lin-46(ma164);lin-28(n719)*

(n=17) mutants, post-dauer *lin-28(n719)* (n=9), and wild type (n=4). (C) Embryo production of *lin-2(e1309)* (n=10), *lin-28(n719)* (n=12)*, lin-28(n719);let-7(mn112)* (n=24)*, lin-28(n719);lin-29(n836)* (n=15) mutants.(D) Embryonic viability of *lin-2(e1309), lin-28(n719), lin-28(n719);let-7(mn112), lin-28(n719);lin-29(n836)*, *lin-46(ma164);lin-28(n719)* mutants, post-dauer *lin-28(n719)*, and wild type. (Number of animlals≥15 per each assay; number of independent replicate assays = 11 for *lin-28(n719),* 4 for *lin-2(e1309),* 5 for *lin-28(n719);let-7(mn112)*, and 3 for all other strains.) The reduction in the number of progeny of *lin-28(n719)* mutants is increased by loss of *let-7*, *lin-29* or *lin-46.* (B). Both embryo production (C) and embryo viability (D) are improved by loss of *let-7*, *lin-29* or *lin-46*. Total number of progeny and embryonic viability of *lin-28(lf)* mutants are also improved by post-dauer development (B,D). (B-D: Data are shown as mean ± SD, unpaired t-test compared to *lin-28(lf)*, NS; not significant, **p<0.01,***p<0.001,****p<0.0001.) (E) The genetic regulatory pathway model for somatic gonadal morphogenesis, derived from the results of epistasis experiments presented in Fig 5A–D, is highly similar to the model for temporal regulation of hypodermal cell fates derived from previous studies (Ambros, 2011; Resnik & Rougvie 2010, See Discussion for *lin-41* involvement in the somatic gonadal morphogenesis).

Figure 2.10

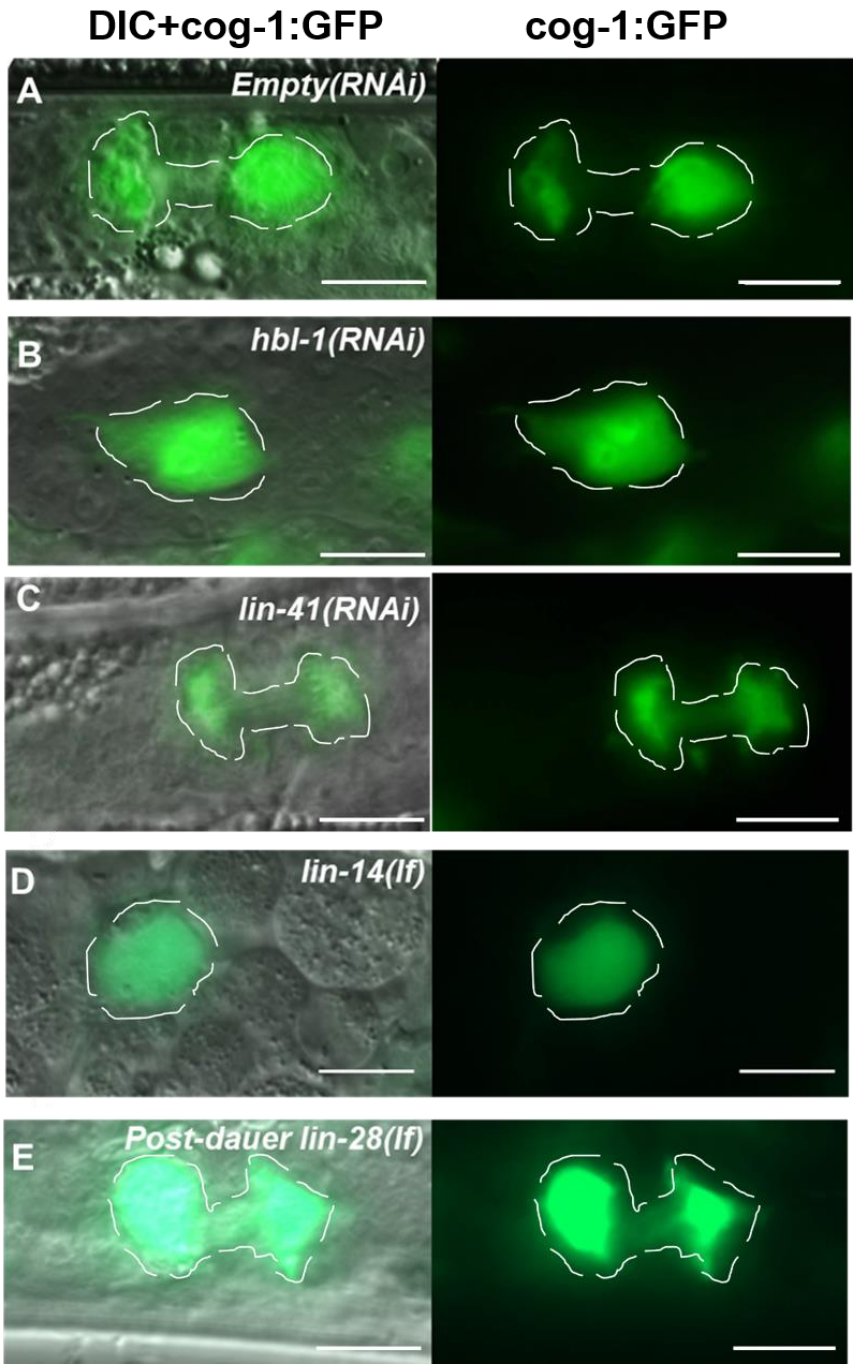
DIC+cog-1:GFP
cog-1:GFP
A
Empty(RNAi)
B
hbl-1(RNAi)
C
lin-41(RNAi)
D
lin-14(lf)
E
Post-dauer lin-28(lf)

Figure 2.10. Sp-Ut valve core cell morphology of *hbl-1(lf), lin-41(lf) and lin-14(lf)* mutants, and post-dauer suppression of *lin-28(lf)* morphological defects.

(A-E) Sp-Ut valve core morphology is visualized by *cog-1:GFP,* shown alone (right panel), and overlaid with DIC (left panel). (A) Animals treated with empty vector RNAi have normal Sp-Ut morphology. (B) *hbl-1*(RNAi) animals. (C) The Sp-Ut valve of *lin-41*(RNAi) animals appeared essentially WT in morphology, except for a somewhat reduced size. (D) *lin-14(n179)* exhibit abnormal Sp-Ut morphology. (E) Post-dauer development of *lin-28(n719)* mutants restored an Sp-Ut valve morphology similar to wild type animals.

In addition, a normal uterine lumen was observed in ~50% of *lin-28(n719);let-7(mn112)* mutants (Fig 2.5D). Most *lin-28(n719)*;*lin-29(n836)* and *lin-28(n719)*;*lin-46(ma164)* mutants showed complete uterine lumen formation (Fig 2.5E,F). Utse migration defects of *lin-28(lf)* mutants were also partially suppressed by loss of either *let-7* or *lin-46* (Fig 2.6G-J).

Consistent with the genetic epistasis observed above for somatic gonadal morphogenesis, *lin-46(lf), let-7(lf)* and *lin-29(lf)* were also epistatic to *lin-28(lf)* for fertility and embryonic viability. The total numbers of live progeny per animal produced by the *lin-28(n719);let-7(mn112)* and *lin-28(n719)*;*lin-29(n836)* double mutants were significantly higher than that produced by the *lin-28(n719)* mutants (Fig 2.9B). Also, the number of live progeny of *lin-28(n719)*;*lin-46(ma164)* was even greater than that of *lin-2(e1309)*, because the loss of *lin-46* rescued the vulva and egg-laying defects of *lin-28(n719)* mutants. *lin-28(n719);let-7(mn112)* and *lin-28(n719);lin-29(n836)* mutants produced more embryos per animal than *lin-28(n719)* mutants (Fig 2.9C), and embryonic viability was similarly suppressed in these double mutants, compared to *lin-28(n719) (*Fig 2.9D).

Overall, our findings indicate that *let-7*, *lin-46*, *hbl-1*, and *lin-29* act downstream of *lin-28* for somatic gonadal development in a network configuration essentially identical to that previously-described for the control of hypodermal cell fate timing by these same genes (Fig 2.9E).

To further investigate the relationship between hypodermal developmental timing and somatic gonadal morphogenesis, we examined whether post-dauer

development can rescue the somatic gonadal defects in *lin-28(n719)* mutants. A previous study showed that the hypodermal heterochronic developmental defects of *lin-28(n719)* mutants, (including precocious vulva, precocious adult cuticle, and altered seam cell number) are efficiently suppressed if the mutants develop through the dauer larva (an alternative, temporarily arrested, third larval stage) followed by “post-dauer” developmental stages (Euling and Ambros VR, 1995; Liu and Ambros, 1991). We observed that after post-dauer development, *lin-28(n719)* adults exhibited restored fertility and embryo viability, normal morphology of the Sp-Ut valve core cell, uterine lumen, and normal utse migration (Fig 2.9B, 2.9D, 2.10E, 2.5G, 2.6E, and 2.6F). This suppression of somatic gonadal defects in *lin-28(n719)* animals by post-dauer development supports the supposition that *lin-28* acts indirectly, via downstream genes and events, to mediate normal somatic gonadal morphogenesis.

Heterochronic development between hypodermal tissue and somatic gonadal tissues in *lin-28(lf)* mutants

Based on the above observations indicating parallels between the control of hypodermal developmental timing and somatic gonadal morphogenesis by *lin-28* mutants, we investigated whether the stage-specificity of somatic gonadal developmental events might be altered in *lin-28(n719)* hermaphrodites, in analogy to their precocious hypodermal development. As a marker to monitor the expression of stage-specific programs in the somatic gonad and hypodermis, we employed *cog-1:GFP* (Palmer et al., 2002), which is expressed in the wild type dorsal uterus and Sp-Ut valve core, beginning from late-L3/early-L4 stage (Fig 2.11A). *cog-1:GFP* is also expressed in the ventral hypodermis (vulval cell lineages) beginning in the mid L4 stage, which is after the onset of *cog-1:GFP* somatic gonadal expression (Fig 2.11B). Thus in the wild type, the somatic gonadal expression of *cog-1:GFP* appears first (late-L3/early-L4 stage) followed later (mid L4) by vulval expression.

We examined whether the normal relative order of *cog-1:GFP* expression in the somatic gonad and vulva is altered in *lin-28(n719)* mutants. In *lin-28(n719)* hermaphrodites, *cog-1:GFP* expression in the vulva was observed precociously in the mid-3rd larval stage (Fig 2.11D), consistent with the previously-described precocious vulva cell divisions of *lin-28(lf)* mutants (Euling and Ambros, 1996). However, the onset of somatic gonadal expression of *cog-1:GFP* was normal, beginning from the late 3rd larval stage in both *lin-28(n719)* and in the wild type

(Fig 2.11E). Thus, the expression of *cog-1:GFP* in the vulva precedes the expression in somatic gonads in *lin-28(n719)* mutants. These data suggest that the somatic gonadal development, at least as reflected by *cog-1::GFP* expression, is not precocious in *lin-28(n719)*. Therefore, developmental events in hypodermal tissues and somatic gonadal tissues are temporally discoordinated in *lin-28(n719)* mutants (Fig 2.11F). We hypothesize that this discord, between the precociously-developing hypodermis, and normally-timed somatic gonad, causes abnormal somatic gonadal morphogenesis.

Figure 2.11

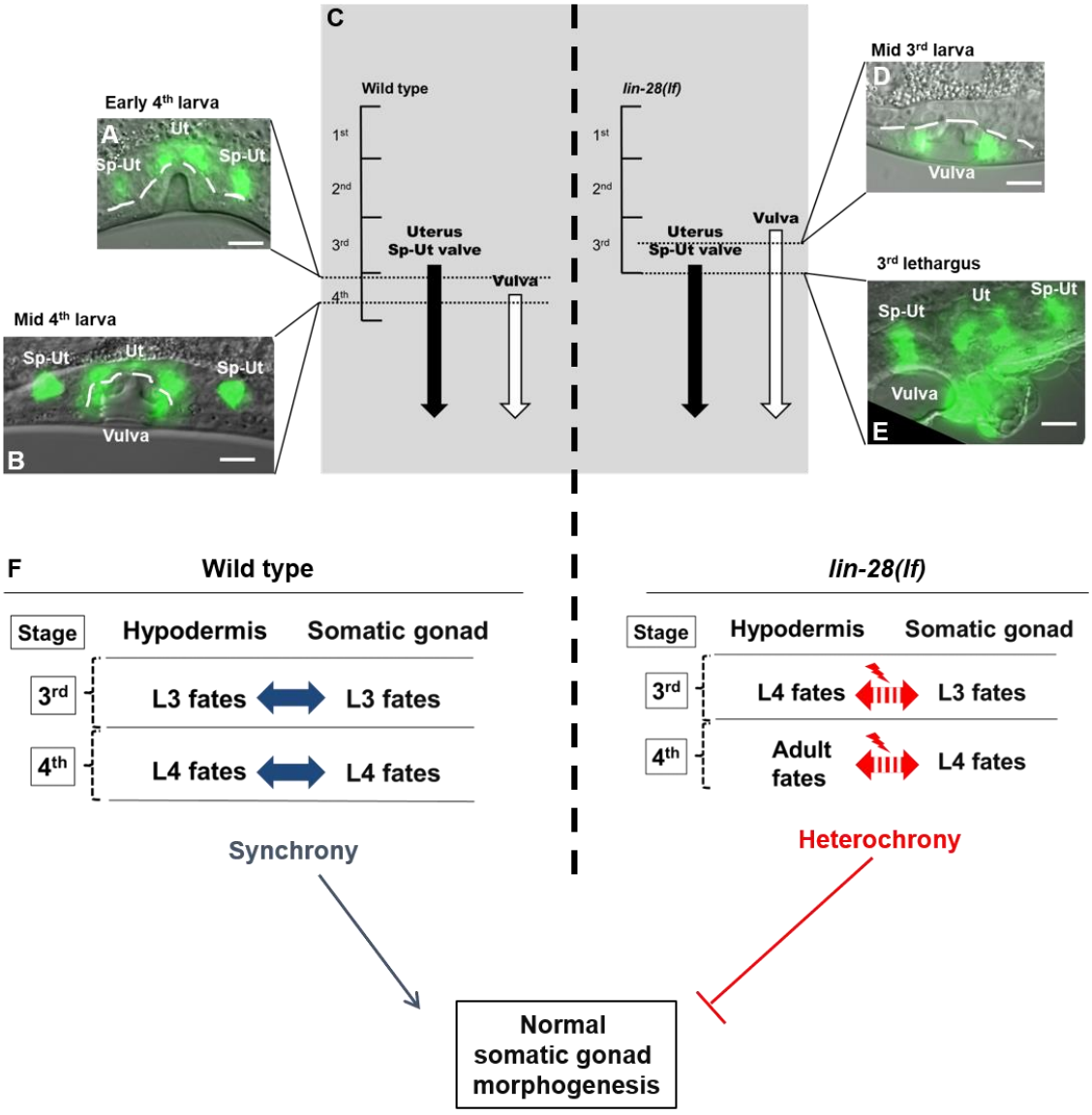
C
Wild type
lin-28(lf)
1st
2nd
3rd
4th
Uterus
Sp-Ut valve
Vulva
Early 4th larva
A
Ut
Sp-Ut
Sp-Ut
Mid 4th larva
Sp-Ut
Ut
Sp-Ut
Vulva
B
Mid 3rd larva
D
Vulva
3rd lethargus
Sp-Ut
Ut
Sp-Ut
Vulva
E
F
Wild type
lin-28(lf)
Stage
Hypodermis
Somatic gonad
3rd
L3 fates
L3 fates
4th
L4 fates
L4 fates
Stage
Hypodermis
Somatic gonad
3rd
L4 fates
L3 fates
4th
Adult fates
L4 fates
Synchrony
Heterochrony
Normal somatic gonad morphogenesis

Figure 2.11. Heterochronic development of the hypodermis, relative to the somatic gonad, in *lin-28(lf)* hermaphrodites.

(A,B,D,E) *cog-1:GFP* expression patterns in wild type and *lin-28(n719)* hermaphrodites at indicated developmental stages. The temporal order of the onset of *cog-1*:GFP expression in the somatic gonad and vulva is reversed in *lin-28(lf)* compared to the wild type. *cog-1*:GFP is expressed in both somatic gonadal tissues (uterus and Sp-Ut valve) and hypodermal tissue (vulva). The timing of expression in wild type and *lin-28(n719)* mutants is summarized in (C). In wild type, *cog-1:GFP* is expressed in somatic gonadal tissues at the late 3rd larval stage (A) and in the vulva in the middle of the 4th larval stage (B). In *lin-28(n719)* mutants, vulva expression of *cog-1:GFP* occurs precociously in the middle of the L3 stages (D), while somatic gonadal expression of *cog-1:GFP* starts at the normal time, in the late 3rd larval stage (E). Both vulval and somatic gonadal expression are detected at 3rd lethargus (E). (F) Model for the importance of *lin-28* activity for somatic gonadal development: In wild type animals, timing of hypodermis development and somatic gonadal development are synchronized. In *lin-28(lf)* mutants, hypodermal development happens precociously while somatic gonadal development does not, resulting in heterochronic development between two tissues. This heterochrony causes somatic gonadal morphogenesis defects.

Hypodermal expression, but not somatic gonadal expression, of *lin-28* rescues abnormal somatic gonadal development, and embryonic lethality in *lin-28(n719)* hermaphrodites

If the somatic gonadal morphological defects of *lin-28(n719)* mutants originate from discoordination between the timing of hypodermal and somatic gonadal development, suppressing the precocious hypodermal development in *lin-28(n719)* mutants should also rescue the somatic gonadal phenotypes. To test whether *lin-28* expression specifically in the hypodermis could rescue the Sp-Ut morphological defects of *lin-28(n719)*, we employed Mos1-mediated single copy insertion (MosSCI) transformation to generate transgenic worms expressing *lin-28*:GFP::*lin-28* 3' UTR driven by tissue-specific promotors; these included *lin-28* endogenous promoter sequences, a *dpy-7* hypodermal promoter (Gilleard et al., 1997), and an *ehn-3A* early somatic gonadal promoter (Large and Mathies, 2010). The endogenous *lin-28* promoter drives *lin-28:GFP* expression in neurons and hypodermis, where *lin-28* is known to be expressed (Moss et al., 1997). Using spinning disk microscopy we also detected *Plin-28::lin-28::GFP* expression in Z1 and Z4 cells, which are precursors of somatic gonadal tissues, (Fig 2.12A,B). *Pdpy-7:lin-28*:*GFP* was expressed in the hypodermis during the embryonic and L1 stages, and *Pehn-3A*::*lin-28*:GFP expression was strongest in Z1 and Z4 from the late embryo to L1 stages (Fig 2.12C,D). *lin-28*:*GFP* levels decreased from the L2 stage in all three strains, presumably due to repression mediated by the *lin-28* 3' UTR.

Figure 2.12

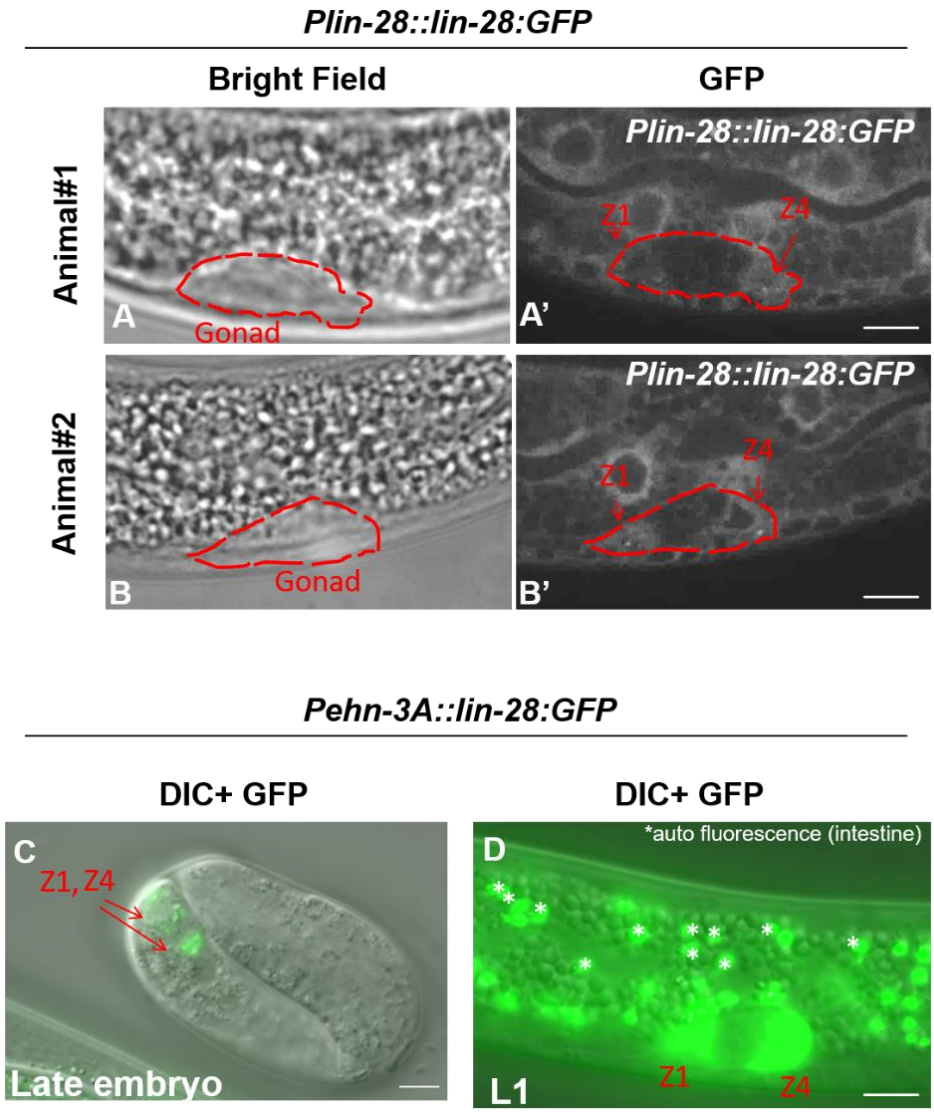
Plin-28::lin-28:GFP
Bright Field
GFP
Animal#1
Plin-28::lin-28:GFP
Z1
Z4
A
Gonad
A'
Animal#2
Plin-28::lin-28:GFP
Z1
Z4
B
Gonad
B'
Pehn-3A::lin-28:GFP
DIC+ GFP
DIC+ GFP
C
Z1, Z4
Late embryo
D
*auto fluorescence (intestine)
L1
Z1
Z4

Figure 2.12. Both *lin-28* endogenous promoter and *ehn-3A* promoter drives early somatic gonadal expression of *lin-28*:GFP.

(A,B) Two *Plin-28::lin-28:GFP* L1 larvae where *GFP* expression was detected in Z1 and Z4 cell by spinning disk microscopy. (C,D) Z1 and Z4 expression of *lin-28:GFP* driven by early somatic gonadal promoter (*Pehn-3A::lin-28:GFP*). GFP expression in Z1 and Z4 cells were detected by fluorescence microscopy beginning in late embryogenesis (C) also L1 larvae (D).

We next crossed those MosSCI strains with *lin-28(n719)*;*cog-1:GFP* hermaphrodites to assess the relative timing of somatic gonadal and hypodermal *cog-1:GFP* expression. *cog-1:GFP* was expressed in somatic gonadal tissues prior to the vulva in wild-type animals, whereas *cog-1:GFP* expression in the vulva was precocious in the *lin-28(n719)* mutants (Fig 2.11, 2.13A,2.13B). *lin-28* expression via its endogenous promoter (P*lin-28*::*lin-28*:GFP:*lin-28* 3'UTR) restored the normal relative timing of somatic gonadal and hypodermal *cog-1:GFP* expression in *lin-28(n719)* mutants (Fig 2.13C). Similarly, in *Pdpy-7::lin-28:GFP;lin-28(n719);cog-1:GFP* animals, *cog-1:GFP* expression in the vulva occurred at the normal time, following somatic gonadal expression. Thus, hypodermal expression of *lin-28* efficiently rescues precocious hypodermal development of *lin-28(n719)* (Fig 2.13D). By contrast, somatic gonadal expression of *lin-28* via the *Pehn-3A*::*lin-28*:GFP transgene did not rescue the precocious expression of hypodermal *cog-1:GFP* in *lin-28(n719)* mutants (Fig 2.13E). These results are consistent with cell-intrinsic activity of *lin-28* in the hypodermis to control hypodermal developmental timing.

Does hypodermal expression of *lin-28* also rescue the somatic gonadal morphogenesis defects of *lin-28(n719)* hermaphrodites? Indeed, *Pdpy-7::lin-28*:*GFP* did rescue wild-type morphology of the Sp-Ut valve core cell in *lin-28(n719)*, (Fig 2.13F, H and I), normal uterine lumen formation (Fig 2.5I), and normal utse migration (Fig 2.6M,N). By contrast, somatic gonadal *lin-28* expression

did not rescue *lin-28(n719)* somatic gonadal defects (Fig 2.13G, 2.13J, 2.5J,2.5K, 2.6O and 2.6P).

Figure 2.13

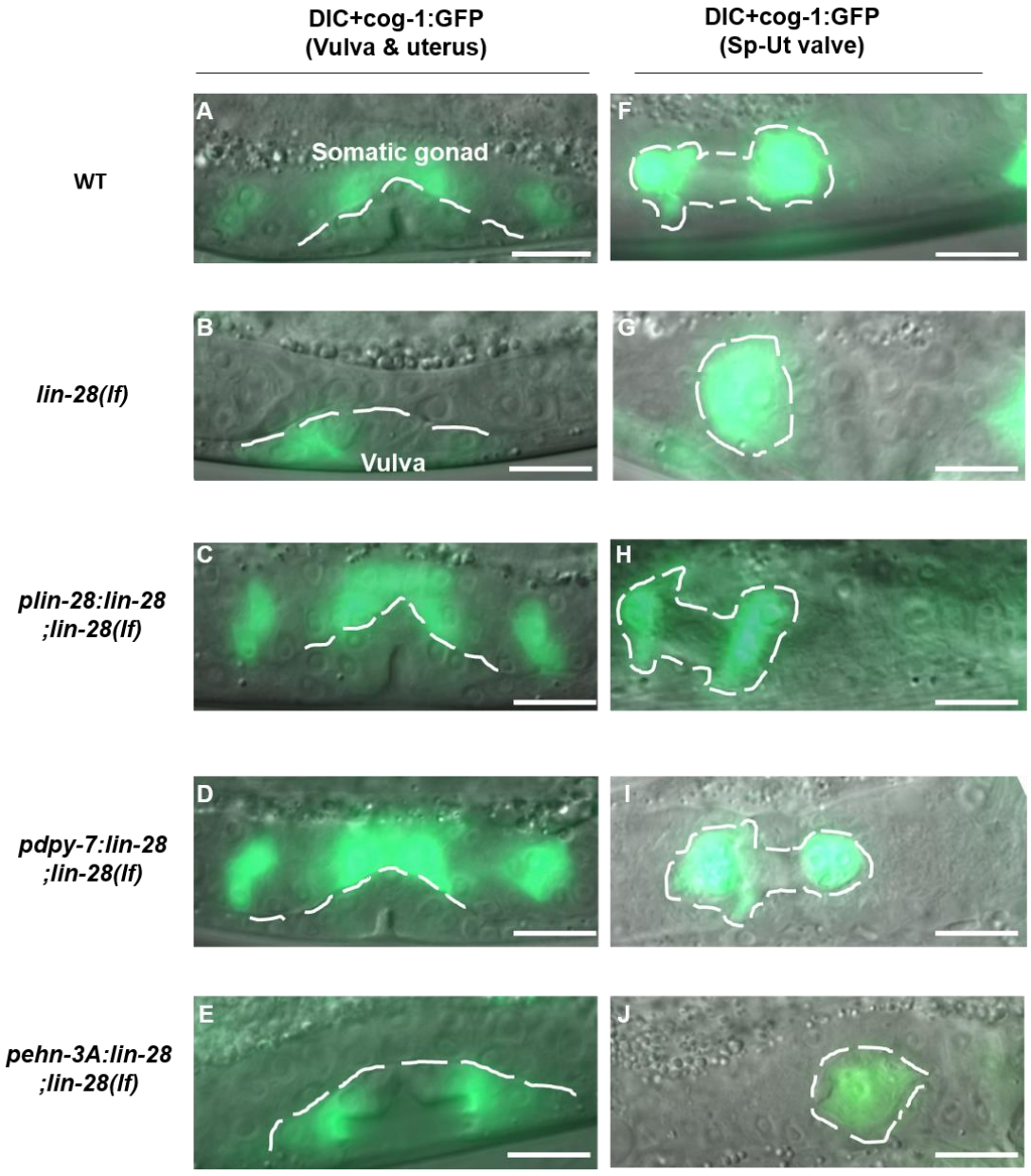
DIC+cog-1:GFP
(Vulva & uterus)
DIC+cog-1:GFP
(Sp-Ut valve)
WT
lin-28(lf)
plin-28:lin-28
;lin-28(lf)
pdpy-7:lin-28
;lin-28(lf)
pehn-3A:lin-28
;lin-28(lf)
A
Somatic gonad
F
B
Vulva
G
C
H
D
I
E
J

Figure 2.13. Hypodermal expression of *lin-28* can rescue developmental timing defects and Sp-Ut valve core cell morphogenesis in *lin-28(lf)* mutants.

cog-1:*GFP* expression in the somatic gonad and vulva in late 3rd or early 4th larval stage hermaphrodites (A-E), or in the Sp-Ut valve core cell in adult or 4th stage hermaphrodites (F-J), of the wild type (A, F), *lin-28(lf)* (B, G), and *lin-28(f)* with *lin-28* expression driven by various promoters (C-E, H-J). *Pdpy-7* (D, I) is a hypodermal-specific promoter (Gilleard et al., 1997) and *Pehn-3A* (E, J) is an early somatic gonadal-specific promoter (Large and Mathies, 2010) . Note: In these experiments, the promoter-driven *lin-28* transgene (C-E, H-J) is also tagged with GFP, but *lin-28:GFP* expression is not detectable at these stages, so all the GFP signal shown here corresponds to *cog-1:GFP. Plin-28::lin-28:GFP;lin-28(n719)* (C) and *Pdpy-7::lin-28:GFP;lin-28(n719)* (D) expresses *cog-1*:*GFP* in the somatic gonad earlier than in the vulva, as in wild type (A). In contrast, both *lin-28(n719)* mutants (B) and *Pehn-3A::lin-28:GFP;lin-28(n719)* (E) expresses *cog-1:GFP* precociously in the vulva. *Plin-28::lin-28:GFP;lin-28(n719)* (H) and *Pdpy-7::lin-28:GFP;lin-28(n719)* (I) restores the Sp-Ut core dumbbell structure observed in wild type (F). However, the Sp-Ut valve core structure remains as a single lobe shape in both *Pehn-3A::lin-28:GFP;lin-28(n719)* (J) and *lin-28(n719)* (G). These data suggest that hypodermal expression of *lin-28* is sufficient to rescue heterochronic development (A-E) and abnormal Sp-Ut valve core morphogenesis (F-J) in *lin-28(n719)* mutants, but somatic gonadal expression of *lin-28* cannot rescue either defect

Because the hypodermal expression of *lin-28* suppresses the morphological defects of the somatic gonad in *lin-28(n719)* mutants, we investigated whether it also rescues the embryonic lethality and fertility defects of these mutants. Expression of either *Plin-28::lin-28::GFP* or *Pdpy-7::lin-28::GFP* restored the embryo viability of *lin-28(n719)* progeny, whereas *Pehn-3A::lin-28:GFP* expression did not restore viability of *lin-28(n719)* progeny (Fig 2.14A).

The total number of live progeny was greater for the *Pdpy-7::lin-28:GFP;lin-28(n719)* strain that for the *lin-28(n719)* mutants. However, only ~15% of animals had numbers of progeny comparable with wild-type values, and the other ~85% of animals produced fewer than 20 progeny at 25°C (Fig 2.14B). In addition, *Pdpy-7*::*lin-28*:GFP insertional strains in the wild-type background led to a similar number of progeny, indicating that the expression of *Pdpy-7*::*lin-28*:GFP intrinsically induces the fertility defects. We found that egg-laying is defective for *Pdpy-7::lin-28:GFP*;*lin-28(n719)* and *Pdpy-7::lin-28:GFP* hermaphrodites (Fig 2.14C). Vulval functions for egg-laying in those strains were intact, because the animals were able to lay eggs occasionally. In contrast, somatic gonadal promoter-driven *lin-28*:GFP expression did not affect the total number of progeny in *lin-28(n719)* animals (Fig 2.14B).

Figure 2.14

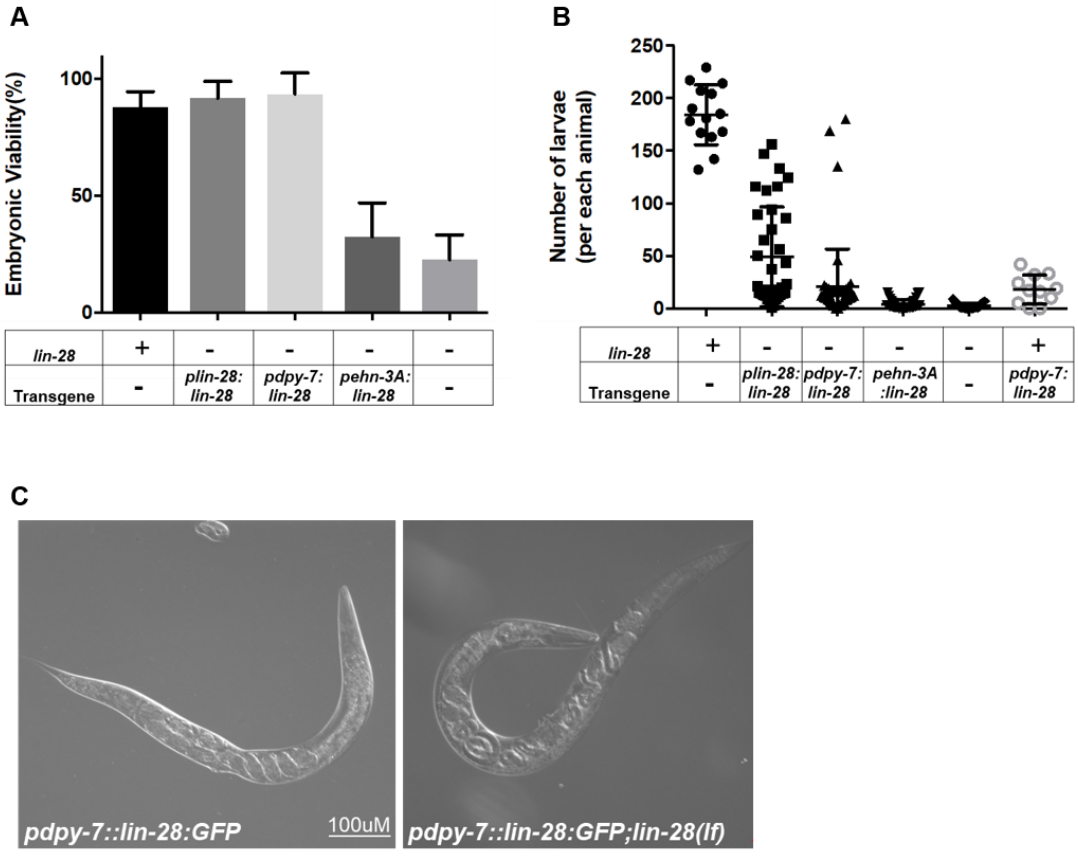
A
Embryonic Viability(%)
100
50
0
lin-28 + - - - -
Transgene - plin-28: lin-28 pdpy-7: lin-28 pehn-3A: lin-28 -
B
Number of larvae (per each animal)
250
200
150
100
50
0
lin-28 + - - - - +
Transgene - plin-28: lin-28 pdpy-7: lin-28 pehn-3A :lin-28 - pdpy-7: lin-28
C
pdpy-7::lin-28:GFP
100uM
pdpy-7::lin-28:GFP;lin-28(lf)

Figure 2.14. Hypodermal expression of *lin-28* enhances fertility of *lin-28(lf)* mutants.

(A) Embryonic viability of *Plin-28::lin-28:GFP;lin-28(n719)* and *Pdpy-7::lin-28:GFP;lin-28(n719)* are restored to a level similar to that in wild type or *lin-2(e1309)* mutants. However, expression of *Pehn-3A::lin-28:GFP* does not enhance the viability of *lin-28(n719)* embryos. (Number of animlals≥15 per each assay; number of independent replicate assays = 4 for *lin-28(n719),* 3 for all other strains.) (B) The number of live larva progeny is increased in *Plin-28::lin-28:GFP;lin-28(n719)* (n=36) and slightly enhanced in *Pdpy-7::lin-28:GFP;lin-28(n719)* (n=53) compared to *lin-28(n719)* mutants (n=25). Progeny numbers for *Pdpy-7:lin-28::GFP* insertional lines without *lin-28(n719)* (n=11) are similar to those of *Pdpy-7::lin-28:GFP;lin-28(n719)* (p value=0.80), suggesting that expression of *Pdpy-7:lin-28::GFP* induces fertility defects regardless of *lin-28(n719)*. Progeny numbers for *Pehn-3A::lin-28:GFP;lin-28(n719)* (n=40) are similar to those of *lin-28(n719)* mutants. (A,B: Unpaired t-test compared to *lin-28(lf),* NS; not significant, *p<0.05,,****p<0.0001) (C) Embryos of *Pdpy-7::lin-28:GFP* (upper panel) and *Pdpy-7::lin-28:GFP;lin-28(n719)* (lower panel) are trapped inside adult hermaphrodites, indicating that defective egg laying is a cause of the reduced fertility in these animals. (Scale bar = 100 μm).

Discussion

C. elegans lin-28(lf) hermaphrodites exhibit a dramatic reduction in fertility, in excess of what would be expected as a simple consequence of their vulval morphogenesis defects. In principle, it was possible that *lin-28* could promote fertility entirely via a germline-specific activity, analogous to the demonstrated role of mammalian Lin28 in promoting pluripotency and stem cell proliferation (Yu et al., 2007; Zhang et al., 2016). Indeed, *lin-28* has been reported to regulate the germ cell pool size in mice and in *C. elegans* hermaphrodites (Shinoda et al., 2013; Wang et al., 2017a). However, the reported effects on germ cell pool size in *C. elegans,* after germline knockdown of *lin-28,* did not include substantially reduced fertility (Wang et al., 2017a). We performed tissue-specific RNAi experiments using *rrf-1(lf)* and *ppw-1(lf)*, and observed that somatic knockdown of *lin-28* caused greater reduction of live progeny number than did germline knockdown of *lin-28* (Fig 2.15). This suggests that the dramatically reduced reproduction of *lin-28(lf)* hermaphrodites is caused by fertility-promoting activities of *lin-28* outside of the germline, that is, within somatic cell lineages of the gonad and/or other tissues. Other examples in which *lin-28* controls the development of reproductive tissues other than germ cells have been reported in flies and mice. The *Drosophila* egg chamber is fused abnormally early in *lin-28* null mutants, and the development of mice vaginal openings is delayed in *lin-28a* transgenic mice (Stratoulias et al., 2014; Zhu et al., 2010).

Figure 2.15

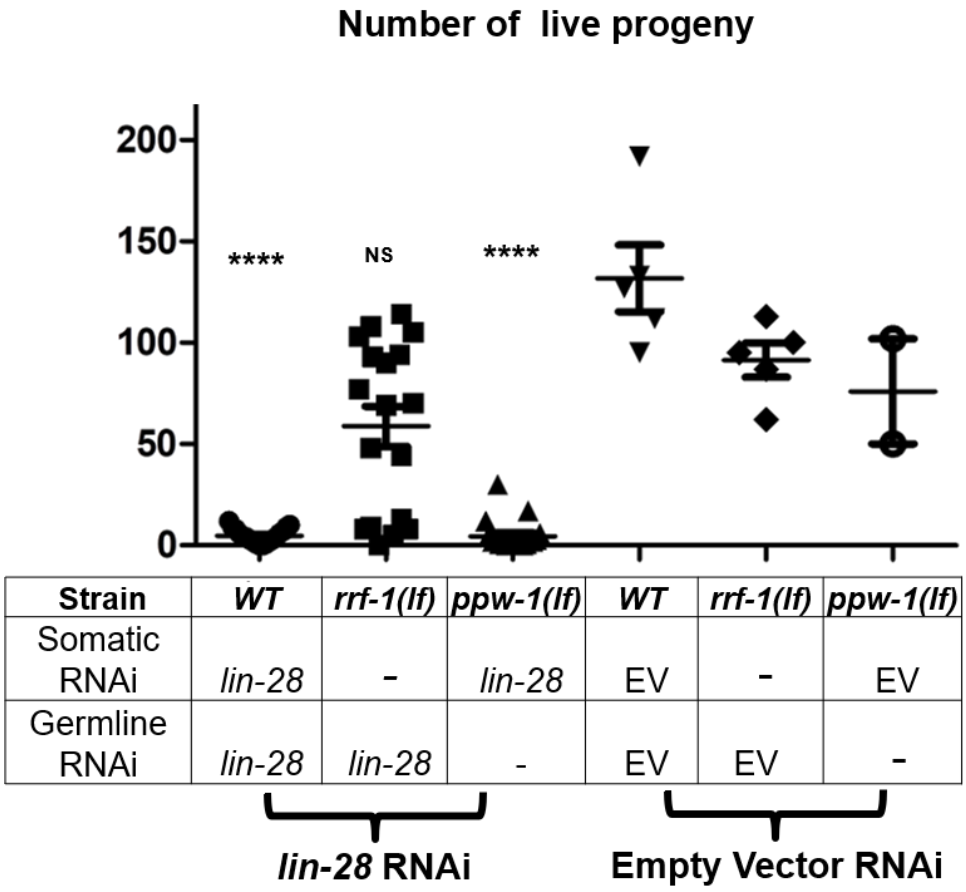
Number of live progeny
200
150
100
50
0
****
NS
****
Strain
WT
rrf-1(lf)
ppw-1(lf)
WT
rrf-1(lf)
ppw-1(lf)
Somatic RNAi
lin-28
-
lin-28
EV
-
EV
Germline RNAi
lin-28
lin-28
-
EV
EV
-
lin-28 RNAi
Empty Vector RNAi

Figure 2.15. Reduction of *lin-28* function in the soma decreases fertility of hermaphrodites more than does reduction of *lin-28* function in the germline.

Wild type, *rrf-1(pk1417)* mutants, and *ppw-1(pk2505)* mutants were fed with *lin-28* RNAi and empty vector RNAi, and the number of progeny produced by each animal was determined. *ppw-1(pk2505) lin-28(RNAi)* animals all exhibited reduced fertility, similar to *lin-28(RNAi)* animals. However, *rrf-1(pk1417) lin-28(RNAi)* animals were, overall, less affected by *lin-28(RNAi)*, with only a minority of animals exhibiting reduced fertility. (Error bar shows standard deviation. unpaired t-test, each strain with *lin-28*(RNAi) was compared to corresponding strain with empty vector (RNAi). NS; not significant, ****p<0.0001.)

Here we investigated the somatic function of *lin-28* in promoting *C. elegans* hermaphrodite fertility. Our results show that *lin-28* is required for the completion of certain somatic gonadal morphogenetic events, specifically, the enlargement of the uterine lumen, the migration of utse nuclei, and extension of the Sp-Ut valve core, and that these somatic gonadal morphogenesis defects likely underlie the reduced fertility of *lin-28(lf)* hermaphrodites. In particular, the abnormal Sp-Ut valve of *lin-28(lf)* animals has a potent impact on fertility by preventing fertilized embryos from entering the uterus, thereby inhibiting ovulation and resulting in reduced embryo production.

We found that egg shell integrity is also compromised in *lin-28(lf)* mutants, which negatively affects embryonic viability, similarly to other egg shell defective mutants (Johnston et al., 2006; Johnston et al., 2010; Maruyama et al., 2007). Moreover, we found that another spermathecal exit mutant *fln-1(lf)* has egg shell-defective phenotypes similar to *lin-28(lf)* (Fig 2.8C), suggesting a causal link between spermathecal retention and egg shell integrity. We speculate that physical damage to the egg shells may occur when the embryos are trapped in the spermatheca. Interestingly, deficiency of *cbd-1*, an essential component of *C. elegans* egg shell, leads to pinched off embryos reflecting incomplete spermathecal exit (Johnston et al., 2010). This suggests that damage to the egg shell of embryos lingering too long in the spermatheca could further aggravate an underlying spermathecal exit defect. Further research is needed to clarify the relationship between spermathecal exit and egg shell integrity.

Our results point to a close coupling between the hypodermal and somatic gonadal phenotypes in *lin-28(lf)* mutants. First, we found that a very similar configuration of the known heterochronic genes mediates the effects of *lin-28(lf)* on hypodermal developmental timing and on somatic gonadal morphogenesis (Fig 2.9E). The exception is *lin-41*; we could not find evidence that *lin-41*, a downstream target of *let-7* for hypodermal developmental timing (Slack et al., 2000), is involved in Sp-Ut valve core morphogenesis. The *lin-41*(RNAi) animals displayed a superficially normal dumbbell-shaped Sp-Ut valve, albeit somewhat smaller than the wild-type valve (Fig 2.10C). This result may reflect either an insufficient knockdown of *lin-41* by RNAi in these experiments, or that *lin-41* does not participate in somatic gonadal development. In the latter case, *hbl-1* would appear to function as a main downstream target of *let-7* in somatic gonadal morphogenesis.

Our second finding indicating a linkage between *lin-28(lf)* hypodermal and somatic gonadal phenotypes, is that post-dauer development suppresses both the hypodermal and the somatic gonadal developmental defects of *lin-28(lf)* hermaphrodites. This result in particular accentuates that the somatic gonadal defects of *lin-28(lf)* do not reflect a direct role of *lin-28* in somatic gonadal development, *per se*; rather, that somatic gonadal morphogenesis fails in *lin-28* mutants as an indirect consequence of precocious development. Consistent with this idea, another precocious mutant, *lin-14(lf)* (Ambros and Horvitz, 1984a), showed similar Sp-Ut valve defects to *lin-28(lf)* mutants (Fig 2.10D).

Importantly, we did not find evidence for precocious development of somatic gonadal events in *lin-28(lf)*. In particular, we observed that the timing of the onset of expression of certain fluorescent markers of L3 and L4 somatic gonadal developmental events was not altered in *lin-28(lf)*, even though subsequent morphogenesis failed. Assuming that the somatic gonad and the hypodermis each has its own developmental clock, it would appear that the hypodermal developmental clock of *lin-28(lf)* mutants is accelerated, while the somatic gonadal developmental clock runs normally, resulting in discoordination of developmental timing between the two tissues during the L3 and L4 stages (Fig 2.11F). We propose that it is this temporal discord between the accelerated hypodermis, and the normally-scheduled somatic gonad, that results in failure of somatic gonadal morphogenesis.

The apparent absence of precocious development of the somatic gonad of *lin-28(lf)* animals suggests that *lin-28* may affect somatic gonadal morphogenesis cell non-autonomously, by controlling one or more signals from the hypodermis to the somatic gonad. In strong support for this model, we found that expression of *lin-28* specifically in the hypodermis could rescue the somatic gonadal developmental defects of *lin-28(lf)* mutants. Conversely, expression of *lin-28* specifically in the somatic gonadal precursor lineage did not rescue any *lin-28(lf)* phenotypes. Based on these observations, we propose that the principle function of *lin-28* with regards to somatic gonadal development is to act within the hypodermis to specify a schedule of hypodermal events that is properly

coordinated with a corresponding schedule of somatic gonadal developmental events. Accordingly, normal somatic gonadal morphogenesis is proposed to require a coordinated agenda of signaling between the hypodermis and the somatic gonad during the L3 and/or L4 stages.

Then, by what mechanisms could hypodermal activity of *lin-28* regulate the development of a different tissue? There are precedents in *C. elegans* for cell non-autonomous developmental signals originating from the hypodermis. A recent study showed that heterochronic genes acting in the hypodermis can modulate mTOR signaling in the intestine (Dowen et al., 2016). This signaling requires the mTORC2 complex specifically and its downstream factors including r*ict-1/rictor, sinh-1/sin, and sgk-1/sgk1* in the intestine. However, it is unlikely that somatic gonadal development is related to mTORC2 signaling, because we found that *rict-1* (RNAi) in *lin-28(lf)* mutants did not induce or suppress Sp-Ut valve defects (data not shown). In another example, it has been reported that migration of the hermaphrodite-specific neurons and arborization of sensory neurons are regulated by hypodermal expression of the microRNA *mir-79* and MNR-1/menorin, respectively (Pedersen et al., 2013; Salzberg et al., 2013). Hypodermal glycosylated cell surface molecules or signaling cell adhesion molecules are key downstream factors for neuronal morphogenesis in each case, implying this nonautonomous signaling may require physical contact with other tissues.

Indeed, seam cells in the hypodermis become physically connected to the utse (uterine seam cell) of *C. elegans* hermaphrodites. The connection between

these two tissues is thought to be formed during the mid to late L4 stages in wild-type animals (Newman et al., 1996). The precocious hypodermal maturation in *lin-28(lf)* animals might cause this connection to be formed aberrantly, or not at all. Alternatively, the reduced number of seam cells in *lin-28(lf)* mutants may alter positioning of seam cells in the hypodermis, disrupting the normal connection between seam cells and utse. However, there is evidence that utse defects may not necessarily be associated with Sp-Ut abnormality. *lin-29* expression in the anchor cell induces signals for utse precursor cells to adopt utse fates, and *lin-29(lf)* mutants do not form a proper utse (Newman et al., 2000). However, loss of *lin-29* does not cause any detectable abnormality in Sp-Ut valve core morphology (Fig 2.9A). Moreover, it has been reported that anchor cell invasion genes (*fos-1, mig-10, egl-43, cdh-3, and zmp-1*) are involved in utse development (Ghosh and Sternberg, 2014), but we did not observe any abnormality in the Sp-Ut valve upon RNAi knockdown of these genes (data not shown). Nevertheless, it will be interesting to examine whether the physical connection between the hypodermal seam and gonadal utse is formed properly in *lin-28(lf)* hermaphrodites.

It is striking that *lin-28(lf)* mutants exhibit coordinated defects in the final stages of morphogenesis in at least three distinct somatic gonadal structures: extension of the Sp-Ut valve core, positioning of the uterine seam cell nuclei, and expansion of the lumen of the uterus. Since all three of these defects are highly penetrant in *lin-28(lf),* and are coordinately rescued by appropriate *lin-28*-expressing transgenes, we were not able to determine if these defects are

expressed independently, or whether for example, one of them is the primary defect that is linked to hypodermal developmental timing, and the other defects are secondarily precipitated by the first. Further research is needed to identify any cause-effect relationships between utse migration, Sp-Ut valve morphogenesis, and uterine lumen formation.

Overall, our studies of *lin-28* in the context of *C. elegans* reproductive system development provides an informative model for exploring fundamental principles of multicellular development, including how the generation of organized cellular complexity requires precise temporal coordination of events across interacting tissues. Our findings exemplify how a cell-intrinsic developmental timing program can be required not only cell-autonomously to specify temporal cell fates, but also to control cell-nonautonomous signaling that is critical for proper development of interacting tissues. Our identification of cell-nonautonomous hypodermis-to-gonad developmental signaling controlled by *lin-28* and the heterochronic pathway should set the stage for future studies addressing the identity and potential evolutionary conservation of the molecular components of the downstream signal(s).

Material and Methods

Culture of *C. elegans* strains

C. elegans wild type (Strain N2) and mutant strains (listed in Table 2.2) were grown and maintained (at 25^{o}C unless otherwise noted) on nematode growth media (NGM) agar plates seeded with *E. coli* (strain HB101). A list of genotyping primers for allele confirmation can be found in Table 2.3. Synchronized populations of larvae at defined developmental stages were obtained as previously described (Stiernagle, 2006). Briefly, embryos were collected using sodium hypochlorite and 5N NaOH, washed with M9 buffer, and incubated in M9 buffer overnight at 20℃, placed on NGM plates seeded with HB101, incubated for defined lengths of time at 20℃ or 25℃, and developmental stage was assessed by DIC microscopy of a sample of worms from the population (Byerly et al., 1976).

Table 2.2. *C. elegans* strains used in this study

Strain Name	Genotype
N2	
VT2932	*lin-28(n719)I*
CB1309	*lin-2(e1309)X*
PS3662	*syIs63[cog-1::GFP + unc-119(+)]*
DZ325	*ezIs2[fkh-6::GFP + unc-119(+)]; III; him-8(e1489) IV*
VT2929	*lin-28(n719)I;syIs63*
VT2930	*lin-28(n719)I;ezIs2*
VT866	*lin-28(n719)I;let-7(mn112) unc-3(e151) X*
MT2001	*lin-28(n719)I;lin-29(n333) II.*
VT937	*lin-28(n719)I;lin-46(ma164) V*
AG212	*unc-119(ed3); avIs143 [pDNL10 (unc-119(+) + cbd-1 prom::CBD-1::mCherry::cbd-1 3'UTR)]*
VT3454	*lin-28(n719);avIs143*
UN0810	*fln-1 (tm545)*
VT3660	*lin-14(n179);syIs63*
VT3730	*let-7(mn112);mnDP1;syIs63*
VT3580	*lin-29(n836);syIs63*
VT3581	*lin-46(ma164) maIs105 [col-19:GFP]; syIs63*
MH1319	*kuIs29 [egl-13p::GFP+unc-119(+)]*
VT3661	*lin-28(n719);kuIs29*
VT3731	*lin-28(n719);let-7(mn112);kuIs29*
VT3665	*lin-2(e1309);syIs63*
VT3664	*lin-2(e1309);lin-28(n719);syIs63*
VT3733	*lin-2(e1309);kuIs29*
VT3732	*lin-2(e1309);lin-28(n719);kuIs29*
EG4322	*ttTi5605 II; unc-119(ed3) III;*
WM186	*avr-14(ad1302) I; ttTi5605 II; unc-119(ed3) III; avr-15(ad1051) glc-1(pk54) V*
VT3392	*avr-14(ad1302) I;maIs402[unc-119(+);pehn-3A:ln-28:GFP:lin-28 3'UTR];unc-119(ed3) III;avr-15(ad1051) glc-1(pk54) V*
VT3486	*avr-14(ad1302) I;maIs403[unc-119(+);plin-28:ln-28:GFP:lin-28 3'UTR];unc-119(ed3) III;avr-15(ad1051) glc-1(pk54) V*
VT3702	*maIs409[unc-119(+); pdpy-7:ln-28:GFP:lin-28 3'UTR]II;unc-119(ed3) III*
VT3517	*lin-28(n719);maIs402;syIs63*
VT3516	*lin-28(n719);maIs403;syIs63*
VT3703	*lin-28(n719);maIs409;syIs63*
VT3734	*lin-28(n719);maIs402;kuIs29*
VT3735	*lin-28(n719);maIs403;kuIs29*
VT3736	*lin-28(n719);maIs409;kuIs29*
NL2098	*rrf-1(pk1417)*
NL2550	*ppw-1(pk2505)*

Table 2.3. Primer sequences used in this study

Primers		Sequences	
1	lin-28(n719) genotyping F	ttataaataaaagtcggag	sequencing to confirm n719
2	lin-28(n719) genotyping R	cctttcagtccttgtccttctac	
3	let-7(mn112) genotyping F	gataccatggaggacgacgg	WT :476 bp mn112: 263 bp
4	let-7(mn112) genotyping R	gtagaaaattgcatagttca	
5	lin-29(n836) genotyping F	ggcttatcagtttgatggca	WT:273bp n836: 200bp
6	lin-29(n836) genotyping R	cccgcaaatttccggaatc	
7	lin-46(ma164) genotyping F	gaacttcaagattcctactgtag	sequencing to confirm ma164
8	lin-46(ma164) genotyping R	gaaatcacgacaattgtagacattg	
9	lin-14(n179) genotyping F	gaaacagctccaccactc	sequencing to confirm n179
10	lin-14(n179) genotyping R	gttctgacactggtcgg	
11	attB4+ lin-28 promoter F	ggggcaactttgtatagaaaagttggatttcggtaaaactcttcaagc	lin-28 Promoter:PCR ampliifed, followed by BP reaction with pDONR P4P1r
12	attB1r+ lin-28 pormoter R	ggggctgctttttgtacaaacttgtcctgaaaaagatttttaaaattttt	
13	attB4+ dpy-7 promoter F	ggggcaactttgtatagaaaagttgga aatctcattccacgatttct	dpy-7 promoter: PCR ampliifed, followed by BP reaction with pDONR P4P1r
14	attB1r + dpy-7 promoter R	ggggctgctttttgtacaaacttgt ttatctggaacaaaatgta	
15	attB4+ehn-3 promoter F	ggggcaactttgtatagaaaagttggactaatctagaaaaatacgaca	enh-3A promoter:PCR ampliifed, follwed by BP reaction with pDONR P4P1r
16	attB1r+ ehn-3 promoter R	ggggctgctttttgtacaaacttgttttgtaatttggaagctgg	
17	attB1+lin-28 gene F	ggggacaagtttgtacaaaaagcaggcttcgttcagcaatgcttttaatta	100bp+lin-28:GFP (P:Primer, T:template, PCR product:A~D) 1. A: (P) 20/18, (T) gDNA 2. B: (P) 19/22, (T) gDNA 3. C: (P)20/22 (T) A,B -> Removal of the first exon 4. D: (P) 21/23, (T) XW12 (Wei et al., 2012) 5. E : (P) 17/24 (T) C,D ->GFP fusion 6. BP reaction E with pDONR 221
18	lin-28 1st exon 3'(overlapping)	aggtgttggtgacgggagcctctcgaaggaag	
19	lin-28 2nd exon 5'(overlapping)	gaggctcccgtcaccaacacctcgatactttgg	
20	lin-28 100bp of 5' upstream	gttcagcaatgcttttaatta	
21	Primer for GFP fusionF	ggcgcgcctctagaggatc	
22	Primer for GFP fusion R(Overaping)	cggggatcctctagaggcgcgccttcatcagaggaattactattcttttc	
23	GFP R	ctatttgtatagttcatccatgcca	
24	attB2+lin-28::GFP gene R	ggggaccactttgtacaagaaagctgggtt ctatttgtatagttcatccatgcca	
25	attB2r+lin28_3UTR(5)	ggggcagctttcttgtacaaagtggga aatcatctagacactgagaata	lin-28 3'UTR:PCR ampliifed, follwed by BP reaction with pDONR P2R-P3
26	attB3 +lin-28_3UTR(3)	ggggcaactttgtataataaagttgt gccaacttgttgaggattgttaa	
27	ttTi5605 genotyping F	tgacattgtcgaaatgtcctc	ttTi5605: 1411bp transgene inserted: 7kb<
28	ttTi5605 genotyping R	gttatacagaagaccgttacg	
29	ttTi5605 genotyping 2F	tctggctctgcttcttcgtt	ttTi5605: 0bp transgene inserted: 1772bp
30	ttTi5605 genotyping 2R	caattcatcccggtttctgt	

Microscopy

For DIC and fluorescence microscopy, worms were anesthetized with 0.2 mM levamisol and mounted on 2% agarose pads. All images except the following were obtained with a ZEISS Axiocam 503 mono: Figure 2.4. (Leica DM 5500Q confocal microscopy), Figure 2.12 (3i (Intelligent imaging Innovations) Everest spinning disk confocal microscopy). The videos were taken with a Zeiss Axioplan2. For gonad DAPI staining, hermaphrodites were cut with a syringe needle and the extruded gonads were fixed with 95% ethanol. After washing twice with M9, the dissected gonads were incubated with 4'6'-diamidino-2-phenylindole solution (100 ng/ml) for 10 min in a humidified chamber and washed again with M9 (Modified from (Shaham, 2004)).

RNAi

RNAi by feeding worms with *E. coli* expressing double-stranded RNA was conducted as previously described (Conte et al., 2015). HT115 bacterial RNAi strains (*lin-28*, *hbl-1*, *lin-29*, *lin-46*, *rict-1, fos-1, mig-10, egl-43, cdh-3, zmp-1*) and an empty vector strain (L4440) from the Ahringer library were used (Kamath and Ahringer, 2003).

Analysis of fertility and embryonic lethality

Individual young adult hermaphrodites were placed, one per plate, on a NGM plates seeded with HB101, and the number of live progeny from each hermaphrodite was counted 3~4 days later. To determine embryo viability, gravid

adult hermaphrodites were dissected with a syringe, the released embryos were collected, and transferred to NGM plates seeded with HB101. The total number of embryos was counted immediately, and after 36 hrs incubation at 25 ℃, the number of live animals was counted. Viability was calculated as (Number of live animals / Total number of embryos seeded) X 100%.

Egg shell integrity

Egg shell permeability was accessed using FM 4-64 dye (Sigma,T13320), as described (Johnston et al., 2006). Briefly, embryos were dissected from gravid hermaphrodites in 150 mM KCl with 30 μM of FM4-64, and the proportion of embryos infiltrated by FM4-64 was measured using fluorescence microscopy.

Construction of plasmids

To generate transgenic strains containing tissue specific promoters driving *lin-28:GFP*, we removed the sequence between the first exon and second exon (I:8409341-I:8410415) of *lin-28a* to prevent the sequence from serving as an endogenous promoter (Moss et al., 1997). GFP sequences were adapted from XW12 (Wei et al., 2012) and were fused in frame to the carboxy terminus of *lin-28* coding sequence. The primers used for the overlapping PCRs for these procedures are listed in Table 2.3. We used Gateway® Technology (Invitrogen, cat 12535-019) to construct transgenic vectors. *lin-28:GFP* was cloned into the gateway entry vector pDONR P2P3 by BP reaction. Also, the promoter regions of *enh-3A*, *lin-28*, and *dpy-7* were cloned into pDONR P4P1r by BP reaction. *lin-28*

3’UTR was cloned into pDONR P2rP3. LR reactions of these three entry vectors with pCJF150 yielded final vectors containing the following transgenes for injection: pSW40(*plin-28*), pSW42(*pehn-3A*), and pSW43(*pdpy-7*). The sequences for all primers used in this procedure can be found in Table 2.3 and the maps of pSW40, pSW42, and pSW43 can be found in Figure 2.16.

Figure 2.16. Vector maps of pSW40, pSW42, and pSW43 injected to make transgenic animals.

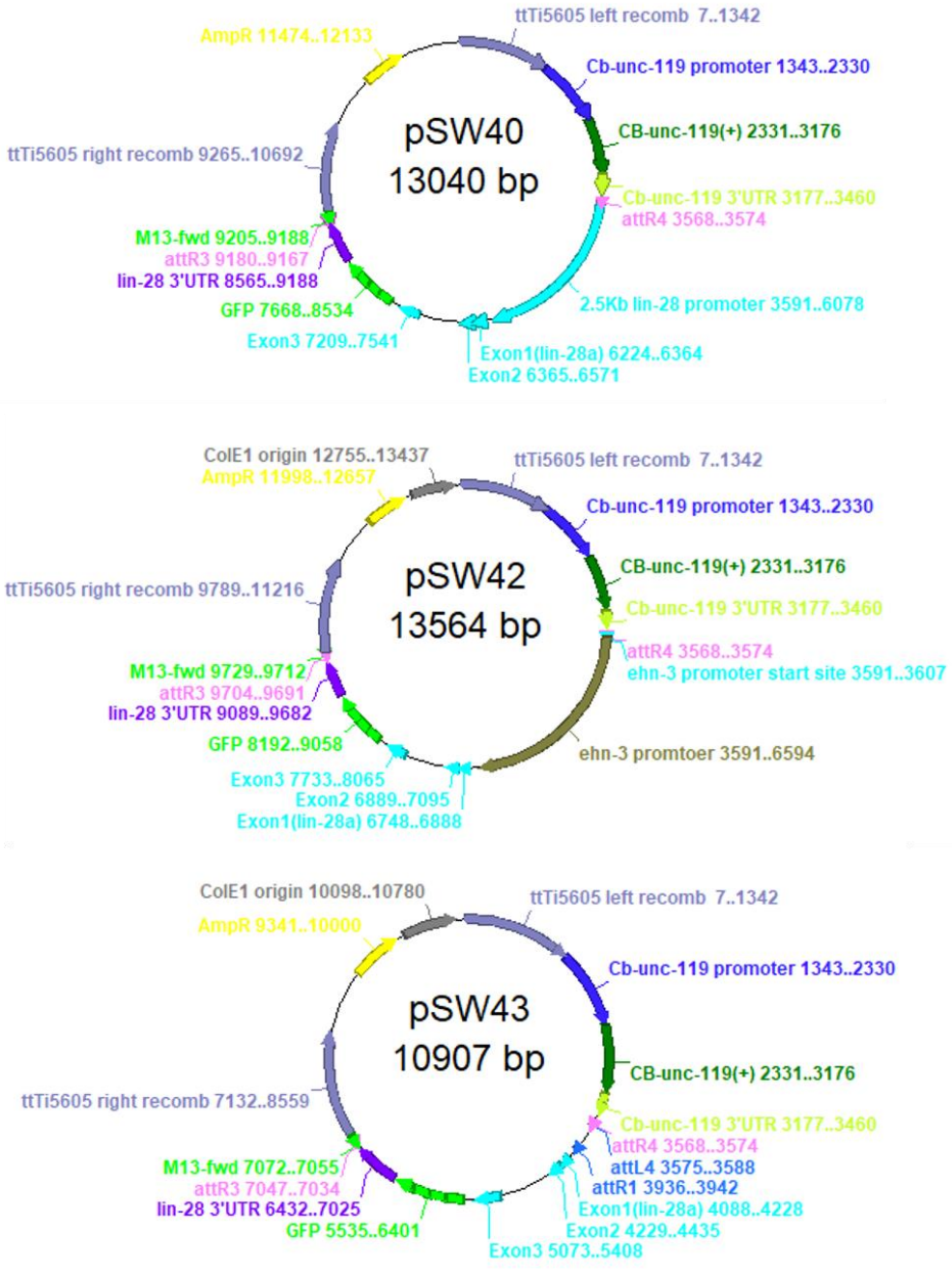

Generation of MosSCI transgenic lines

MosSCI single-copy insertions (into the *ttTi5605* Mos1 allele, near the center of chromosome II) were obtained using the protocol previously described on the "wormbuilder" website (http://www.wormbuilder.org/). For each plasmid construct, MosSCI transformation was generally conducted using the direct injection approach (Frøkjær-Jensen et al., 2012), and also using the approach employing extrachromosomal array intermediates and ivermectin selection for insertion (Shirayama et al., 2012). To prepare plasmids for injection, the following plasmids were purified using a midiprep kit (Qiagen, Cat.12143): pSW40, pSW42, PSW43, pCFJ601 (Peft-3::transposase), pMA122 (Phsp::peel-1), pGH8 (Prab-3::mCherry), pCFJ90 (Pmyo-2::mCherry), pCFJ104(Pmyo-3::mCherry), pJL44(Phsp-16.48::MosTase::glh-2 3'UTR), pCCM416(Pmyo-2::avr-15), and pRF4(*rol-6(su1006)*). For the direct injection method, injection mixtures consisted of pCFJ601(50 ng/µl), pMA122(10 ng/µl), pGH8(10 ng/µl), pCFJ90(2.5 ng/µl), pCFJ104 (5 ng/ul), and one of the transgene-containing plasmids (pSW40, pSW42, or pSW43(25 ng/ul); the mixture was injected into EG4322 hermaphrodites and injected animals were placed singly onto NGM plates seeded with HB101. Following 7~10 days of incubation at 25 ℃, cultures were heat-shocked (35 ℃, 1hr) to kill any worms with an extrachromosomal array and surviving animals were cloned. After allowing them to produce progeny, worms are genotyped to identify single copy transgene inserted strains. For the approach using ivermectin selection, we injected a mixture of pJL44(50 ng/µl), pCCM416(50 ng/µl), and pRF4(50 ng/µl)

with one of pSW40, pSW42, or pSW43(15 ng/ul) into WM186 hermaphrodites. After allowing the progeny of injected animals to grow for multiple generations, they were heat-shocked (35 ℃, 1 hr) to induce heat shock promoter driven transposase expression from extra chromosomal arrays, and single single-copy transgene inserted strains were selected by invermectin resistance (10 ng/ml) against extrachromosomal arrays. We obtained VT3702 by the direct injection method, and VT3486 and VT3392 by the extrachromosomal array intermediate method. We crossed those strains to VT2929 to obtain VT3703, VT3517 and VT3516 (Table 2.2).

Chapter III. Characterization of *C. elegans lin-28* Isoforms and Their Functions

-Abstract

-Background and Significance

-Results

-Discussion

-Material and Methods

Abstract

The *C. elegans* genome encodes two isoforms of *lin-28, lin-28a* and *lin-28b,* which differ in their first exons, but have identical second and third exons. Here we investigated the expression patterns and functions of each isoform in hermaphrodites. Only *lin-28a* mRNA is trans-spliced with the spliced leader 1 (SL1) sequence, potentially causing differences in subsequent mRNA regulation relative to *lin-28b*. Our analysis of expression patterns suggests that *lin-28a* and *lin-28b* are co-expressed in the hypodermis, neurons, and muscle. To determine the function of each isoform, we generated two individual knock-out mutants, *lin-28a(lf)* and *lin-28b(lf)*, using CRISPR-Cas9 technology. We found that *lin-28a* and *lin-28b* function essentially redundantly. Single-isoform knockout mutations of either isoform do not show defects in fertility, embryonic viability, or somatic gonadal development. However, our findings indicate a slightly lesser contribution of *lin-28b* compared to *lin-28a* in the context of seam cell fate progression.

Background and Significance

The *C. elegans* genome encodes two isoforms of *lin-28*, *lin-28a* and *lin-28b*, which differ in their first exons. The function of *lin-28* in developmental timing has been investigated extensively, and most studies have used *lin-28(n719)*, a putative null mutation. The *n719* allele contains a point mutation at the splicing donor sequence right after the second exon. Because *lin-28a* and *lin-28b* share second and third exons, the *n719* mutation leads to loss of function of both isoforms.

In the present study, we examined the expression and function of individual *lin-28* isoforms. For this purpose, we constructed a reporter strain that can distinguish between the spatial expression patterns of the two isoforms. We also generated selective isoform-specific knock-out mutations using CRISPR-cas9 technology. Our results suggest overall functional redundancy of *lin-28a* and *lin-28b*, consistent with their overlapping expression in diverse tissues. In addition, our study established reporter strains and genetic mutants that can be employed to further characterize the two *lin-28* isoforms in other biological contexts, for example under stress conditions or sensitized genetic backgrounds.

Results

Genomic structure of *C. elegans lin-28*

The two isoforms of LIN-28 differ in their first exons (Fig 3.1A). The genomic locus of *lin-28* spans from chromosome I:8407802~8412955, which includes four different exons. The first exons of each isoform encode 47-amino-acids and 16-amino-acids, respectively. The second and third exons, which are shared by the two isoforms, encode two RNA-binding domains, the CSD and the ZFD. Therefore, both isoforms contain the conserved RNA binding domains of LIN-28. Although the first exons of the two isoforms do not contain any recognizable functional domains, both are well conserved among other nematodes including *C. brenneri*, *C. briggsae*, and *C. tropicalis* suggesting they might have conserved functions (Fig 3.1B,C).

Figure 3.1

A

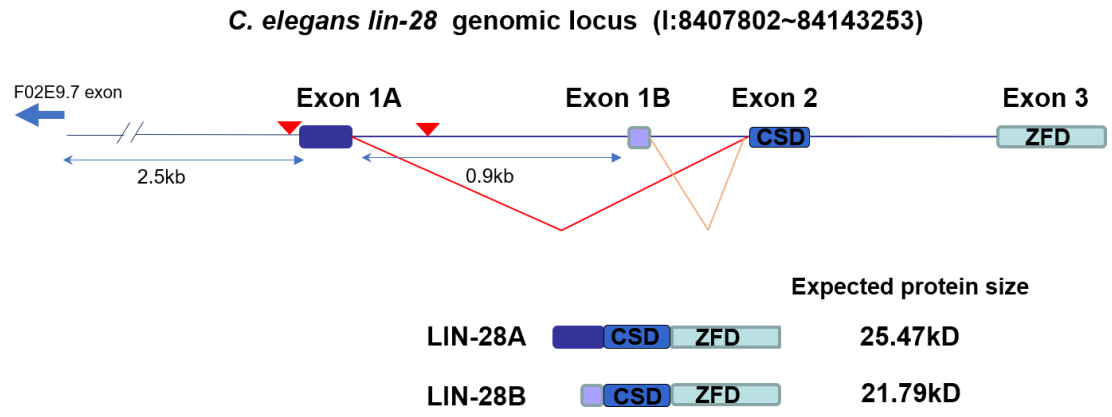

B. Exon 1A amino acid sequences

```
C. elegans      MSTVVSEGRNDGNNRYSPQDEVEDRLPDVVDNRLTENMRVPSFERLP    (100%)
C. brenneri     MSTVVSEGRNGGNERYSPQD----ELPDLENLKLTDDMRVPSFDRLP    (74.42%)
C. briggsae     MSTVVSEGRNGGNERYSPQDDVSKELPDINGLSLEETMGIPSFDRLP    (65.96%)
C. tropicalis   MT--VSEGRNGGNEGYSPDDNGLDKLPNVEDLKLTDNMRVPSFERLP    (68.89%)
                *:  ******.**: ***:*    .**:: .  * : * :***:***
```

C. Exon 1B amino acid sequences

```
C. elegans      MIEAALENPVPIKSQL   (100%)
C. Brenneri     MIEAALENPVLVKSQL   (87.50%)
C. briggsae     MIEAALENPVLIKSQL   (93.75%)
C. tropicalis   MIEAARENPVPVKSQL   (87.50%)
                ***** **** :****
```

Figure 3.1. Structure of *C. elegans* genes encoding LIN-28 and sequence conservation of first exon of *lin-28* isoforms among nematode species

(A) The first exon differs between *lin-28a* and *lin-28b*. The second and third exons are shared by the two isoforms and encode the cold shock domain (CSD) and zinc finger domain (ZFD), respectively. Red triangles show the locations of the spliced leader 1 (SL1) trans-splicing donor sequence (TTTCAG) upstream of each first exon. The expected protein sizes of each isoform were calculated. (B,C) Homology of peptides encoded by the first exon in different nematode species. The sequences were obtained from the UCSC genome browser (https://genome.ucsc.edu/cgi-bin/hgGateway), and amino acids were aligned using the T-coffee program (http://www.tcoffee.org/Projects/tcoffee/). The homology scores compared to *C. elegans* are shown in parentheses.

Expression patterns of *lin-28a* and *lin-28b*

We speculated that the two isoforms might be expressed differently for several reasons. First, they appear to potentially use different promoters for transcription. In the 5' direction upstream of *lin-28,* the closest coding sequence of another gene is 2488 bp away from the start of the first exon of *lin-28a*, and thus, the promoter region of *lin-28a* could be located between these sequences (Fig 3.1A). The first exon of *lin-28b* is 931 bp downstream from the end of the first exon of *lin-28a*, and a sequence in this region might function as the promoter region of *lin-28b* (Fig 3.1A). Nonetheless, we cannot exclude the possibility that *lin-28a* and *lin-28b* are spliced from the same transcript via alternative splicing events. The levels of their cDNAs are likely also affected by the individual splicing efficiency between the first exon of *lin-28a* and *lin-28b* with their second exons. High-throughput RNA sequencing presented in wormbase homepage showed the expression level of the first exon of *lin-28a* was higher than that of *lin-28b* (Fig 3.2A).

To investigate the spatial expression pattern of each isoform, we generated a *lin-28* transcriptional reporter strain with differential fluorescent protein tagging of the two isoforms. We generated a "minigene," which contained the sequence I: 8409314~8412955 of *lin-28*. The minigene included 2488 bp upstream of *lin-28a* up to another coding sequence of F02.E9.7, the first exon of *lin-28a*, the first exon of *lin-28b*, and the first 27 bp of their second exon (Fig 3.2B). Because *lin-28a* and *lin-28b* have the same frame to encode their peptides, splicing with common

second and third exons, we artificially added one base pair inside the first exon of *lin-28b* to change its frame. We added the green fluorescent protein (GFP) coding sequence in the frame with the *lin-28a* coding sequence and the mCherry coding sequence in the frame with the *lin-28b* coding sequence. Therefore, this reporter expresses GFP if *lin-28a* is transcribed and spliced and mCherry if *lin-28b* is transcribed and spliced (Fig 3.2B). Extrachromosomal arrays with this construct showed that GFP and mCherry were co-expressed in neurons, hypodermis, and muscle tissues, indicating that both *lin-28a* and *lin-28b* are expressed in these tissues (Fig 3.2 C-E). Thus, the spatial expression patterns of *lin-28a* and *lin-28b* isoforms appear to be largely identical.

Figure 3.2

A ***lin-28*** **RNA-seq data uploaded in worm base homepage(www.wormbase.org)**

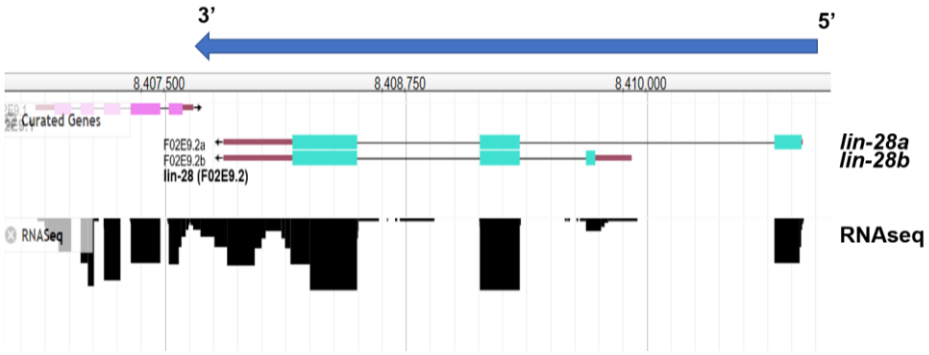

B **Isoform dependent differential expression reporter system**

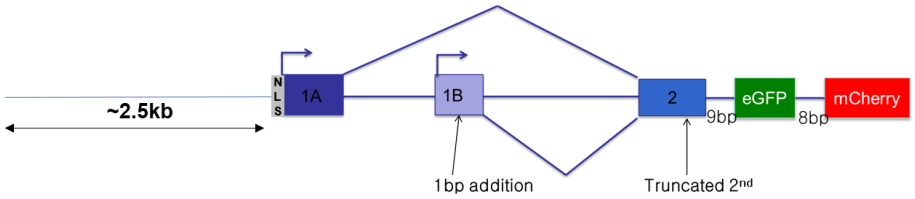

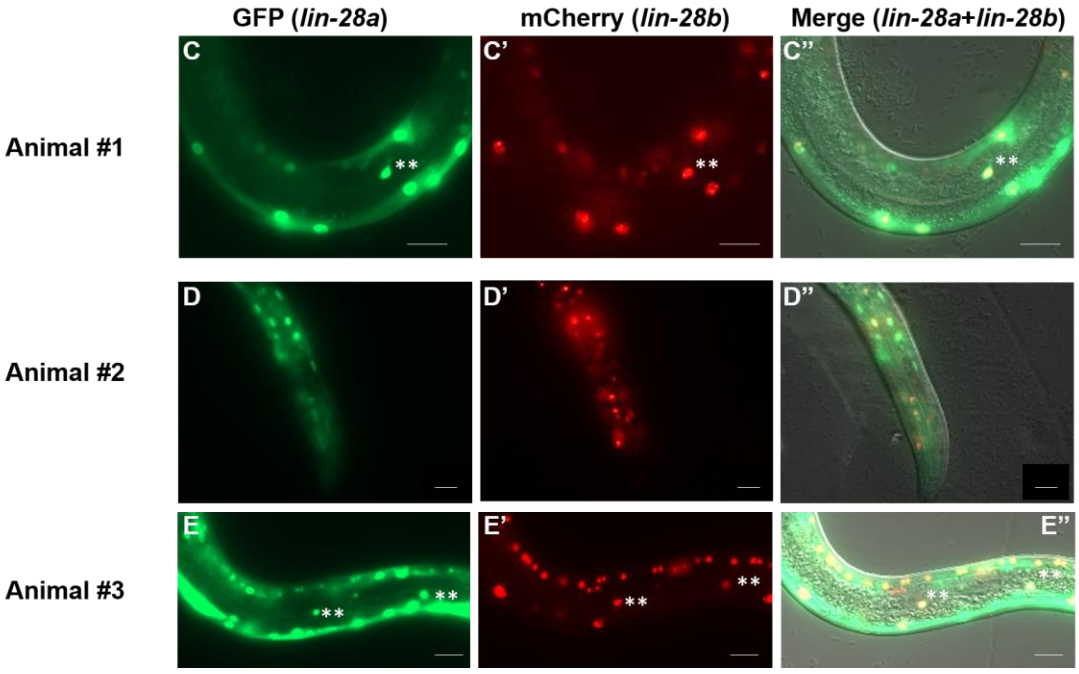

Figure 3.2. Expression patterns of *lin-28a* and *lin-28b*

(A) RNA-seq data presented in wormbase shows that expression of the first exon of *lin-28a* was higher than that of *lin-28b*.(B) “Minigene” structure with expression of GFP or mcherry depending on expression of *lin-28a* or *lin-28b*, respectively. One base pair was added inside the *lin-28b* sequence to make *lin-28b* in frame with mCherry but not GFP. (C-E) Extrachromosomal array expression patterns using “minigene” containing vector in (B). GFP and mCherry expression overlapped in hypodermis (C,E, depicted by **), neural cells (D), and muscle cells (C,E), indicating spatial co-expression of LIN-28 isoforms.

Only *lin-28a* is trans-spliced by SL1 sequence

More than half of *C. elegans* mRNAs are trans-spliced with the 22 nt spliced leader sequence 1 (SL1). Spliceosomes catalyze this trans-splicing, connecting the 5' splice leader of the 100-bp SL1 RNA to a 5' exon of the pre-mRNA, and in the process removing 5' ("outtron") sequences from the pre-mRNA (Blumenthal, 2012) (Fig 3.3A). The sequence TTTCAG, which can be transcribed to the 3' splice splice acceptor sequence UUUCAG (Conrad et al., 1991; Conrad et al., 1993), is found 1 bp upstream of the first codon of *lin-28a* and 705 bp upstream of the first codon of *lin-28b* in the *C. elegans* genome (Fig 3.1A). To determine whether either of the *lin-28* isoforms is trans-spliced by SL1, we conducted reverse transcription polymerase chain reaction (RT-PCR) experiments. We generated cDNA pools from mixed stage *C. elegans* hermaphrodites. PCR using the SL1 sequence-specific primer and a primer specific to each isoform showed that cDNA was amplified with the *lin-28a* specific primer, but not with the *lin-28b* specific primer (Fig 3.3B). We confirmed that the sequence of the amplified product was matched to SL1 spliced *lin-28a* as expected by Sanger sequencing. This result indicates that only *lin-28a* is trans-spliced by the SL1 sequence. The 5' cap of the SL1 leader sequence is tri-methylated rather than mono-methylated (Hastings, 2005). Thus, only *lin-28a* mRNA may contain a tri-methyl guanosine cap, which may induce a subsequent translational process that differs from those of *lin-28b* mRNA.

Figure 3.3

A

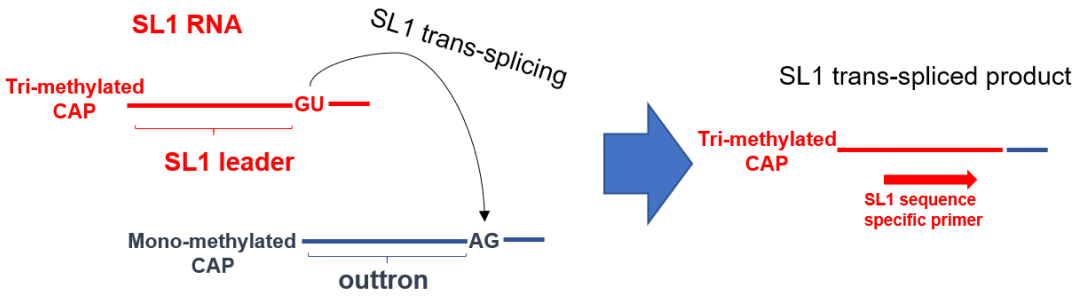
SL1 RNA
SL1 trans-splicing
Tri-methylated CAP
GU
SL1 leader
Mono-methylated CAP
AG
outtron
SL1 trans-spliced product
Tri-methylated CAP
SL1 sequence specific primer

B

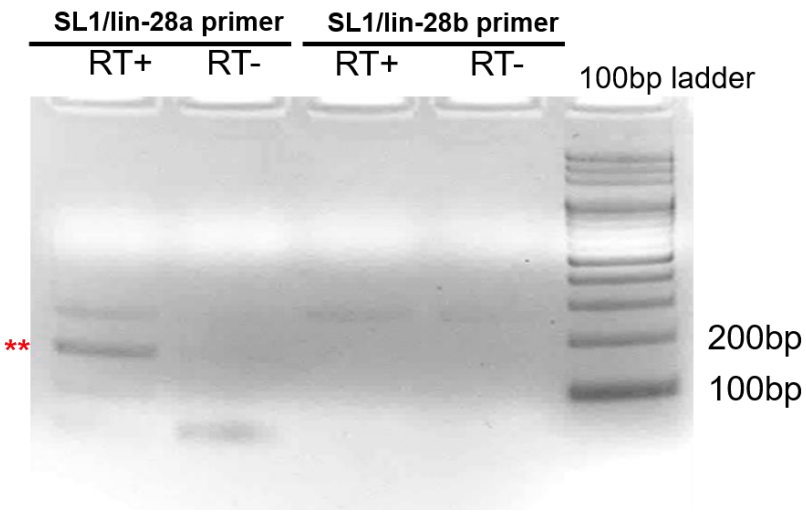
SL1/lin-28a primer
SL1/lin-28b primer
RT+
RT-
RT+
RT-
100bp ladder
**
200bp
100bp

Figure 3.3. *lin-28a* transcripts are SL-1 trans-spliced.

(A) Schematic representation of SL-1 trans-splicing process. More than half of *C. elegans* transcripts are trans-spliced with the SL1 leader sequences, which contain a tri-methylated 5' cap. (B) RT-PCR results using cDNA of wild-type *C. elegans* hermaphrodites. PCR was performed with primer binding to the SL1 leader sequence and each isoform-specific primer. PCR band is only amplified with the SL1 primer/*lin-28a* specific primer set (**). This band was purified and confirmed by Sanger sequencing.

Construction of *lin-28a(lf)* and *lin-28b(lf)* mutants

To investigate the functions of *lin-28a* and *lin-28b*, we generated loss of function mutants of each isoform, *lin-28a(lf)* and *lin-28b(lf)*, using CRISPR-Cas9 technology. We obtained a mutant with a 4-bp deletion *(ma289)* in the coding sequence of the first *lin-28a*-specific exon and a mutant with a 4-bp deletion *(ma331)* in the coding sequence of the first *lin-28b*-specific exon (Fig 3.4A).

The *ma289* and *ma331* 4 bp deletions are expected to express frame-shifted peptides of LIN-28A or LIN-28B respectively, leading to isoform-specific early translational termination. We performed western blotting of mixed stage animals using LIN-28 anti-serum to assess expression of *lin-28a* and *lin-28b* in the mutants. The western blot pattern of LIN-28 in wild-type *C. elegans* consisted of two bands, an upper band between 26 kD and 37 kD and a lower band between 19 kD and 26 kD. This pattern is consistent with immunoblots obtained using LIN-28 antibody in previous studies (Morita and Han, 2006; Seggerson et al., 2002). The predicted molecular weights of LIN-28a and LIN-28b are 25.47 kD and 21.79 kD, respectively (Fig 3.1A), suggesting that the faster-running band on the western blot (“B” in Fig 3.1A) corresponds to LIN-28B, and the slower running band corresponds to LIN-28A (apparently running slower than expected for unknown reasons). These assignments appear to be correct, as the upper band is absent in *lin-28a(ma289),* and the lower band is absent in *lin-28b(ma331).*

Figure 3.4

A

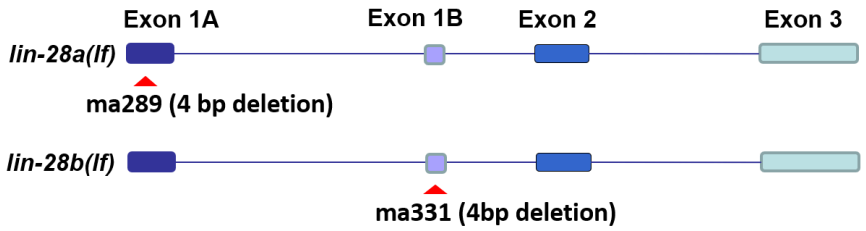

lin-28a (ma289)

wt: atgtcgacggtagtatcg**gagg**gaaggaatgatgggaataa……gaggctcccg

ma289:atgtcgacggtagtatcg____gaaggaatgatgggaataa……gaggctcccg

lin-28b (ma331)

wt: atgattgaagccgct**ttgg**agaatccggtgcccatcaaatctcaattg

ma331: atgattgaagccgct____agaatccggtgcccatcaaatctcaattg

B

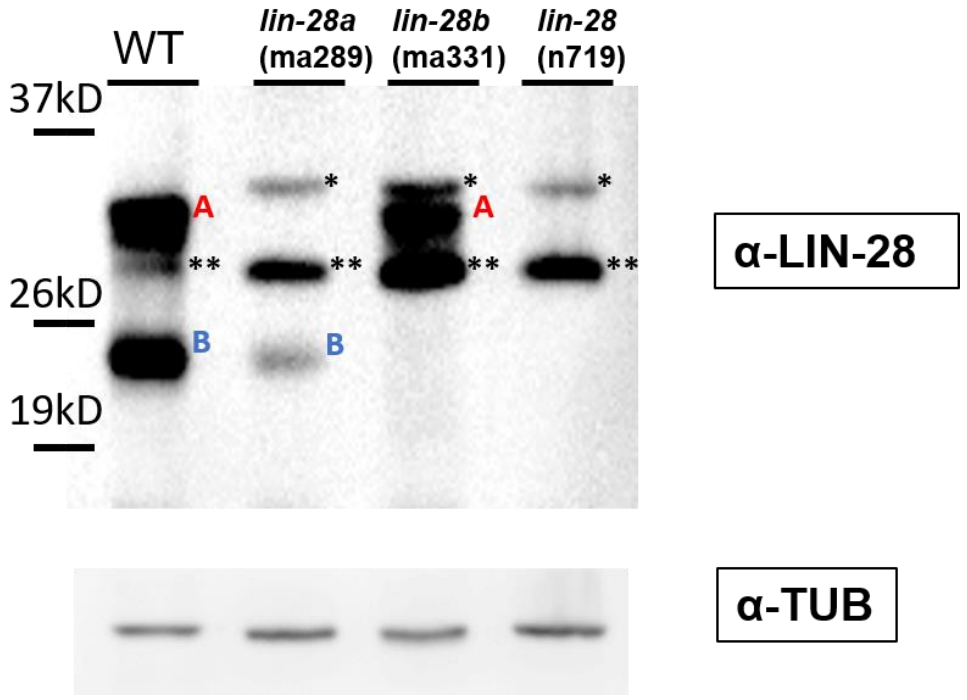

Figure 3.4. Generation of isoform-specific knockout mutants

(A) *lin-28a(ma289)* and *lin-28b(ma331)* mutants were obtained using CRISPR-Cas9 technology. The 4-bp deleted sequences are shown and were expected to cause a frame shift mutation in each isoform (wt=wild type). (B) Western blot analysis of wild-type, *lin-28a(ma289)*, *lin-28b(ma331),* and *lin-28(n719)* using anti-LIN-28 antiserum. Wild-type showed two major bands (A,B), whereas each isoform mutant had only one major band (A or B). *lin-28(n719)* putative null mutant was used as a negative control. Two non-specific bands (* and **) were present for the null mutant control.

Heterochronic phenotypes of *lin-28a(lf)* and *lin-28b(lf)* mutants

We investigated whether the *lin-28a(lf)* and/or *lin-28b(lf)* mutants exhibited the developmental timing defects found in *lin-28(lf)* mutants. Both ventral and lateral hypodermal tissues exhibit developmental defects in *lin-28(0)* mutants(*lin-28(0)* stands for the null mutant *lin-28(n719)*) due to the skipping of the L2 larval stage. *lin-28(0)* mutants do not develop a proper vulva, resulting in complete inability to lay eggs (Euling and Ambros, 1996). The *lin-28(0)* vulva protrudes outside, which is a morphological characteristic of the mutants. Both *lin-28a(lf)* and *lin-28b(lf)* mutants developed a normal vulva and laid embryos as efficiently as wild-type (Fig 3.5). Next, we tested whether one wild type copy of either isoform is sufficient for the development of a functional vulva (Fig 3.6A). To determine this, we first crossed *lin-28(0)* with wild type to obtain heterozygous (*lin-28(0)*/+) males. Then, the heterozygous males were crossed with *lin-28(0)*, or *lin-28a(lf)*, or *lin-28b(lf)* homozygous mutants. From these crosses, we obtained *lin-28(0)/*+, *lin-28a(lf)/lin-28(0)*, and *lin-28b(lf)/lin-28(0)* F1 progeny with a normal vulva and cloned individual animals. We selected F1 heterozygote mutants with a *lin-28(0)* copy, based on their producing *lin-28(0)* homozygous F2s with protruding vulvae (Fig 3.6A). The ratios of animals with a normal vulva to those with a protruding vulva were calculated among F2 self-progeny from individual F1 heterozygotes. If any population of heterozygous F2 (*lin-28(0)/*+, *lin-28a(lf)/lin-280f)*, or *lin-28b(lf)/lin-28(0)*) developed a protruding vulva, the percentage of animals with a protruding vulva was expected to be more than 25% among all F2 animals.

However, the percentages of animals with a protruding vulva among F2s from all three heterozygous F1s were not greater than 25%. This result suggests essentially all of the heterozygous animals (*lin-28(0)/*+, *lin-28a(lf)/lin-28(0)*, or *lin-28b(lf)/lin-28(0)*) develop a normal vulva and lay embryos, indicating that one copy of either *lin-28* isoform is sufficient for vulval development (Fig 3.6B).

Figure 3.5

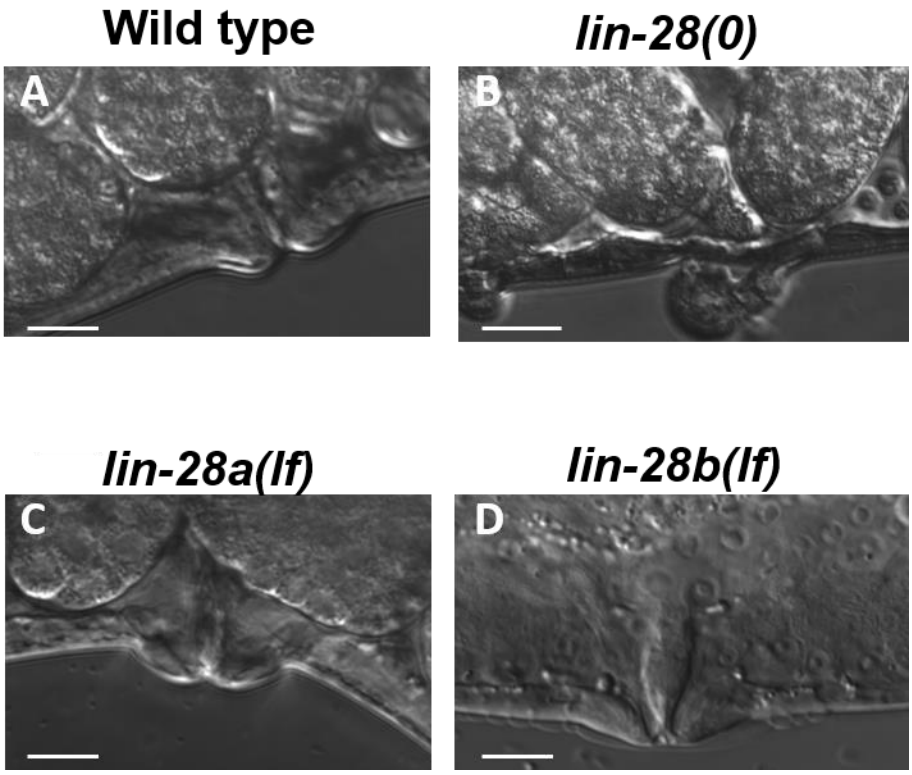

Figure 3.5 Vulval morphology of *lin-28* isoform mutants

Vulval morphology of (A) wild type, (B) *lin-28(0)* mutant, (C) *lin-28a(lf)* mutant, and (D) *lin-28b(lf)* mutant. *lin-28* isoform mutants (C,D) did not show the same vulval defects that the *lin-28(lf)* mutant did (B).

(*lin-28(0)* stands for the null mutant *lin-28(n719)*, *lin-28a(lf)* for *lin-28a(ma289)* and *lin-28b(lf)* for *lin-28b(ma331)*)

Figure 3.6

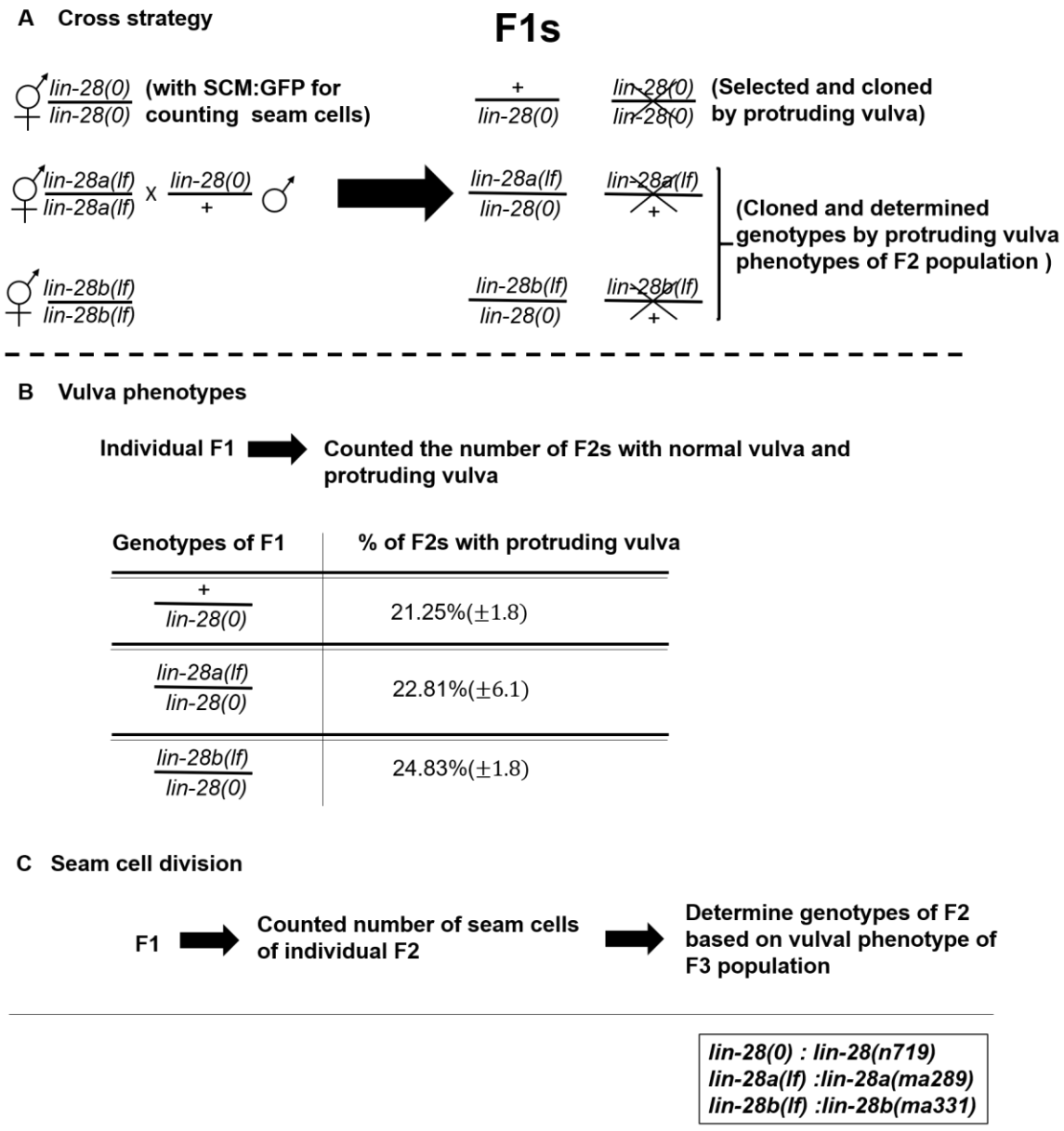

Genotypes of F1	% of F2s with protruding vulva
+ / *lin-28(0)*	21.25%(±1.8)
lin-28a(lf) / *lin-28(0)*	22.81%(±6.1)
lin-28b(lf) / *lin-28(0)*	24.83%(±1.8)

lin-28(0) : lin-28(n719)
lin-28a(lf) :lin-28a(ma289)
lin-28b(lf) :lin-28b(ma331)

Figure 3.6 Experiments for testing haploinsufficiency of *lin-28* isoforms for vulval development and seam cell division

(A) Schematic representation of genetic strategy to obtain heterozygous mutants of *lin-28* isoforms. Homozygous mutants of *lin-28* and its isoform mutants were crossed with *lin-28* heterozygous males to obtain heterozygous F1. We selected heterozygous strains with the *lin-28(0)* allele based on their F2 phenotypes for isoform mutants. (B) To determine whether either isoform showed haploinsufficiency for vulval development, individual F1s were cloned and their number of progeny based on their vulva phenotype was counted. The percentage of F2 animals with a protruding vulva was not more than 25% for all heterozygotes. (C) For seam cell division, individual F2 animals of F1 heterozygous mutants were cloned and their seam cell numbers were counted. Their genotypes were determined based on their F3 vulva phenotypes.

Seam cells are specialized hypodermal structures, which are embedded in hyp7 syncytium, and they are connected to the hypodermis. When an animal hatches,10 seam cells are located laterally on each side of the animal. After the cell divisions that occur during the larval stages, 16 seam cells reside in each side of the L4 animal. *lin-28(0)* mutants skip the L2-specific hypodermal cell division that includes a proliferative cell division of 5 seam cells (See Fig 1.2). As a result, the mutants show a reduced number of seam cells at the adult stages (Ambros and Horvitz, 1984c). We counted the seam cell numbers in *lin-28a(lf)* and *lin-28b(lf)* mutants at the L4 stage using the SCM:GFP reporter, which was expressed in seam cells. At 20°C, both *lin-28a(lf)* and *lin-28b(lf)* mutants showed an average of 16 seam cells, identical to the wild type. The average seam cell number in the *lin-28(0)* mutant at the adult stage by SCM:GFP was 11, as previously reported (Fig 3.7A). We also investigated the seam cell number at 25°C and found that neither the *lin-28a(lf)* or *lin-28b(lf)* mutants showed a reduction in seam cell number (Fig 3.7B).

To test for haploinsufficiency for seam cell division, we generated heterozygous mutants of *lin-28(0)* and each isoform (*lin-28(0)*/+, *lin-28a(lf)/lin-28(0)*, and *lin-28b(lf)/lin-28(0)*) as described above with SCM:GFP reporters (Fig 3.6A,C). We counted seam cell numbers in individual F2s at their L4 stages and later determined their genotype by progeny test. Wild type, *lin-28a(lf)*, and *lin-28b(lf)* homozygotes contained 16 seam cells on average as expected, while an average of 12 seam cells were detected in *lin-28(0)* homozygous mutants. Both *lin-28(0)*/+

and *lin-28b(lf)*/*lin-28(0)* heterozygotes had an average of 16 seam cells. However, the average seam cell number in the *lin-28a(lf)*/*lin-28(0)* mutant was 14, which was mildly but still significantly lower than that in wild type (Fig 3.7C). In summary, these results suggest that one copy of the *lin-28a* isoform is sufficient to execute the seam cell divisions that occur in wild type. However, one copy of *lin-28b* is not sufficient for robustly normal seam cell division patterns, although two copies of *lin-28b* can substitute for normal *lin-28* function. This result shows that *lin-28b* is haplo-insufficient for proper stage-specific seam cell division patterns.

Figure 3.7

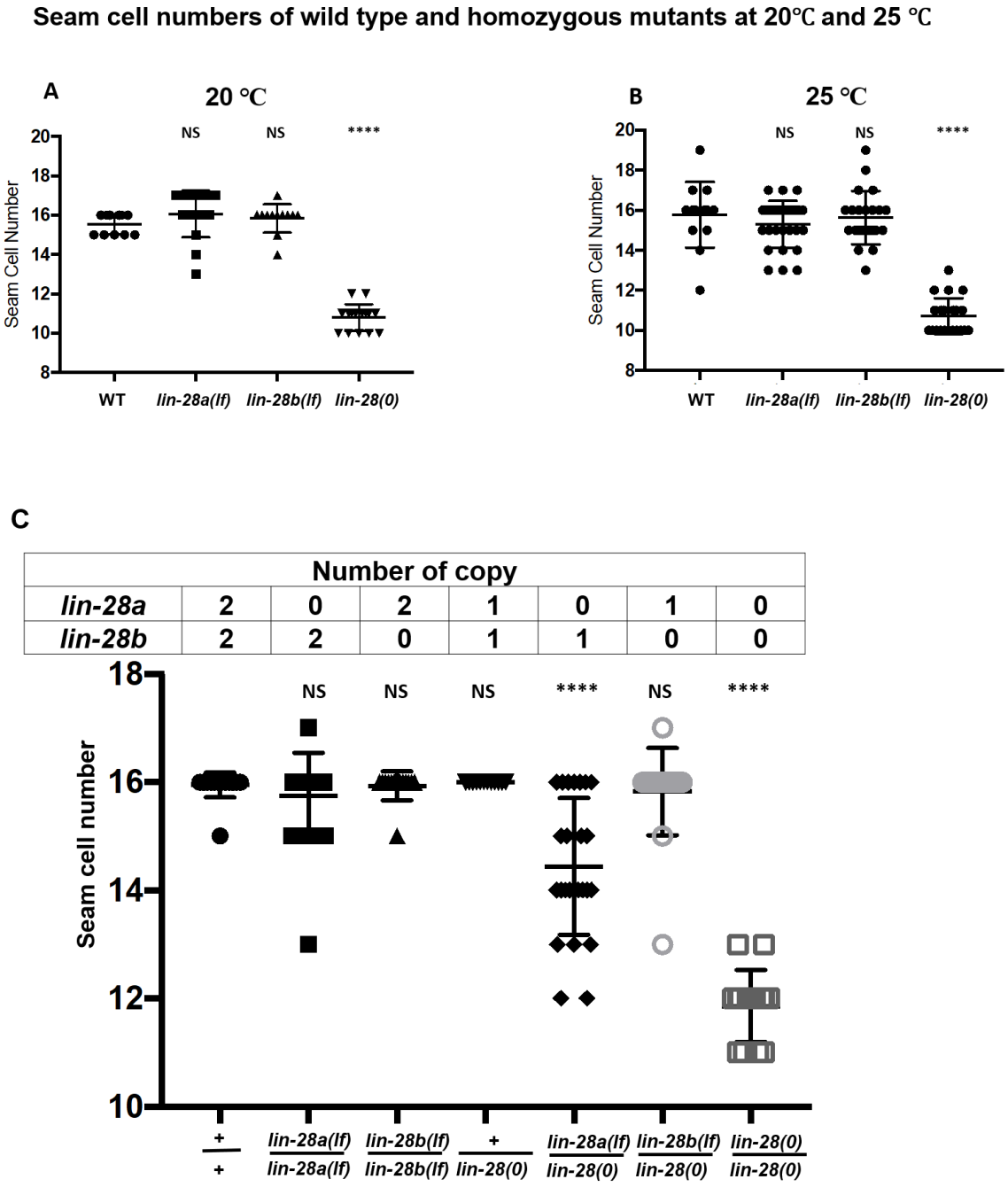
Seam cell numbers of wild type and homozygous mutants at 20℃ and 25 ℃
A
20 ℃
Seam Cell Number
NS
NS
****
WT
lin-28a(lf)
lin-28b(lf)
lin-28(0)
B
25 ℃
C
Number of copy
lin-28a 2 0 2 1 0 1 0
lin-28b 2 2 0 1 1 0 0
Seam cell number
+/+
lin-28a(lf)/lin-28a(lf)
lin-28b(lf)/lin-28b(lf)
+/lin-28(0)
lin-28a(lf)/lin-28(0)
lin-28b(lf)/lin-28(0)
lin-28(0)/lin-28(0)

Figure 3.7. Seam cell numbers in *lin-28(0)*, *lin-28a(lf)*, and *lin-28b(lf)* mutants as well as their heterozygous mutants

(A,B) Seam cell numbers in *lin-28(0)*, *lin-28a(lf)*, and *lin-28b(lf)* homozygous mutants were counted at 20°C (A) and 25°C (B). Both isoform mutants exhibited an average of 16 seam cells, similar to wild type. (C) Seam cell numbers of heterozygous mutants of *lin-28* and its isoforms were counted at 20°C as shown in Fig 3.6. Mutants of all genotypes had seam cell numbers comparable to wild type, except for *lin-28b(lf)* heterozygotes (*lin-28b(lf)/lin-28(0)*) and the *lin-28(lf)* homozygous mutant. (unpaired t-test compared to wild type (WT), NS: not significant, ****p<0.001)

Redundant functions of *lin-28* isoforms in fertility, embryonic phenotype, and somatic gonadal development

In addition to heterochronic defects, *lin-28(0)* mutants also exhibited defects in fertility, embryonic lethality, and somatic gonadal development (Chapter II). We investigated whether either isoform-specific mutant shows these defects. Both *lin-28a(lf)* and *lin-28b(lf)* produced similar numbers of progeny compared with wild type at 25°C, suggesting both isoforms are redundant for fertility function (Fig 3.8A). Also, both *lin-28a(lf)* and *lin-28b(lf)* embryos were oval-shaped similar to wild type and differing from the irregular misshapen *lin-28(lf)* embryos (Fig 3.8B). Consistent with this observation, the embryonic viability of each mutant was comparable to wild type at 25°C (Fig 3.8C). These data suggest that each isoform is sufficient for embryonic morphogenesis and viability.

We also examined the formation of the uterine lumen in isoform mutants (Fig 3.9). The defect in uterine lumen formation is an example of a somatic gonadal abnormality in *lin-28(0)* mutants. However, both the *lin-28a(lf)* and *lin-28b(lf)* mutants formed a normally connected lumen during the L4 stage, implying redundant function of *lin-28a* and *lin-28b* in somatic gonadal development.

Figure 3.8

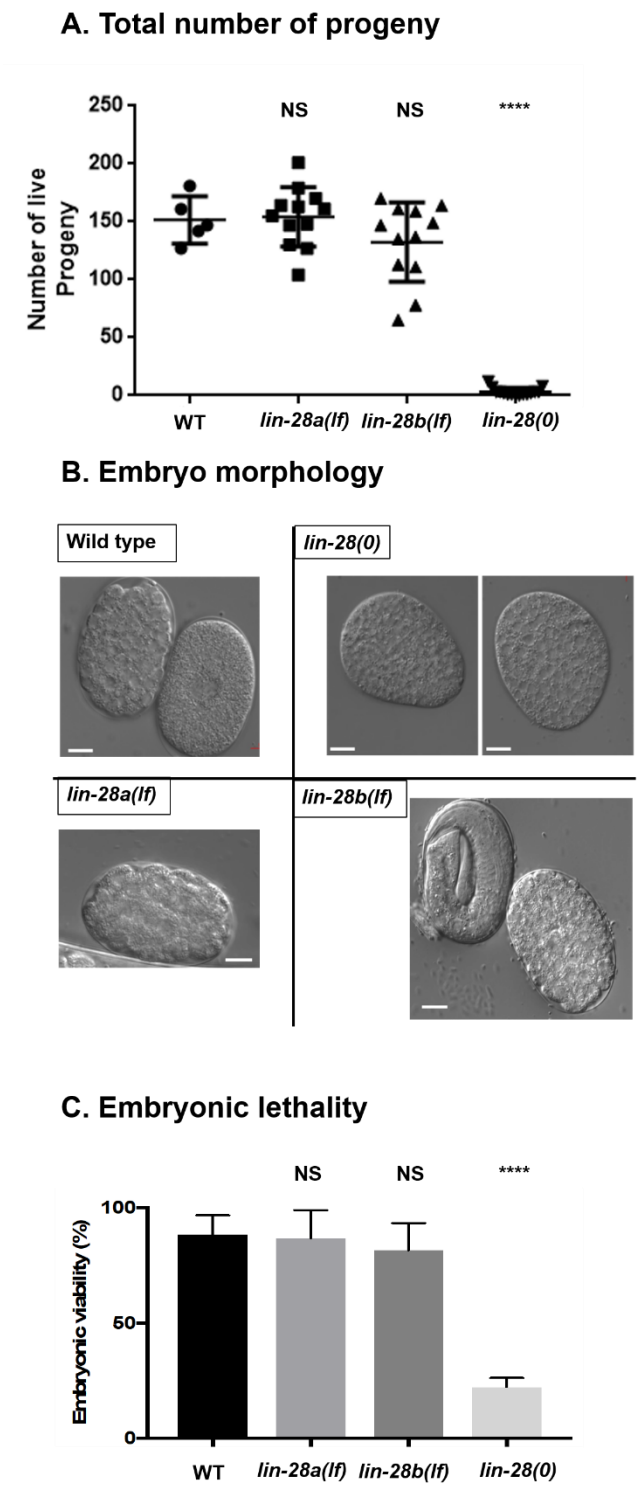
A. Total number of progeny
Number of live Progeny
250
200
150
100
50
0
NS
NS
****
WT
lin-28a(lf)
lin-28b(lf)
lin-28(0)
B. Embryo morphology
Wild type
lin-28(0)
lin-28a(lf)
lin-28b(lf)
C. Embryonic lethality
Embryonic viability (%)
100
50
0
NS
NS
****
WT
lin-28a(lf)
lin-28b(lf)
lin-28(0)

Figure 3.8. Fertility and embryonic phenotypes of isoform mutants

(A) Total number of progeny of *lin-28* and its isoform mutants at 25°C (unpaired t-test compared to wild type, ns: not significant, ****p<0.001). (B) Embryonic morphology of isoform mutants (images of wild type and *lin-28(lf)* mutant embryos were adapted from Figure 2.8A). (C) Embryonic lethality of *lin-28(lf)* mutant and the isoform mutants (number of animals ≥15 per each assay; number of independent replicate assays = 3, unpaired t-test compared to wild type(WT), ****p<0.001).

Figure 3.9

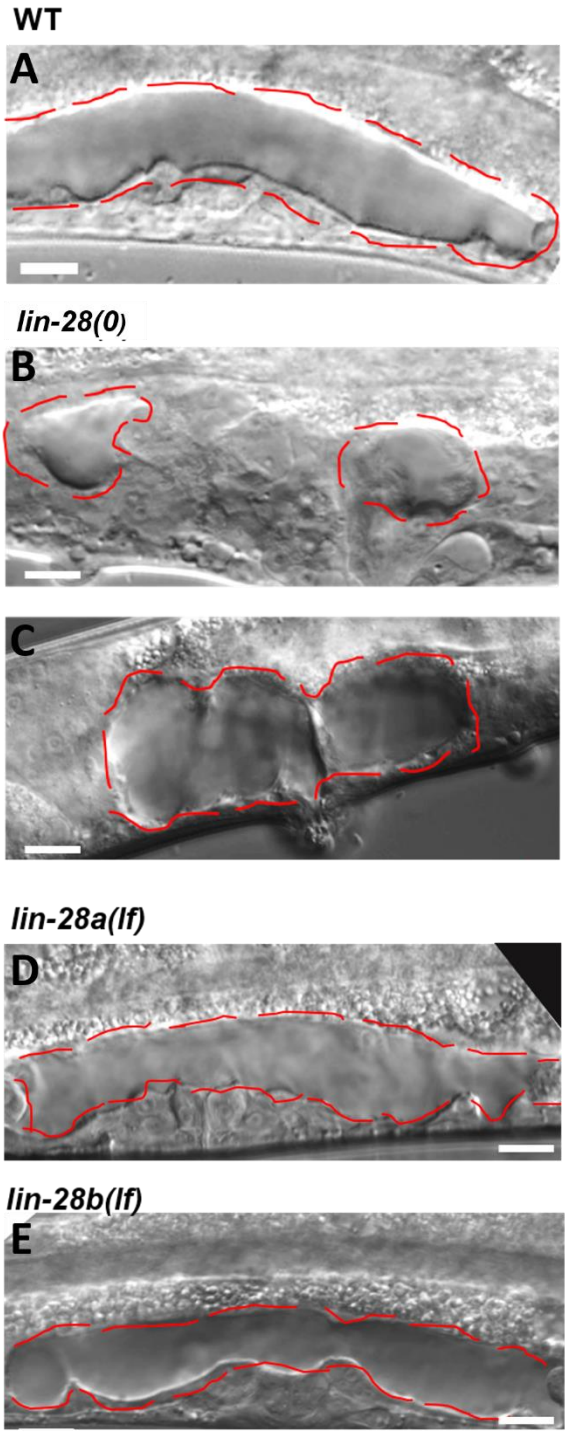

Figure 3.9. Uterine lumen formation in isoform mutants

Uterine lumen formation of (A) wild type (mid L4 stage), (B,C) *lin-28(lf)* mutant (L4 stage, see Figure 2.11 for stages of *lin-28(lf)* mutants), (D) *lin-28a(lf)* mutants (mid L4 stage), and (E) *lin-28b(lf)* mutants (mid L4 stage). ((A-C) are adapted from Figure 2.5 for comparison with (D, E).)

Discussion

Two mammalian paralogs of Lin-28 regulate *let-7* expression by distinct mechanisms, and each paralog is also highly expressed in different subtypes of cancer cell lines (Piskounova et al., 2011). Although *C. elegans* do not have paralogs of *lin-28*, they express two isoforms of LIN-28 from the same locus, and the potential differences in expression and function those isoforms have not been investigated previously. Here, we constructed differential reporter strains for the isoforms and generated isoform knockout mutants using CRISPR-Cas9 to study the expression and function of each isoform.

Our analysis of *lin-28a* and *lin-28b* expression patterns showed that the two isoforms are co-expressed in the hypodermis, neurons, and muscles, indicating that their spatial expression patterns are not appreciably distinct, consistent with our finding that they function redundantly in the hypodermis. The *lin-28a(lf)* and *lin-28b(lf)* mutants did not show defects of vulval morphogenesis or egg-laying capacity. In addition, the seam cell number in each mutant was comparable to that in wild type, not to the *lin-28(lf)* mutants. However, our results suggest that expression of one copy of *lin-28b* is not sufficient to produce the number of seam cells found in wild type. This might imply that the function of *lin-28b*, not *lin-28a*, cannot fully substitute the function of wild-type *lin-28* to execute seam cell division. Another possibility is that this result simply reflects a lower level of *lin-28b* expression compared with *lin-28a*. RNA sequencing data from a previous study shows that *lin-28b* expression is lower than *lin-28a* expression (Fig 3.2A).

Intriguingly, our western blot analysis showed that the LIN-28B protein level was decreased in *lin-28a(lf)* mutants (Fig 3.4B). The effects of a 4-bp deletion in the first exon of *lin-28a* on the expression of *lin-28b* should be further investigated. Nonetheless, it is evident that the two isoforms function almost redundantly in seam cell division. The average number of seam cells in *lin-28b* heterozygous mutant (*lin-28b(lf)/lin-28(0)*) was approximately 14, which is significantly higher than that in *lin-28(0)* homozygous (*lin-28(lf)/lin-28(lf)*) mutants. The two isoform mutants did not show apparent defects in fertility, embryo viability, or somatic gonadal development.

Despite the overall redundancy of the *lin-28* isoforms, several aspects of the *lin-28* isoforms deserve further investigation. First, it will be interesting to study the functions of the different isoforms under various stress conditions. Alternative splicing often occurs under oxidative stress and heat-shock in mammals and plants (Ding et al., 2014; Takechi et al., 1994; Takeo et al., 2009). In addition, the subcellular locations of the isoforms have not been determined yet. The mammalian Lin-28 paralogs have different subcellular locations, although both contain CSD and ZKD in common (Piskounova et al., 2011). This is due to the functional nuclear localization signal in Lin-28B, which neither *C. elegans lin-28* isoform possesses. However, either one or both of the isoforms are expected to be located in the nucleus, based on their nuclear function of inhibiting *let-7* (Van Wynsberghe et al., 2011). Through these studies, the physiological roles and the molecular characteristics of each isoform will be further elucidated.

Material and Methods

Construction of differential reporter strain

To construct the “minigene” which contains differential reporter, we first amplified I: 8411465~8412955 of *C. elegans* genome using primer SW136, SW137, SW138, SW139 (Sequences are in Table 3.1.). SW136 contains sequences complementary to the 1st exon of *lin-28a* with XhoI site, and SW137 contains sequences complementary to first 27bp of the 2nd exon of *lin-28* with NotI site. SW138 and SW139 contains sequences complementary to the 1st exon of *lin-28b* of opposite strands, but each contains C(SW138) and G(SW139) inside the 1st exon of *lin-28b*. PCRs were performed with SW136/SW139 (Fragment A), and SW138/SW137 (Fragment B) using genomic DNA as a template. Then overlapping PCR was performed with SW136/SW137 using prior PCR products (Fragment A and Fragment B) as templates. Then this overlapped PCR product was subcloned into pWASR1 (Gift from John Calarco, University of Toronto) using XhoI and NotI (pSW24). Finally, we performed LR reaction using Gateway® Technology (Invitrogen, cat 12535-019) with 1) pSW24 (attL1-minigene-attL2), 2) pSW33 (attL4-*lin-28* 2.5kb promoter-attR1), and 3) the vector containing unc-54 3’UTR (attR2-*unc-54* ’3 UTR-attL3) to construct pSW41 (Fig 3.10). After construction, we injected mixture of 50µg/µl of pSW41 and 50µg/µl of pRF4(*rol-6(su1006)*) and screened for extrachromosomal array containing strains which are roller with GFP and mCherry expression.

Table 3.1 List of primers and sequences used in this study

Primers		Sequences
SW136	XhoI+ lin-28 gene-Nterm	ggctcgag tcgacggtagtatcggagg
SW137	NotI + lin-28 2nd exon truncated-Cterm	gggcggccgc tgagccaaagtatcgaggtg
SW138	lin-28 1st alternative exon overlapping F	attgaagccgctttgg c agaatccggtgcccatc
SW139	lin-28 1st alternative exon overlapping R	caccggattct g ccaaagcggcttcaatcat
SW181	lin-28a specific primer R	Tgttggtgacgggagcc
SW182	lin-28b specific primer R	Gtgttggtgacaattgaga
SW183	SL1 specific primer F	Ggtttaattacccaagtttgag
SW188	lin-28 RT primer	Ctacctttccattcgatcgctc

Figure 3.10. Plasmid map of pSW41

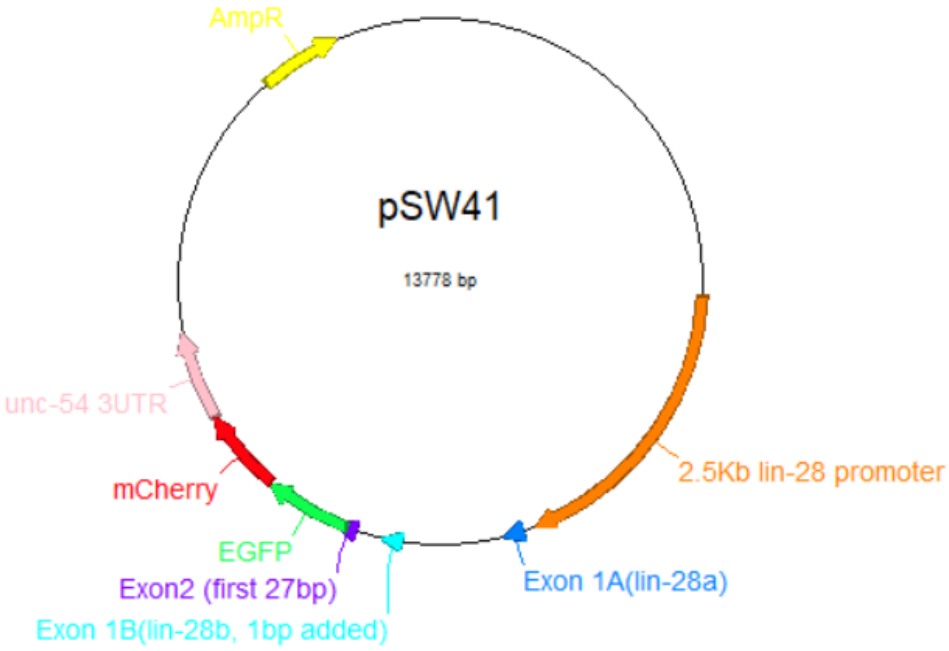

Generation of mutants using CRISPR-Cas9

To generate the *lin-28a* and *lin-28b* mutants, we designed guide sequences as follows: *"*cgacggtagtatcggaggga" for targeting *lin-28a* and "gggcaccggattctccaaag" for targeting *lin-28b*. We cloned the vector which expresses these guide RNAs using protocol in (Friedland et al., 2013). We used the *dpy-10* guide expression vector (Arribere et al., 2014) or *unc-22* guide expression vector as a co-CRISPR markers (Kim et al., 2014). We injected 1) P*eft-3*::Cas-9 expression vector (50ug/ul), 2) *unc-22* or *dpy-10* guide RNA expression vector (50ug/ul), 3) *lin-28a* or *lin-28b* guide RNA expression vector (50ug/ul), and 4) sur-5:GFP expression marker as injection marker (15ug/ul). And we screened F1 animals which have roller/ twitcher (*unc-22(lf)*) or dumpy (*dpy-10(lf)*) phenotypes and clone them to produce F2s. We obtained 10 dumpy F2 animals (from 3 F1s) from P0 injected with *dpy-10* targeting guide and *lin-28a* targeting guide, and among them *lin-28a(ma289)* was identified by Sanger sequencing. We obtained 15 twitcher F2 animals (from 2 F1s) from P0 injected with *unc-22* targeting guide and *lin-28b* targeting guide, and among them *lin-28b(ma331)* was identified by Sanger sequencing.

Culture of *C. elegans* strains

C. elegans wild type (Strain N2) and mutant and reporter strains (*lin-28(n719)*, *lin-28(ma289)*, *lin-28(ma331), lin-28(n719);SCMp:GFP, lin-28(ma289);SCMp:GFP,*

lin-28(ma331);SCMp:GFP) were grown and maintained (at 20 ^{o}C or 25^{o}C) on nematode growth media (NGM) agar plates seeded with *E. coli* (strain HB101). Synchronized populations of larvae at defined developmental stages were obtained as described in Chapter II.

RT-PCR

RNA samples are extracted using mixed-stage N2 animals using TRIzol (Invitrogen Cat No. 15596026), then reverse transcription was done using SuperScript II (Invitrogen,Cat No.18064) following their protocols. *lin-28* specific reverse primer (SW188) was used as a RT-primer The PCR was performed with a SL-1 specific primer (SW183) with either lin-28a specific primer (SW181) or lin-28b specific primer (SW182).

Western Blot

Lysates of mixed staged animals of wild type*, lin-28a(ma289)*, *lin-28b(ma331)*, and *lin-28(n719)* mutants were obtained using lysis buffer composed of 1% NP40, 150mM Nacl, 50mM Tris-Cl(pH8.0), 5mM EDTA, 0.1% of 1M Dithiothreitol, phosphatase inhibitor cocktail (“PhosSTOP“, Roche, Cat No.04906 845 001), and protease inhibitor cocktail (“Complete”, Roche, Cat No. 11 697 489 001). One of each inhibitor cocktail was added for 5ml of lysis buffer. 2X volume of lysis buffer

was added and sonicated. Samples were boiled and loaded on a 15% SDS-polyacrylamide gel. After electrophoresis for 2 hr at 100V, the gel is transferred to PDVF membrane (Thermo science, LC2005). For anti-LIN-28, LIN-28 antisera (used in (Seggerson et al., 2002)) and anti-rabbit antibody (Sigma, Cat. GENA934) were used for primary and secondary antibody. For tubulin, anti-tubulin antibody (Sigma, Cat No.T9822) and anti-mouse antibody(Biorad, Cat 172-1011) were used for primary and secondary antibody.

Microscopy

For DIC and fluorescence microscopy, worms were anesthetized with 0.2mM levamisol and mounted on 2% agarose pads. All images were obtained with a ZEISS Axiocam 503 mono.

Chapter IV. Discussion

- Summary

- Future Directions

1) Remaining questions (Regarding Chapter II & Chapter III)

2) Role of *lin-28* in remodeling Dorsal-D type neurons of *C. elegans*

3) *In vivo* functions of two RNA binding domains in LIN-28

Summary

We investigated two aspects of *lin-28* regulation of *C. elegans* development.

First, we examined how *lin-28* regulates somatic gonadal development and fertility in *C. elegans* hermaphrodites. We demonstrate that *lin-28(lf)* mutants exhibit fertility defects caused by the abnormality of somatic gonadal development including Sp-Ut valve core cell morphogenesis. *lin-28(lf)* mutants also show embryonic lethality. We found evidence that the lack of egg shell integrity of *lin-28(lf)* embryos contributes the embryonic lethality and its association with the defects of spermathecal exit process.

However, the timing of somatic gonadal development in *lin-28(lf)* mutants is essentially normal, despite precocious hypodermal development in the mutants. This discrepancy of developmental timing is an example of “heterochrony” between somatic gonad and hypodermis. Moreover, abnormal morphology of *lin-28(lf)* mutants is restored to normal not by somatic gonadal expression, but by hypodermal expression of *lin-28*. Consistently, the genes downstream of *lin-28* in the regulation of hypodermal developmental timing, including *let-7*, *hbl-1*, *lin-46*, and *lin-29* are also involved in somatic gonadal development. Therefore, our study presents a phenomenon where normal development of one tissue requires properly timed development of other interacting tissues.

Our second project was to characterize expression and the roles of two isoforms of *lin-28* in *C. elegans.* Our study showed that two isoforms have similar

spatial expression patterns. We also confirmed that only *lin-28a* is trans-spliced with SL1 leader sequence. Next, we generated *lin-28a* and *lin-28b* knock out mutants to investigate their phenotypes. Neither isoform mutant exhibit apparent defects in vulva morphology, seam cell division, fertility or somatic gonadal development found in *lin-28(lf)* mutant. This finding indicates the redundant function of *lin-28a* and *lin-28b* in these phenotypes, in line with their overlapped spatial expression patterns. However, *lin-28b*, not *lin-28a*, displayed a partial haplo-insufficiency with regard to specification of the L2-specific seam cell symmetric division. This result reflects either minor functional difference of two isoforms or merely different levels of expression.

Future Directions

1) Remaining questions (Regarding Chapter II & Chapter III)

We do not understand the mechanism by which hypodermal development of *C. elegans* affects somatic gonadal development. Although the utse is the tissue which physically connects hypodermal seam cells to somatic gonads, our data suggest that the absence of utse does not appear to affect Sp-Ut valve core cell morphogenesis (see Discussion in Chapter 2). Nonetheless, it will be still worth to examine the timing and execution of physical connections between the seam cell and somatic gonad in *lin-28(lf)* mutants compared to the wild type, using electron microscopy of precisely-staged fourth stage animals.

Factors involved in the signaling between hypodermis and somatic gonad may be identified by genetic screens. We can generate pools of candidate mutants by treating *lin-28(lf)* mutants with ethyl methanesulfonate (EMS) or N-ethyl-N-nitrosourea (ENU), then screen the animals which show normal Sp-Ut valve core cell morphology. One caveat of this suppressor screening is that many alleles of known *lin-28* downstream genes in heterochronic pathway such as *lin-46*, *let-7*, or *lin-29* will be also identified as the results of the screening. However, it is possible that unknown signaling factors can be uncovered as a result of this screening, which will elucidate the communication process between different tissues.

Two *lin-28* isoforms of *C. elegans* can be further investigated in their expression patterns and physiological roles. First, we can examine their temporal

expression patterns during larval development. Levels of *lin-28* transcripts are consistent during all larval stages, whereas LIN-28 protein level decreases drastically from the 2nd larval stage (Seggerson et al., 2002). It is still unknown whether the two isoforms have similar expression profiles or exhibit distinct patterns of temporal expression. In addition, subcellular location of each isoform has not been investigated. For this purpose, the separation of cytoplasm and nucleus followed by western blot analysis can be done with *lin-28(lf)*, *lin-28a(lf)*, *lin-28b(lf)* mutants, and wild type animals. Previous reporter analysis showed that LIN-28:GFP localizes predominantly to the cytoplasm (Lehrbach et al., 2009; Moss et al., 1997), however it has also been suggested that LIN-28 binds to and regulates *pri-let-7* in the nucleus (Stefani et al., 2015; Van Wynsberghe et al., 2011).

How the *ma289* mutation leads to decrease in LIN-28B protein level (Fig 3.4B) requires further explanations. The western blot analysis should be repeated several times for quantification of LIN-28B levels in *lin-28(ma289)* mutants compared to wild type. We can quantify RNA levels of *lin-28b* in parallel, to determine if the *ma289* mutation causes transcriptional or post-transcriptional change of LIN-28 expression.

It will be also interesting to investigate roles of each *lin-28* isoform under diverse stress conditions, although we concluded that two isoforms function *lin-28(*RNAi) treated animals were more sensitive to UV, oxidative stress and heat stress than control(RNAi) (Wang et al., 2017b), which we can confirm with the *lin-*

28(lf) genetic mutants. At the same time, the roles of each isoform under stress can be addressed using *lin-28a(lf)* and *lin-28b(lf)* mutants. Also, LIN-28 is required for the maintenance of LIN-14 levels during L1 stage (Arasu et al., 1991). We can determine whether LIN-28A and/or LIN-28B is sufficient for this function. These works will provide a comprehensive understanding about characteristics and roles of *lin-28* isoforms.

2) Role of *lin-28* in remodeling Dorsal-D type neurons of *C. elegans*

C. elegans embryos and early L1 hermaphrodites contain only three types of motor neurons among all eight types of motor neurons. Another five types of motor neuron are born post-embryonically (Sulston et al., 1983; White et al., 1978; White et al., 1986). GABAergic ventral D type (VD) neurons are the one of five types of motor neurons that are not born until the early L2 stage. The function of VD neurons in adult animals is to receive synaptic inputs from cholinergic neurons from dorsal sides, and GABAergic dorsal D type (DD) neurons substitute for VD neurons during the L1 stage as they are born in early L1 by forming synapses in ventral sides of the animal. During late L1 and early L2 stages, six DD neurons undergo remodeling by switching their synaptic location to the dorsal side of animals and then onwards the DD neurons begin to receive inputs from ventrally innervating cholinergic neurons (White et al., 1978). DD neuronal remodeling is an example of neural circuit plasticity, which occurs post-embryonically.

DD neuronal remodeling starts from ~12 hours after the embryo hatches and is completed 10 hours later when animals are in the early L2 stage. Many

genes regulate the timing of neuronal remodeling. Among them, the heterochronic gene *lin-14* is the first identified regulator (Hallam and Jin, 1998). *lin-14(lf)* mutants exhibit a precocious DD neuronal remodeling with 5~6 hours earlier initiation compared to the wild type animals. This is in accordance with the role of LIN-14 in determining the timing of transition between L1 and L2 hypodermal cell fates, in that hypodermal development are also precocious in *lin-14(lf)* mutants due to skipping of L1 specific cell division. A later study suggested that LIN-14, together with UNC-30, maintains the expression of immunoglobulin domain protein OIG-1 in DD neurons to inhibit their remodeling during L1 stage (Howell et al., 2015). In VD neurons, the nuclear hormone receptor UNC-55 is expressed to prevent remodeling. Therefore *unc-55(lf)* mutants show remodeling of VD neurons which does not occur in wild type (Shan et al., 2005; Walthall and Plunkett, 1995; Zhou and Walthall, 1998). UNC-55 is not expressed in DD neurons in wild type, but the ectopic expression of UNC-55 in DD neurons blocks their remodeling with their synapses in the ventral side even after the L1 stage (Shan et al., 2005). UNC-55 suppress another heterochronic gene *hbl-1* in VD neuron to prevent remodeling (Thompson-Peer et al., 2012). HBL-1 is required for completion the synapse remodeling in D-type neurons. *hbl-1(lf)* mutants shows a delay in the completion of DD neuronal remodeling. *mir-84*, one of *let-7* family microRNA which suppresses *hbl-1* in hypodermal cells in order to regulate developmental timing, also suppresses *hbl-1* in DD neuronal remodeling. Therefore, *mir-84(lf)* mutants show earlier

completion of DD neuronal remodeling (Thompson-Peer et al., 2012).

In accordance with heterochronic genes determining the transition timing of the hypodermal cell fate, *lin-14, hbl-1,* and *mir-84* are involved in timing of the DD neuronal remodeling. While LIN-14 prevents the precocious DD neuronal remodeling as just as it prevents precocious hypodermal cell fates, HBL-1 promotes completion of DD neuronal remodeling. Previous studies has shown that LIN-28 positively regulates the level of HBL-1 and also forms a positive feedback loop with LIN-14 in regard to determination of hypodermal cell fates (Arasu et al., 1991; Pepper et al., 2004; Tsialikas et al., 2017).

Our preliminary data suggests that LIN-28 is expressed in Dorsal D-type neuron. We used a reporter that expresses mCherry under an *unc-47* promoter in order to label GABAergic motor neurons. This reporter strain was crossed with a strain containing a GFP tag fused at the 3' end coding sequence of the endogenous *lin-28* (Generated by Orkan Ilbay). We observed that LIN-28:GFP is expressed along the ventral neurons, is especially brightly expressed in the DD neuron in L1 larva (Fig 4.1). We confirmed the expression of LIN-28 in DD neuron by merging GFP and mCherry images (Fig 4.1). It will be intriguing to investigate LIN-28 function in DD neuronal remodeling, particularly because the roles in LIN-28 in *C. elegans* neurons has not been understood despite its neuronal expression. One prediction would be that *lin-28* could function upstream of *hbl-1* to promote completion of DD remodeling. Alternatively, *lin-28* could function upstream of *lin-14* to inhibit precocious DD remodeling. To explore

these possibilities, we can generate *lin-28(lf)* mutants with the Punc-25::UNC-57:GFP reporter for monitoring DD neuronal remodeling (Thompson-Peer et al., 2012) and determine relative timing of the remodeling compared to wild type.

Figure 4.1

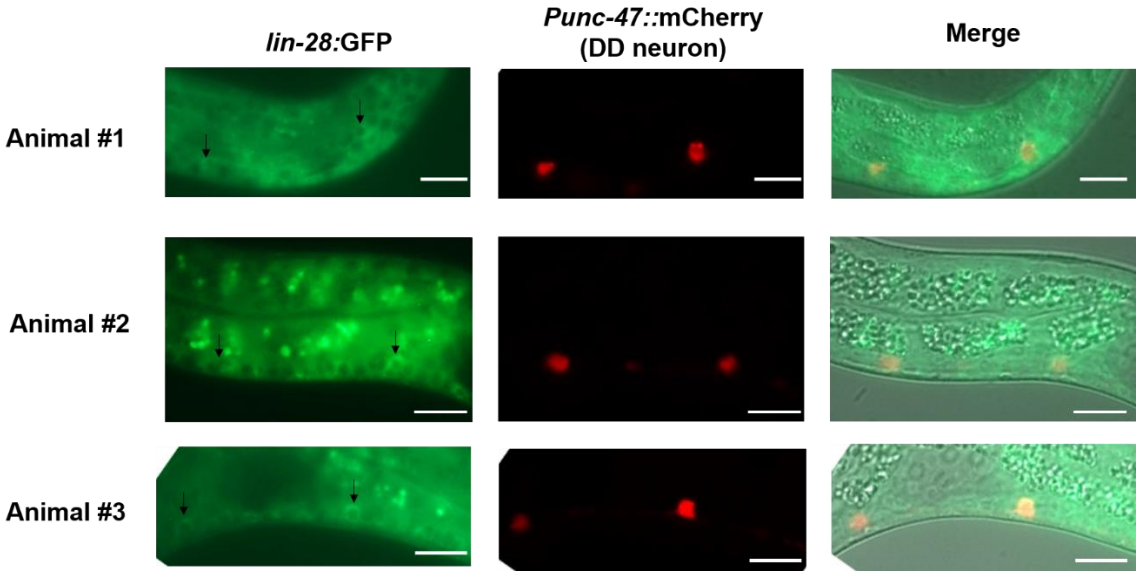
*lin-28:*GFP
*Punc-47::*mCherry
(DD neuron)
Merge
Animal #1
Animal #2
Animal #3

Figure 4.1. LIN-28 is expressed in DD motor neuron

GFP and mCherry images of three animals expressing lin-28:GFP and P*unc-47*::mCherry

The GFP images in left panels show expression of LIN-28 in neurons and other regions.

The positions of DD neuron (based on Punc-47::mCherry) are depicted as arrows.

3) *In vivo* functions of two RNA binding domains in LIN-28

Roles of the cold shock domain (CSD) and zinc-finger domain (ZFD) in mammalian Lin-28 have been studied *in vitro* using cell culture system or crystallography (Mayr et al., 2011; Nam et al., 2011; Triboulet et al., 2015; Wang et al., 2017c). These studies mainly focused on the function of the two domains in the regulation of *let-7* microRNA.

Using CRISPR-Cas9, it will be possible to generate *C. elegans* mutants which contain mutations in essential amino acids of each domain. Exploring the phenotypes of these mutants will allow us to understand the *in vivo* functions of each domain. In addition, we can analyze the RNA sequences bound to either wild type or mutated LIN-28 using CLIP-seq. Through these analyses, we can validate the RNA sequence motifs important for the recognition by CSD or ZFD, which is previously reported as GNGAY and GGAG respectively (Nam et al., 2011). In addition, the analyses will uncover mRNAs, and pri- or pre- forms of microRNAs that could be affected by domain specific mutation of LIN-28. Thus, these data could enable us to identify the domains that are essential for binding or regulating specific RNAs.

REFERENCES

Abbott, A. L., Alvarez-Saavedra, E., Miska, E. A., Lau, N. C., Bartel, D. P., Horvitz, H. R. and Ambros, V. (2005). The let-7 MicroRNA Family Members mir-48, mir-84, and mir-241 Function Together to Regulate Developmental Timing in Caenorhabditis elegans. *Dev. Cell* **9**, 403–414.

Abete-Luzi, P. and Eisenmann, D. M. (2018). Regulation of C. elegans L4 cuticle collagen genes by the heterochronic protein LIN-29. *Genes.* **56**,.

Abrahante, J. E., Daul, A. L., Li, M., Volk, M. L., Tennessen, J. M., Miller, E. A. and Rougvie, A. E. (2003). The Caenorhabditis elegans hunchback-like gene lin-57/hbl-1 controls developmental time and is regulated by microRNAs. *Dev. cell* **4**, 625–637.

Alexander, P. B., Wang, J. and McKnight, S. L. (2011). Targeted killing of a mammalian cell based upon its specialized metabolic state. *Proc. Natl. Acad. Sci. United States Am.* **108**, 15828–15833.

Ambros, V. (1989). A hierarchy of regulatory genes controls a larva-to-adult developmental switch in C. elegans. *Cell* **57**, 49–57.

Ambros, V. (2011). MicroRNAs and developmental timing. *Curr. Opin. Genet. & Dev.* **21**, 511–517.

Ambros, V. and Horvitz, H. (1984a). Heterochronic mutants of the nematode Caenorhabditis elegans. *Science* **226**, 409–416.

Ambros, V. and Horvitz, H. R. (1984b). Heterochronic mutants of the nematode Caenorhabditis elegans. *Sci.* **226**, 409–416.

Ambros, V. and Horvitz, H. R. (1984c). Heterochronic mutants of the nematode Caenorhabditis elegans. *Sci.* **226**, 409–416.

Ambros, V. and Horvitz, H. R. (1987). The lin-14 locus of Caenorhabditis elegans controls the time of expression of specific postembryonic developmental events. *Genes & Dev.* **1**, 398–414.

Arasu, P., Wightman, B. and Ruvkun, G. (1991). Temporal regulation of lin-14 by the antagonistic action of two other heterochronic genes, lin-4 and lin-28. *Genes & Dev.* **5**, 1825–1833.

Arribere, J. A., Bell, R. T., Fu, B. X. H., Artiles, K. L., Hartman, P. S. and Fire, A. Z. (2014). Efficient marker-free recovery of custom genetic modifications with CRISPR/Cas9 in Caenorhabditis elegans. *Genetics* **198**, 837–846.

Balzer, E. and Moss, E. G. (2007). Localization of the Developmental Timing Regulator Lin28 to mRNP Complexes, P-bodies and Stress Granules. *RNA Biol.* **4**, 16–25.

Beachy, S. H., Onozawa, M., Chung, Y. J., Slape, C., Bilke, S., Francis, P., Pineda, M., Walker, R. L., Meltzer, P. and Aplan, P. D. (2012). Enforced expression of Lin28b leads to impaired T-cell development, release of inflammatory cytokines, and peripheral T-cell lymphoma. *Blood* **120**, 1048–1059.

Blumenthal, T. (2012). Trans-splicing and operons in C. elegans. *Wormb. : Online Rev. C. elegans Biol.* 1–11.

Byerly, L., Cassada, R. C. and Russell, R. L. (1976). The life cycle of the nematode Caenorhabditis elegans. I. Wild-type growth and reproduction. *Dev. Biol.* **51**, 23–33.

Carmel-Gross, I., Bollag, N., Armon, L. and Urbach, A. (2016). LIN28: A Stem Cell Factor with a Key Role in Pediatric Tumor Formation. *Stem Cells Dev.* **25**, 367–377.

Chalfie, M., Horvitz, H. R. and Sulston, J. E. (1981). Mutations that lead to reiterations in the cell lineages of C. elegans. *Cell* **24**, 59–69.

Chang, W., Tilmann, C., Thoemke, K., Markussen, F.-H., Mathies, L. D., Kimble, J. and Zarkower, D. (2004). A forkhead protein controls sexual identity of the C. elegans male somatic gonad. *Dev.* **131**, 1425–36.

Chatterjee, I., Richmond, A., Putiri, E., Shakes, D. C. and Singson, A. (2005). The Caenorhabditis elegans spe-38 gene encodes a novel four-pass integral membrane protein required for sperm function at fertilization. *Dev.* **132**, 2795–808.

Chen, C., Cao, F., Bai, L., Liu, Y., Xie, J., Wang, W., Si, Q., Yang, J., Chang, A., Liu, D., et al. (2015a). IKKβ Enforces a LIN28B/TCF7L2 Positive Feedback Loop That Promotes Cancer Cell Stemness and Metastasis. *Cancer Res.* **75**, 1725–1735.

Chen, C.-H., Luhur, A. and Sokol, N. (2015b). Lin-28 promotes symmetric stem cell division and drives adaptive growth in the adult Drosophila intestine. *Dev.* **142**, 3478–3487.

Cho, J., Chang, H., Kwon, S. C., Kim, B., Kim, Y., Choe, J., Ha, M., Kim, Y. K. and Kim, V. N. (2012). LIN28A Is a Suppressor of ER-Associated Translation in Embryonic Stem Cells. *Cell* **151**, 765–777.

Clandinin, T. R., DeModena, J. A. and Sternberg, P. W. (1998). Inositol trisphosphate mediates a RAS-independent response to LET-23 receptor tyrosine kinase activation in C. elegans. *Cell* **92**, 523–533.

Conrad, R., Thomas, J., Spieth, J. and Blumenthal, T. (1991). Insertion of part of an intron into the 5' untranslated region of a Caenorhabditis elegans gene converts it into a trans-spliced gene. *Mol. Cell. Biol.* **11**, 1921–1926.

Conrad, R., Liou, R. F. and Blumenthal, T. (1993). Functional analysis of a C. elegans trans-splice acceptor. *Nucleic acids Res.* **21**, 913–919.

Conte, D., MacNeil, L. T., Walhout, A. J. M. and Mello, C. C. (2015). RNA Interference in Caenorhabditis elegans. *Curr. Protoc. Mol. Biol.* **109**, 26.3.1-26.330.

Cox, J. L., Mallanna, S. K., Luo, X. and Rizzino, A. (2010). Sox2 uses multiple domains to associate with proteins present in Sox2-protein complexes. *PloS one* **5**, e15486.

Detwiler, M. R., Reuben, M., Li, X., Rogers, E. and Lin, R. (2001). Two zinc finger proteins, OMA-1 and OMA-2, are redundantly required for oocyte maturation in C. elegans. *Dev. cell* **1**, 187–199.

Ding, F., Cui, P., Wang, Z., Zhang, S., Ali, S. and Xiong, L. (2014). Genome-wide analysis of alternative splicing of pre-mRNA under salt stress in Arabidopsis. *BMC Genomic-* **15**, 431.

Dong, Q., Meng, P., Wang, T., Qin, W., Qin, W., Wang, F., Yuan, J., Chen, Z., Yang, A. and Wang, H. (2010). MicroRNA let-7a inhibits proliferation of human prostate cancer cells in vitro and in vivo by targeting E2F2 and CCND2. *PloS one* **5**, e10147.

Dowen, R. H., Breen, P. C., Tullius, T., Conery, A. L. and Ruvkun, G. (2016). A microRNA program in the C. elegans hypodermis couples to intestinal mTORC2/PQM-1 signaling to modulate fat transport. *Genes Dev* **30**, 1515–1528.

Euling, S. and Ambros, V. (1996). Heterochronic genes control cell cycle progress and developmental competence of C. elegans vulva precursor cells. *Cell* **84**, 667–676.

Euling, S. and Ambros VR (1995). Reversal of cell fate determination in Caenorhabditis elegans vulval development. *Development* **122**, 2507–15.

Faas, L., Warrander, F. C., Maguire, R., Ramsbottom, S. A., Quinn, D., Genever, P. and Isaacs, H. V. (2013). Lin28 proteins are required for germ layer specification in Xenopus. *Development* **140**, 976–986.

Fay, D. S., Stanley, H. M., Han, M. and Wood, W. B. (1999). A Caenorhabditis elegans homologue of hunchback is required for late stages of development but not early embryonic patterning. *Dev. Biol.* **205**, 240–253.

Friedland, A. E., Tzur, Y. B., Esvelt, K. M., Colaiácovo, M. P., Church, G. M. and Calarco, J. A. (2013). Heritable genome editing in C. elegans via a CRISPR-Cas9 system. *Nat. methods* **10**, 741–743.

Frøkjær-Jensen, C., Davis, M. W., Ailion, M. and Jorgensen, E. M. (2012). Improved Mos1-mediated transgenesis in C. elegans. *Nat. methods* **9**, 117–118.

Gartner, A., Boag, P. R. and Blackwell, T. K. (2008). Germline survival and apoptosis. *WormBook: Online Rev. C. elegans Biol.* 1–20.

Ghosh, S. and Sternberg, P. W. (2014). Spatial and molecular cues for cell outgrowth during C. elegans uterine development. *Dev. Biol.* **396**, 121–135.

Gilleard, J. S., Barry, J. D. and Johnstone, I. L. (1997). cis regulatory requirements for hypodermal cell-specific expression of the Caenorhabditis elegans cuticle collagen gene dpy-7. *Mol. Cell. Biol.* **17**, 2301–2311.

Gissendanner, C. R., Kelley, K., Nguyen, T. Q., Hoener, M. C., Sluder, A. E. and Maina, C. V. (2008). The Caenorhabditis elegans NR4A nuclear receptor is required for spermatheca morphogenesis. *Dev. Biol.* **313**, 767–786.

Gorelick, R. J., Henderson, L. E., Hanser, J. P. and Rein, A. (1988). Point mutants of Moloney murine leukemia virus that fail to package viral RNA: evidence for specific RNA recognition by a "zinc finger-like" protein sequence. *Proc. Natl. Acad. Sci. United States Am.* **85**, 8420–8424.

Grant, B. and Hirsh, D. (1999). Receptor-mediated endocytosis in the Caenorhabditis elegans oocyte. *Mol. Biol. cell* **10**, 4311–4326.

Graumann, P. and Marahiel, M. A. (1996). A case of convergent evolution of nucleic acid binding modules. *BioEssays: news Rev. Mol. Cell. Dev. Biol.* **18**, 309–315.

Hafner, M., Max, K. E. A., Bandaru, P., Morozov, P., Gerstberger, S., Brown, M., Molina, H. and Tuschl, T. (2013). Identification of mRNAs bound and regulated by human LIN28 proteins and molecular requirements for RNA recognition. *RNA* **19**, 613–626.

Hall, D. H., Winfrey, V. P., Blaeuer, G., Hoffman, L. H., Furuta, T., Rose, K. L., Hobert, O. and Greenstein, D. (1999). Ultrastructural features of the adult hermaphrodite gonad of Caenorhabditis elegans: relations between the germ line and soma. *Dev. Biol.* **212**, 101–123.

Hallam, S. J. and Jin, Y. (1998). lin-14 regulates the timing of synaptic remodelling in Caenorhabditis elegans. *Nature* **395**, 78–82.

Hastings, K. E. M. (2005). SL trans-splicing: easy come or easy go? *Trends Genet. : TIG* **21**, 240–247.

Heo, I., Joo, C., Cho, J., Ha, M., Han, J. and Kim, V. N. (2008). Lin28 mediates the terminal uridylation of let-7 precursor MicroRNA. *Mol. cell* **32**, 276–84.

Heo, I., Joo, C., Kim, Y.-K., Ha, M., Yoon, M.-J., Cho, J., Yeom, K.-H., Han, J. and Kim, V. N. (2009). TUT4 in concert with Lin28 suppresses microRNA biogenesis through pre-microRNA uridylation. *Cell* **138**, 696–708.

Hoskins, R., Hajnal, A. F., Harp, S. A. and Kim, S. K. (1996). The C. elegans vulval induction gene lin-2 encodes a member of the MAGUK family of cell junction proteins. *Dev.* **122**, 97–111.

Howell, K., White, J. G. and Hobert, O. (2015). Spatiotemporal control of a novel synaptic organizer molecule. *Nature* **523**, 83–87.

Iwasaki, K., McCarter, J., Francis, R. and Schedl, T. (1996). emo-1, a Caenorhabditis elegans Sec61p gamma homologue, is required for oocyte development and ovulation. *J. cell Biol.* **134**, 699–714.

Jiang, S. and Baltimore, D. (2016). RNA-binding protein Lin28 in cancer and immunity.

Cancer Lett. **375**, 108–113.
Jin, J., Jing, W., Lei, X.-X., Feng, C., Peng, S., Boris-Lawrie, K. and Huang, Y. (2011). Evidence that Lin28 stimulates translation by recruiting RNA helicase A to polysomes. *Nucleic acids Res.* **39**, 3724–3734.
Johnston, W. L. and Dennis, J. W. (2011). The eggshell in the C. elegans oocyte-to-embryo transition. *Genes.* **17**, 1–17.
Johnston, W. L., Krizus, A. and Dennis, J. W. (2006). The eggshell is required for meiotic fidelity, polar-body extrusion and polarization of the C. elegans embryo. *BMC Biol.* **4**, 35.
Johnston, W. L., Krizus, A. and Dennis, J. W. (2010). Eggshell chitin and chitin-interacting proteins prevent polyspermy in C. elegans. *Curr. Biol. CB* **20**, 1932–7.
Kamath, R. S. and Ahringer, J. (2003). Genome-wide RNAi screening in Caenorhabditis elegans. *Methods* **30**, 313–321.
Kariya, K.-I., Bui, Y. K., Gao, X., Sternberg, P. W. and Kataoka, T. (2004). Phospholipase Cepsilon regulates ovulation in Caenorhabditis elegans. *Dev. Biol.* **274**, 201–210.
Kaur, S., Gupta, S., Chaudhary, M., Khursheed, M. A., Mitra, S., Kurup, A. J. and Ramachandran, R. (2018). let-7 MicroRNA-Mediated Regulation of Shh Signaling and the Gene Regulatory Network Is Essential for Retina Regeneration. *Cell reports* **23**, 1409–1423.
Keyte, A. L. and Smith, K. K. (2011). Heterochrony and developmental timing mechanisms: Changing ontogenies in evolution. *Semin. Cell & Dev. Biol.* **34**, 99–107.
Kim, H. H., Kuwano, Y., Srikantan, S., Lee, E. K., Martindale, J. L. and Gorospe, M. (2009). HuR recruits let-7/RISC to repress c-Myc expression. *Genes & Dev.* **23**, 1743–1748.
Kim, H., Ishidate, T., Ghanta, K. S., Seth, M., Conte, D., Shirayama, M. and Mello, C. C. (2014). A co-CRISPR strategy for efficient genome editing in Caenorhabditis elegans. *Genetics* **197**, 1069–1080.
Kimble, J. and Hirsh, D. (1979). The postembryonic cell lineages of the hermaphrodite and male gonads in Caenorhabditis elegans. *Dev. Biol.* **70**, 396–417.
Kimble, J. E. and White, J. G. (1981). On the control of germ cell development in Caenorhabditis elegans. *Dev. Biol.* **81**, 208–219.
King, C. E., Cuatrecasas, M., Castells, A., Sepulveda, A. R., Lee, J.-S. and Rustgi, A. K. (2011). LIN28B promotes colon cancer progression and metastasis. *Cancer Res.* **71**, 4260–4268.
Klingenberg, C. P. (1998). Heterochrony and allometry: the analysis of evolutionary change in ontogeny. *Biol. Rev. Camb. Philos. Soc.* **73**, 79–123.
Kovacevic, I. and Cram, E. J. (2010). FLN-1/filamin is required for maintenance of actin and exit of fertilized oocytes from the spermatheca in C. elegans. *Dev. Biol.* **347**, 247–257.
Kovacevic, I., Orozco, J. M. and Cram, E. J. (2013). Filamin and phospholipase C-ε are required for calcium signaling in the Caenorhabditis elegans spermatheca. *PLoS Genet.* **9**, e1003510.
Kroft, T. L., Gleason, E. J. and L\textquotesingleHernault, S. W. (2005). The spe-42 gene is required for sperm–egg interactions during C. elegans fertilization and encodes a sperm-specific transmembrane protein. *Dev. Biol.* **286**, 169–181.
Landsman, D. (1992). RNP-1, an RNA-binding motif is conserved in the DNA-binding cold shock domain. *Nucleic acids Res.* **20**, 2861–2864.
Large, E. E. and Mathies, L. D. (2010). hunchback and Ikaros-like zinc finger genes control reproductive system development in Caenorhabditis elegans. *Dev. Biol.* **339**, 51–64.

Lee, Y. S. and Dutta, A. (2007). The tumor suppressor microRNA let-7 represses the HMGA2 oncogene. *Genes & Dev.* **21**, 1025–1030.

Lee, R. C., Feinbaum, R. L. and Ambros, V. (1993). The C. elegans heterochronic gene lin-4 encodes small RNAs with antisense complementarity to lin-14. *Cell* **75**, 843–854.

Lee, Y. T., de Vasconcellos, J. F., Yuan, J., Byrnes, C., Noh, S.-J., Meier, E. R., Kim, K. S., Rabel, A., Kaushal, M., Muljo, S. A., et al. (2013). LIN28B-mediated expression of fetal hemoglobin and production of fetal-like erythrocytes from adult human erythroblasts ex vivo. *Blood* **122**, 1034–1041.

Lehrbach, N. J., Armisen, J., Lightfoot, H. L., Murfitt, K. J., Bugaut, A., Balasubramanian, S. and Miska, E. a (2009). LIN-28 and the poly(U) polymerase PUP-2 regulate let-7 microRNA processing in Caenorhabditis elegans. *Nat. Struct. & Mol. Biol.* **16**, 1016–20.

Lin, S. Y., Johnson, S. M., Abraham, M., Vella, M. C., Pasquinelli, A., Gamberi, C., Gottlieb, E. and Slack, F. J. (2002). The C. elegans hunchback homolog, hbl-1, controls temporal patterning and is a probable MicroRNA target. *Dev. Cell* **4**, 639–650.

Liu, Z. and Ambros, V. (1991). Alternative temporal control systems for hypodermal cell differentiation in Caenorhabditis elegans. *Nature* **350**, 162–165.

Liu, Z., Kirch, S. and Ambros, V. (1995). The Caenorhabditis elegans heterochronic gene pathway controls stage-specific transcription of collagen genes. *Dev.* **121**, 2471–2478.

Liu, Y., Li, H., Feng, J., Cui, X., Huang, W., Li, Y., Su, F., Liu, Q., Zhu, J., Lv, X., et al. (2013). Lin28 induces epithelial-to-mesenchymal transition and stemness via downregulation of let-7a in breast cancer cells. *PloS one* **8**, e83083.

Luhur, A., Buddika, K., Ariyapala, I. S., Chen, S. and Sokol, N. S. (2017). Opposing Post-transcriptional Control of InR by FMRP and LIN-28 Adjusts Stem Cell-Based Tissue Growth. *Cell reports* **21**, 2671–2677.

Ma, W., Ma, J., Xu, J., Qiao, C., Branscum, A., Cardenas, A., Baron, A. T., Schwartz, P., Maihle, N. J. and Huang, Y. (2013). Lin28 regulates BMP4 and functions with Oct4 to affect ovarian tumor microenvironment. *Cell Cycle* **12**, 88–97.

Mallo, M., Wellik, D. M. and Deschamps, J. (2010). Hox genes and regional patterning of the vertebrate body plan. *Dev. Biol.* **344**, 7–15.

Marson, A., Levine, S. S., Cole, M. F., Frampton, G. M., Brambrink, T., Johnstone, S., Guenther, M. G., Johnston, W. K., Wernig, M., Newman, J., et al. (2008). Connecting microRNA genes to the core transcriptional regulatory circuitry of embryonic stem cells. *Cell* **134**, 521–533.

Maruyama, R., Velarde, N. V., Klancer, R., Gordon, S., Kadandale, P., Parry, J. M., Hang, J. S., Rubin, J., Stewart-Michaelis, A., Schweinsberg, P., et al. (2007). EGG-3 regulates cell-surface and cortex rearrangements during egg activation in Caenorhabditis elegans. *Curr. Biol. CB* **17**, 1555–60.

Mayr, F., Schütz, A., Döge, N. and Heinemann, U. (2011). The Lin28 cold-shock domain remodels pre-let-7 microRNA. *Nucleic Acids Res.* **40**, 7492–7506.

McCarter, J., Bartlett, B., Dang, T. and Schedl, T. (1999). On the control of oocyte meiotic maturation and ovulation in Caenorhabditis elegans. *Dev. Biol.* **205**, 111–128.

Miller, M. A., Nguyen, V. Q., Lee, M. H., Kosinski, M., Schedl, T., Caprioli, R. M. and Greenstein, D. (2001). A sperm cytoskeletal protein that signals oocyte meiotic maturation and ovulation. *Sci.* **291**, 2144–2147.

Miller, M. A., Ruest, P. J., Kosinski, M., Hanks, S. K. and Greenstein, D. (2003). An Eph receptor sperm-sensing control mechanism for oocyte meiotic maturation in Caenorhabditis elegans. *Genes & Dev.* **17**, 187–200.

Mogilyansky, E. and Rigoutsos, I. (2013). The miR-17/92 cluster: a comprehensive update on its genomics, genetics, functions and increasingly important and numerous roles in health and disease. *Cell death Differ.* **20**, 1603–1614.

Morita, K. and Han, M. (2006). Multiple mechanisms are involved in regulating the expression of the developmental timing regulator lin-28 in Caenorhabditis elegans. *EMBO J.* **25**, 5794–804.

Moss, E. G. and Tang, L. (2003). Conservation of the heterochronic regulator Lin-28, its developmental expression and microRNA complementary sites. *Dev. Biol.* **258**, 432–442.

Moss, E. G., Lee, R. C. and Ambros, V. (1997). The Cold Shock Domain Protein LIN-28 Controls Developmental Timing in C. elegans and Is Regulated by the lin-4 RNA. *Cell* **88**, 637–646.

Nam, Y., Chen, C., Gregory, R. I., Chou, J. J. and Sliz, P. (2011). Molecular basis for interaction of let-7 microRNAs with Lin28. *Cell* **147**, 1080–91.

Newman, A. P. and Sternberg, P. W. (1996). Coordinated morphogenesis of epithelia during development of the Caenorhabditis elegans uterine-vulval connection. *Proc. Natl. Acad. Sci. United States Am.* **93**, 9329–9333.

Newman, A. P., White, J. G. and Sternberg, P. W. (1995). The Caenorhabditis elegans lin-12 gene mediates induction of ventral uterine specialization by the anchor cell. *Dev.* **121**, 263–271.

Newman, A. P., White, J. G. and Sternberg, P. W. (1996). Morphogenesis of the C. elegans hermaphrodite uterus. *Dev.* **122**, 3617–3626.

Newman, A. P., Inoue, T., Wang, M. and Sternberg, P. W. (2000). The Caenorhabditis elegans heterochronic gene lin-29 coordinates the vulval–uterine–epidermal connections. *Curr. Biol.* **10**, 1479–1488.

Newman, M. A., Thomson, J. M. and Hammond, S. M. (2008). Lin-28 interaction with the Let-7 precursor loop mediates regulated microRNA processing. *RNA* **14**, 1539–1549.

Nishimura, H. and L'Hernault, S. (2008). Spermatogenesis-defective (spe) mutants of the nematodeCaenorhabditis elegansprovide clues to solve the puzzle of male germline functions during reproduction. *Dev. Dyn.*

Oh, J.-S., Kim, J.-J., Byun, J.-Y. and Kim, I.-A. (2010). Lin28-let7 modulates radiosensitivity of human cancer cells with activation of K-Ras. *Int. J. Radiat. Oncol. Biol. Phys.* **76**, 5–8.

Ouchi, Y., Yamamoto, J. and Iwamoto, T. (2014). The heterochronic genes lin-28a and lin-28b play an essential and evolutionarily conserved role in early zebrafish development. *PloS one* **9**, e88086.

Palmer, R. E., Inoue, T., Sherwood, D. R., Jiang, L. I. and Sternberg, P. W. (2002). Caenorhabditis elegans cog-1 Locus Encodes GTX/Nkx6.1 Homeodomain Proteins and Regulates Multiple Aspects of Reproductive System Development. *Dev. Biol.* **252**, 202–213.

Pappalardo, L., Borer, P. N., … M. S.- and 1998 (1997). Structure of the HIV-1 nucleocapsid protein bound to the SL3 Ψ-RNA recognition element.

Parry, J. M., Velarde, N. V., Lefkovith, A. J., Zegarek, M. H., Hang, J. S., Ohm, J., Klancer, R., Maruyama, R., Druzhinina, M. K., Grant, B. D., et al. (2009). EGG-4 and EGG-5 Link Events of the Oocyte-to-Embryo Transition with Meiotic Progression in C. elegans. *Curr. Biol. : CB* **19**, 1752–1757.

Pedersen, M. E., Snieckute, G., Kagias, K., Nehammer, C., Multhaupt, H. A. B., Couchman, J. R. and Pocock, R. (2013). An epidermal microRNA regulates neuronal

migration through control of the cellular glycosylation state. *Sci.* **341**, 1404–1408.

Peng, S., Chen, L.-L., Lei, X.-X., Yang, L., Lin, H., Carmichael, G. G. and Huang, Y. (2011). Genome-wide studies reveal that Lin28 enhances the translation of genes important for growth and survival of human embryonic stem cells. *Stem cells* **29**, 496–504.

Pepper, A. S.-R., McCane, J. E., Kemper, K., Yeung, D. A., Lee, R. C., Ambros, V. and Moss, E. G. (2004). The C. elegans heterochronic gene lin-46 affects developmental timing at two larval stages and encodes a relative of the scaffolding protein gephyrin. *Dev.* **131**, 2049–59.

Piskounova, E., Polytarchou, C., Thornton, J. E., LaPierre, R. J., Pothoulakis, C., Hagan, J. P., Iliopoulos, D. and Gregory, R. I. (2011). Lin28A and Lin28B inhibit let-7 microRNA biogenesis by distinct mechanisms. *Cell* **147**, 1066–1079.

Polesskaya, A., Cuvellier, S., Naguibneva, I., Duquet, A., Moss, E. G. and Harel-Bellan, A. (2007). Lin-28 binds IGF-2 mRNA and participates in skeletal myogenesis by increasing translation efficiency. *Genes & Dev.* **21**, 1125–1138.

Qiu, C., Ma, Y., Wang, J., Peng, S. and Huang, Y. (2010). Lin28-mediated post-transcriptional regulation of Oct4 expression in human embryonic stem cells. *Nucleic acids Res.* **38**, 1240–8.

Reinhart, B. J., Slack, F. J., Basson, M., Pasquinelli, a E., Bettinger, J. C., Rougvie, a E., Horvitz, H. R. and Ruvkun, G. (2000). The 21-nucleotide let-7 RNA regulates developmental timing in Caenorhabditis elegans. *Nature* **403**, 901–6.

Resnick, T. D., McCulloch, K. A. and Rougvie, A. E. (2010). miRNAs give worms the time of their lives: small RNAs and temporal control in Caenorhabditis elegans. *Dev. Dyn. Off. Publ. Am. Assoc. Anat.* **239**, 1477–1489.

Rougvie, A. E. (2001). Control of developmental timing in animals. *Nat. Rev. Genet.* **2**, 690–701.

Rougvie, A. E. and Ambros, V. (1995). The heterochronic gene lin-29 encodes a zinc finger protein that controls a terminal differentiation event in Caenorhabditis elegans. *Dev.* **121**, 2491–2500.

Roush, S. and Slack, F. J. (2008). The let-7 family of microRNAs. *Trends cell Biol.* **18**, 505–16.

Ruvkun, G. and Giusto, J. (1989). The Caenorhabditis elegans heterochronic gene lin-14 encodes a nuclear protein that forms a temporal developmental switch. *Nature* **338**, 313–319.

Salzberg, Y., Díaz-Balzac, C. A., Ramirez-Suarez, N. J., Attreed, M., Tecle, E., Desbois, M., Kaprielian, Z. and Bülow, H. E. (2013). Skin-Derived Cues Control Arborization of Sensory Dendrites in Caenorhabditis elegans. *Cell* **155**, 10.1016/j.cell.2013.08.058.

Seggerson, K., Tang, L. and Moss, E. G. (2002). Two genetic circuits repress the Caenorhabditis elegans heterochronic gene lin-28 after translation initiation. *Dev. Biol.* **243**, 215–25.

Shaham, S. (2004). Methods in cell biology. *WormBook*.

Shan, G., Kim, K., Li, C. and Walthall, W. W. (2005). Convergent genetic programs regulate similarities and differences between related motor neuron classes in Caenorhabditis elegans. *Dev. Biol.* **280**, 494–503.

Shinoda, G., de Soysa, T. Y., Seligson, M. T., Yabuuchi, A., Fujiwara, Y., Yi Huang, P., Hagan, J. P., Gregory, R. I., Moss, E. G. and Daley, G. Q. (2013). Lin28a Regulates Germ Cell Pool Size and Fertility. *Stem cells* **2013**,.

Shirayama, M., Seth, M., Lee, H.-C., Gu, W., Ishidate, T., Conte, D. and Mello, C. C.

(2012). piRNAs initiate an epigenetic memory of nonself RNA in the C. elegans germline. *Cell* **150**, 65–77.

Shyh-Chang, N., Locasale, J. W., Lyssiotis, C. A., Zheng, Y., Teo, R. Y., Ratanasirintrawoot, S., Zhang, J., Onder, T., Unternaehrer, J. J., Zhu, H., et al. (2013). Influence of threonine metabolism on S-adenosylmethionine and histone methylation. *Sci.* **339**, 222–226.

Singson, a., Mercer, K. B. and L'Hernault, S. W. (1998). The C. elegans spe-9 gene encodes a sperm transmembrane protein that contains EGF-like repeats and is required for fertilization. *Cell* **93**, 71–9.

Slack, F. J., Basson, M., Liu, Z., Ambros, V., Horvitz, H. R. and Ruvkun, G. (2000). The lin-41 RBCC Gene Acts in the C. elegans Heterochronic Pathway between the let-7 Regulatory RNA and the LIN-29 Transcription Factor. *Mol. Cell* **5**, 659–669.

Stefani, G., Chen, X., Zhao, H. and Slack, F. J. (2015). A novel mechanism of LIN-28 regulation of let-7 microRNA expression revealed by in vivo HITS-CLIP in C. elegans. *RNA* **21**, 985–996.

Stiernagle, T. (2006). Maintenance of C. elegans (February 11, 2006), WormBook, ed. The C. elegans Research Community, WormBook, doi/10.1895/wormbook. 1.101. 1.

Stratoulias, V., Heino, T. I. and Michon, F. (2014). Lin-28 regulates oogenesis and muscle formation in Drosophila melanogaster. *PloS one* **9**, e101141.

Sulston, J. E., Schierenberg, E., White, J. G. and Thomson, J. N. (1983). The embryonic cell lineage of the nematode Caenorhabditis elegans. *Dev. Biol.* **100**, 64–119.

Takechi, H., Hosokawa, N., Hirayoshi, K. and Nagata, K. (1994). Alternative 5' splice site selection induced by heat shock. *Mol. Cell. Biol.* **14**, 567–575.

Takeo, K., Kawai, T., Nishida, K., Masuda, K., Teshima-Kondo, S., Tanahashi, T. and Rokutan, K. (2009). Oxidative stress-induced alternative splicing of transformer 2beta (SFRS10) and CD44 pre-mRNAs in gastric epithelial cells. *Am. J. Physiol. Cell Physiol.* **297**, C330–C338.

Thompson-Peer, K. L., Bai, J., Hu, Z. and Kaplan, J. M. (2012). HBL-1 Patterns Synaptic Remodeling in C. elegans. *Neuron* **73**, 453–465.

Triboulet, R., Pirouz, M. and Gregory, R. I. (2015). A Single Let-7 MicroRNA Bypasses LIN28-Mediated Repression. *Cell Reports* **13**, 260–266.

Tsialikas, J., Romens, M. A., Abbott, A. and Moss, E. G. (2017). Stage-Specific Timing of the microRNA Regulation of lin-28 by the Heterochronic Gene lin-14 in Caenorhabditis elegans. *Genetics* **205**, 251–262.

Vadla, B., Kemper, K., Alaimo, J., Heine, C. and Moss, E. G. (2012). lin-28 controls the succession of cell fate choices via two distinct activities. *PLoS Genet.* **8**, e1002588.

Van Wynsberghe, P. M., Kai, Z. S., Massirer, K. B., Burton, V. H., Yeo, G. W. and Pasquinelli, A. E. (2011). LIN-28 co-transcriptionally binds primary let-7 to regulate miRNA maturation in Caenorhabditis elegans. *Nat. Struct. & Mol. Biol.* **18**, 302–8.

Viswanathan, S. R., Daley, G. Q. and Gregory, R. I. (2008). Selective blockade of microRNA processing by Lin28. *Sci.* **320**, 97–100.

Viswanathan, S. R., Powers, J. T., Einhorn, W., Hoshida, Y., Ng, T. L., Toffanin, S., O'Sullivan, M., Lu, J., Phillips, L. a, Lockhart, V. L., et al. (2009). Lin28 promotes transformation and is associated with advanced human malignancies. *Nat. Genet.* **41**, 843–8.

Walthall, W. W. and Plunkett, J. A. (1995). Genetic transformation of the synaptic pattern of a motoneuron class in Caenorhabditis elegans. *J. Neurosci. Off. J. Soc. Neurosci.* **15**, 1035–1043.

Wang, J., Alexander, P., Wu, L., Hammer, R., Cleaver, O. and McKnight, S. L. (2009). Dependence of mouse embryonic stem cells on threonine catabolism. *Sci.* **325**, 435–439.

Wang, D., Hou, L., Nakamura, S., Su, M., Li, F., Chen, W., Yan, Y., Green, C. D., Chen, D., Zhang, H., et al. (2017a). LIN-28 balances longevity and germline stem cell number in Caenorhabditis elegans through let-7/AKT/DAF-16 axis. *Aging Cell* **16**, 113–124.

Wang, D., Hou, L., Nakamura, S., Su, M., Li, F., Chen, W., Yan, Y., Green, C. D., Chen, D., Zhang, H., et al. (2017b). LIN-28 balances longevity and germline stem cell number in Caenorhabditis elegans through let-7/AKT/DAF-16 axis. *Aging cell* **16**, 113–124.

Wang, L., Nam, Y., Lee, A. K., Yu, C., Roth, K., Chen, C., Ransey, E. M. and Sliz, P. (2017c). LIN28 Zinc Knuckle Domain Is Required and Sufficient to Induce let-7 Oligouridylation. *Cell reports* **18**, 2664–2675.

Warrander, F., Faas, L., Kovalevskiy, O., Peters, D., Coles, M., Antson, A. A., Genever, P. and Isaacs, H. V. (2015). lin28 proteins promote expression of 17sim92 family miRNAs during amphibian development. *Dev. Dyn.* **245**, 34–46.

Wei, X., Potter, C. J., Luo, L. and Shen, K. (2012). Controlling gene expression with the Q repressible binary expression system in Caenorhabditis elegans. *Nat. methods* **9**, 391–5.

White, J. G., Albertson, D. G. and Anness, M. A. (1978). Connectivity changes in a class of motoneurone during the development of a nematode. *Nature* **271**, 764–766.

White, J. G., Southgate, E., Thomson, J. N. and Brenner, S. (1986). The structure of the nervous system of the nematode Caenorhabditis elegans. *Philos. Trans. R. Soc. London. Ser. B, Biol. Sci.* **314**, 1–340.

Wightman, B., Bürglin, T. R., Gatto, J., Arasu, P. and Ruvkun, G. (1991). Negative regulatory sequences in the lin-14 3'-untranslated region are necessary to generate a temporal switch during Caenorhabditis elegans development. *Genes & Dev.* **5**, 1813–1824.

Wilbert, M. L., Huelga, S. C., Kapeli, K., Stark, T. J., Liang, T. Y., Chen, S. X., Yan, B. Y., Nathanson, J. L., Hutt, K. R., Lovci, M. T., et al. (2012). LIN28 binds messenger RNAs at GGAGA motifs and regulates splicing factor abundance. *Mol. cell* **48**, 195–206.

Wirshing, A. C. E. and Cram, E. J. (2017). Myosin activity drives actomyosin bundle formation and organization in contractile cells of the spermatheca. *Mol. Biol. cell* **28**, 1937–1949.

Yao, K., Qiu, S., Tian, L., Snider, W. D., Flannery, J. G., Schaffer, D. V. and Chen, B. (2016). Wnt Regulates Proliferation and Neurogenic Potential of Müller Glial Cells via a Lin28/let-7 miRNA-Dependent Pathway in Adult Mammalian Retinas. *Cell reports* **17**, 165–178.

Yin, X., Gower, N. J. D., Baylis, H. A. and Strange, K. (2003). Inositol 1,4,5-Trisphosphate Signaling Regulates Rhythmic Contractile Activity of Myoepithelial Sheath Cells in Caenorhabditis elegans. *Mol. Biol. cell* **15**, 3938–3949.

Yu, J., Vodyanik, M. A., Smuga-Otto, K., Antosiewicz-Bourget, J., Frane, J. L., Tian, S., Nie, J., Jonsdottir, G. A., Ruotti, V., Stewart, R., et al. (2007). Induced Pluripotent Stem Cell Lines Derived from Human Somatic Cells. *Science* **318**, 1917–1920.

Yuan, J., Nguyen, C. K., Liu, X., Kanellopoulou, C. and Muljo, S. A. (2012). Lin28b reprograms adult bone marrow hematopoietic progenitors to mediate fetal-like lymphopoiesis. *Sci.* **335**, 1195–1200.

Zhang, Y., Foster, J. M., Nelson, L. S., Ma, D. and Carlow, C. K. S. (2005). The chitin synthase genes chs-1 and chs-2 are essential for C. elegans development and responsible for chitin deposition in the eggshell and pharynx, respectively. *Dev. Biol.* **285**, 330–9.

Zhang, J., Ratanasirintrawoot, S., Chandrasekaran, S., Wu, Z., Ficarro, S. B., Yu, C., Ross, C. A., Cacchiarelli, D., Xia, Q., Seligson, M., et al. (2016). LIN28 Regulates Stem Cell Metabolism and Conversion to Primed Pluripotency. *Cell stem cell* **19**, 66–80.

Zhou, H. M. and Walthall, W. W. (1998). UNC-55, an orphan nuclear hormone receptor, orchestrates synaptic specificity among two classes of motor neurons in Caenorhabditis elegans. *J. Neurosci. Off. J. Soc. Neurosci.* **18**, 10438–10444.

Zhou, Y., Li, Y.-S., Bandi, S. R., Tang, L., Shinton, S. A., Hayakawa, K. and Hardy, R. R. (2015). Lin28b promotes fetal B lymphopoiesis through the transcription factor Arid3a. *J. Exp. Med.* **212**, 569–580.

Zhu, H., Shah, S., Shyh-Chang, N., Shinoda, G., Einhorn, W. S., Viswanathan, S. R., Takeuchi, A., Grasemann, C., Rinn, J. L., Lopez, M. F., et al. (2010). Lin28a transgenic mice manifest size and puberty phenotypes identified in human genetic association studies. *Nat. Genet.* **42**, 626–30.